POLITECNICO DI TORINO

POLITECNICO DI TORINO

Master's Degree course in Aerospace Engineering

Master's Degree Thesis

Techno-economic and environmental assessment of hydrogen production for the aerospace industry: Italian and European scenarios

Supervisors
Prof. Roberta Fusaro
Prof. Davide Ferretto

Candidate
Mattia Bracci

Academic Year 2024-2025

Contents

List of Figures

List of Tables

Introduction

For over a century of aviation history, many groundbreaking innovations have been witnessed, leading in just a few decades from the Wright brothers' rudimentary first flight (1903) to the achievement of supersonic flight (1947) and space exploration (with Yuri Gagarin becoming the first man in space in 1961). Since then, efforts to push the boundaries of human flight have continued unabated, but have seen the birth of different directions of technological development, meant to increase the efficiency of aircraft (such as with the turbofan engine in the 1960s) and to reduce atmospheric emissions (as with the introduction of SAF[1] in recent years).
Upon this latter direction of further progress, recent research has focused on decarbonising aviation through the use of hydrogen as a propellant. The only two feasible ways, in fact, are SAF fuels themselves, which would reduce total emissions without eliminating them, and electric batteries, whose weight/power ratio is inadequate for long-haul flights.
Concerning SAF, the worries highlighted by Bardon and Massol (2025) are significant, remarking that «more ambitious policies are needed to bridge further the gaps between technologically ready and cheap fossil fuels and SAF. [...] Otherwise, aviation will either not decarbonise or capture an excessive quantity of resources critically needed to smooth other sectors' transition. Such resource displacement across sectors would only transfer the problem and could even worsen it, considering the very low carbon abatement efficiencies of such resources in aviation» [97].
Keeping in mind the growing interest in electric propulsion, the study conducted by Sismanidou et al. (2024) carried out various simulations to evaluate the workability of electric aircraft on long-haul routes. The results clearly show how these flights would require several stops to recharge the batteries, with the overall amount of time more than doubling.
It is also stated by the authors how «the intermediate stops and low speeds mean travellers would need to accept a considerable increase in travel time and reduction in comfort» [98].
Setting out the results from its 2022 report on Climate Change, the IPCC states that aviation accounts for 2.4% of global CO_2 emissions [99]. The role of hydrogen in the decarbonisation of air transport could be crucial due to the following pros [100]:

- H_2 is a sustainable power source, if produced from renewable energy.
- It has three times the power density of kerosene (120 MJ/kg vs 43 MJ/kg).

[1] Sustainable Aviation Fuel

- Using H_2 to power aircraft would eliminate aviation carbon emissions from aircraft operations[2].

Reflecting on hydrogen potential as a solution for the coming decades, several opinions highlight the disproportionate enthusiasm surrounding it. Some of the drawbacks pointed up by the critics of hydrogen are listed below [101]:

- Hydrogen is not a drop-in fuel, so aircraft fleets would need to be retrofitted or completely renewed to enable its adoption. The changes would not only affect the aircraft propulsion system but also its overall structure, with the need for longer fuselages to accommodate the cylindrical tanks, leaving less space to accommodate passenger seats (in airliners).
- Green H_2 production could damage local communities and nature in many countries. Its exports could clash with delivering energy transition goals, taking renewables away from other applications; for the same reason, it could also hinder the achievement of the 2030 *Sustainable Development Goal* of universal energy access.
- A lot of the current market predictions are based on highly speculative assumptions and uncertain technological innovations. The strongest supporters of hydrogen are the fossil fuel industry itself and countries with vested interests in keeping their fossil fuel infrastructure working.

Additionally, as stated in a 2022 report from the *Arab Reform Initiative*, green hydrogen production is vulnerable to replicating the extractive pattern that has been in place for decades, referred to as "green neo-colonialism". This process is built upon the overexploitation of the natural resources in the country, such as land and water, the neglect of the local people's needs (particularly social and environmental risks) and the exclusion of local stakeholders [104].
Expanding on this background, this thesis seeks to investigate the current level of technological maturity of hydrogen, analysing its production pathways, costs, and integration into airport hubs. The aim is to assess, considering nowadays conditions, the technological challenges that must be overcome if hydrogen is to become an available fuel. The main issues that will be addressed are:

1. How is hydrogen currently produced? How should it be produced to be carbon neutral throughout its entire life cycle?
2. How much does it cost to produce hydrogen from fossil sources compared to renewable ones? How higher is its final cost than that of fossil fuels currently in use?
3. What scales can be used to measure the state of the art of hydrogen technologies employed in aviation?

[2]Assuming no emissions in the manufacturing process. Although eliminating carbon footprints, hydrogen would not completely abate emissions, as it would lead to significantly higher releases of water vapour, which is to all effects a greenhouse gas.

4. How can hydrogen production be integrated into the airport structure in order to avoid transport costs? Is this a feasible scenario for Turin Caselle Airport?

Laying out the approach to these questions, this thesis is structured as follows: the first chapter describes the methodologies of the research, which led to the selection of the papers used as sources; the second chapter analyses the various alternatives to produce hydrogen, comparing their costs and emissions; the third one focuses on the cost of electrolysis, making an estimate of the Italian and European LCOH[3]; the fourth chapter shows the various scales of technological maturity, demonstrating their application in a few case studies; the fifth one compares the three main pathways to produce hydrogen, considering the distance between the production site and the airport of end use; the last chapter shows how the on-site production could be realised in the specific case of Turin Caselle Airport.

[3]Levelized Cost Of Hydrogen, see section 2.4.1

Chapter 1

Systematic literature review

1.1 Literature review in Scopus

The systematic literature review conducted for this study is modelled on the methodology exposed in Athia et al. (2024) [1]. It was mainly conducted on Scopus, a multidisciplinary bibliographic database for peer-reviewed literature (scientific journals, books, and conference proceedings) published by Elsevier [2] [3].

The two ways to look for a document in Scopus are the *basic search* and the *advanced search*. The first one allows to find a specific document, an author or an organization. Searching for a document is by far the most common way of using Scopus, and the database offers a large selection of *search field* to choose from. The default fields of research are *title*, *abstract* and *keywords* of the papers contained in the database.

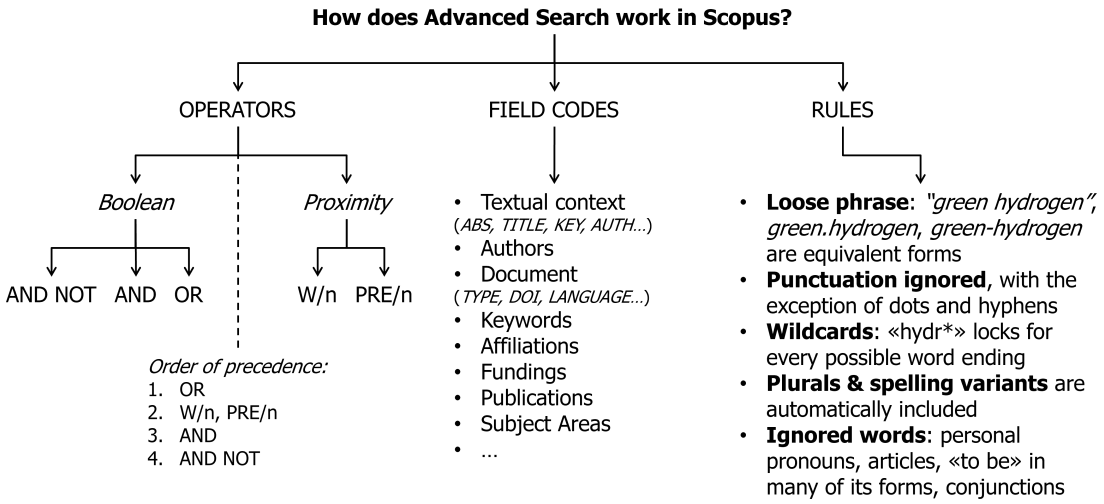

Figure 1.1: Scopus *advanced search* chart [4]

1.2 Scopus' advanced search

The *advanced search* is the best way for a user to conduct meticulous research in the database. It relies on *operators*, that are used in the query string to connect the research words, and *field codes*, namely the research fields of interest. Figure 1.1 resumes the three features that make up the *advanced search* tool: the flow chart was developed with informations from *Elsevier* [4].

Operators Divided into two categories:

- Boolean operators (AND, OR, AND NOT), useful to combine different search queries.
- Proximity operators (W/n, PRE/n), to find words within a specified distance ("n" must be a number) of each other.

Scopus follows a precise *order of precedence* between operators, in which the OR has top priority, followed by the two proximity operators, while the AND NOT is the one with the least priority.

Field codes A large number of categories from which the user can choose the one of his interest. The most common are:

- Textual context: ABS (abstract), TITLE, KEY (keywords), ALL (all fields)
- Authors: AUTH (author), AUTHLASTNAME
- Document: DOCTYPE, DOI (Digital Object Identifier), LANGUAGE, LOADDATE
- Affiliations: AFFILORG (affiliation organization), AFFILCOUNTRY
- Fundings: FUND-SPONSOR, FUND-ACR (funding sponsor acronym)
- Publication: PUBDATETXT (date of publication), ISBN (International Standard Book Number), PUBSTAGE, PUBYEAR (year of publication)
- Subject Areas: Health sciences (MEDI: medicine), Life sciences (AGRI: agricultural and biological sciences), Physical sciences (ENGI: engineering), Social sciences (ECON: economics and finance)

These field codes can be combined to search the query string in more than one at the same time: a useful example is the default search field, defined TIT-ABS-KEY, that looks for the query string in the article title, abstract and keywords.

Rules The last relevant aspect of the Scopus' advanced search tool is represented by the general rules. It is helpful for the user to know these rules, because many of them expand the number of results obtained when they're deemed as too few and vice versa. The *loose phrase* rule implies that Scopus treats two adjacent words in the query string as if there's an AND operator between them; this doesn't apply when the words are between quote marks, or if a dot or a hyphen separates them. *Wildcards* are blunt words that allow Scopus to search for every possible word ending; the search tool also performs other actions, such as removing grammatical particles (articles, pronouns, etc.) and punctuation or adding plurals and spelling variants.

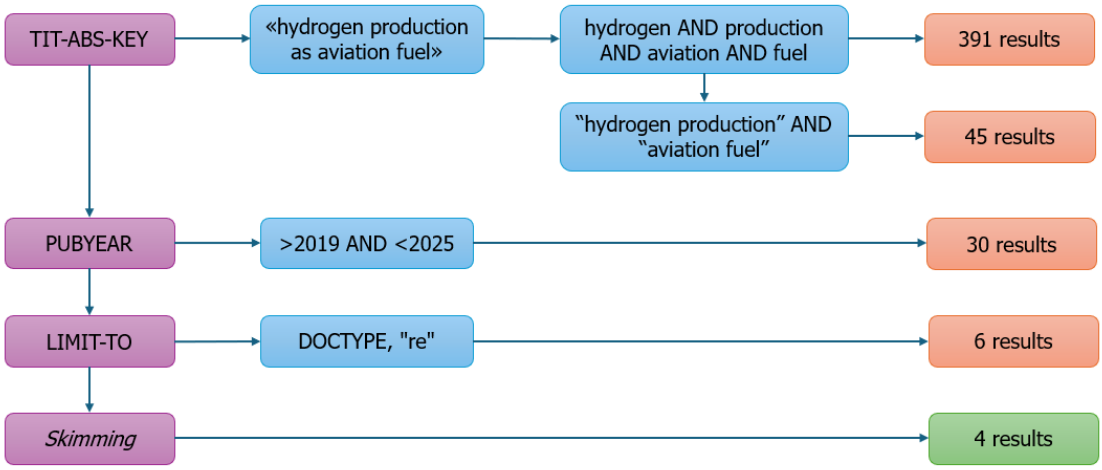

Figure 1.2: Case study 1

1.3 Sample cases

Figure 1.2 displays an actual advanced research carried out in this work. The first line of the flowchart shows the results obtained through a *basic search* on Scopus, which looks for correspondences in the title, abstract, or keywords of every document in the database. Scopus reads the query string «Hydrogen production as aviation fuel» as if AND operators were placed between the words and 391 matching papers are found. The first way to lower the number of results is to group the four relevant words in the string ("as" is not considered by Scopus because of the above-mentioned rule). Searching for the presence of both "Hydrogen production" and "aviation fuel" in the papers returns 45 results. The following step is to add two more filters: the results are limited to papers published after 2020 and the document type is restricted to review papers. This refining is represented by the query string:

TITLE-ABS-KEY("Hydrogen production" AND "aviation fuel") AND PUBYEAR>2019 AND (LIMIT-TO(DOCTYPE,"re"))

After this limitation, there will be only 6 papers in the results. The last line of the chart contains the skimming operation, which consists of the rapid viewing of the document to check if it pertains to the subject of interest. After this final step, the user is left with 4 papers.

Figure 1.3 displays an utterly more significant reduction of the results' amount. The starting sentence is similar to the previous one, but the number of results for the first search line is far higher, amounting to 2478 documents. The second line shows how to use the PRE\n operator: asking for 0 words between *green* and *Hydrogen* is the same as searching for "*green Hydrogen*". The new filters adopted in the following steps are the document language, set to "English", and one of the paper keywords, which must be "Electrolysis". The *search query* related to these two filters is:

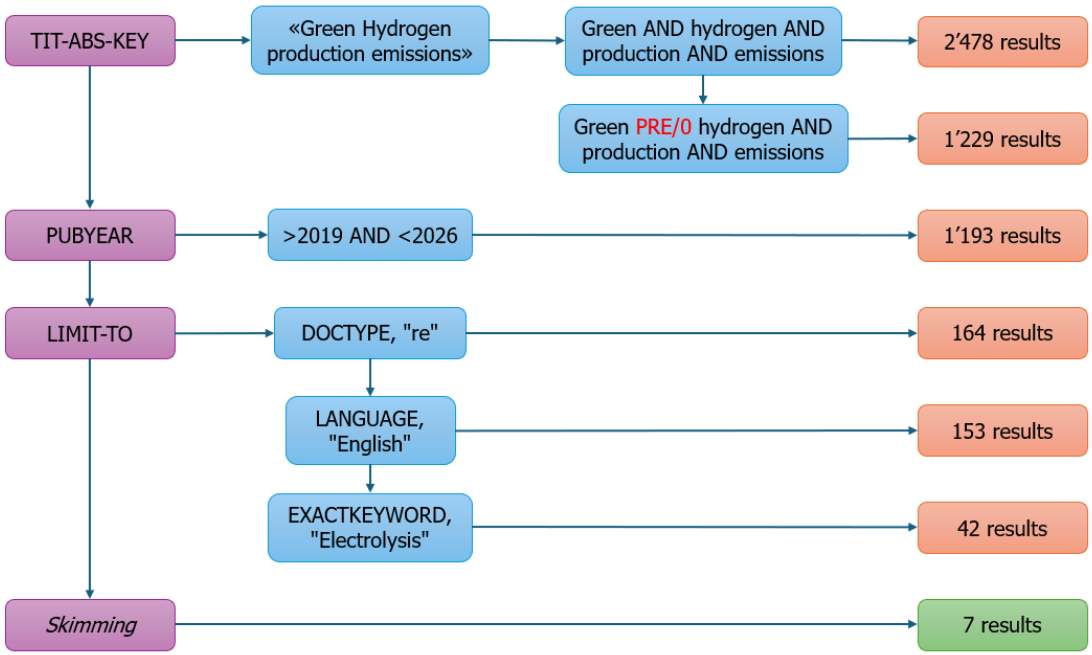

Figure 1.3: Case study 2

(LIMIT-TO(LANGUAGE,"English")) AND
(LIMIT-TO(EXACTKEYWORD,"Electrolysis"))

After the skimming operation, the user is left with 7 review papers.

1.4 Common mistakes

Some possible improvements that can be reported are related to the papers' country of origin and the publication year range. Both these aspects are relevant in studies about hydrogen, being it an emerging technology. The first one because there are regions in which some technologies are deemed more relevant than others: when looking for a particular technology (e.g. electrolysis), limiting the country of source may be beneficial for the user. The publication year is likewise considerable because in recent years hydrogen production technologies have made significant improvements that may alter the worthiness of older papers.

1.5 Results of literature review

To present the results of the literature review conducted, the papers used as sources for the thesis are listed below. The papers are divided by topic, each of which can be related to a chapter.

1.5.1 Topics covered

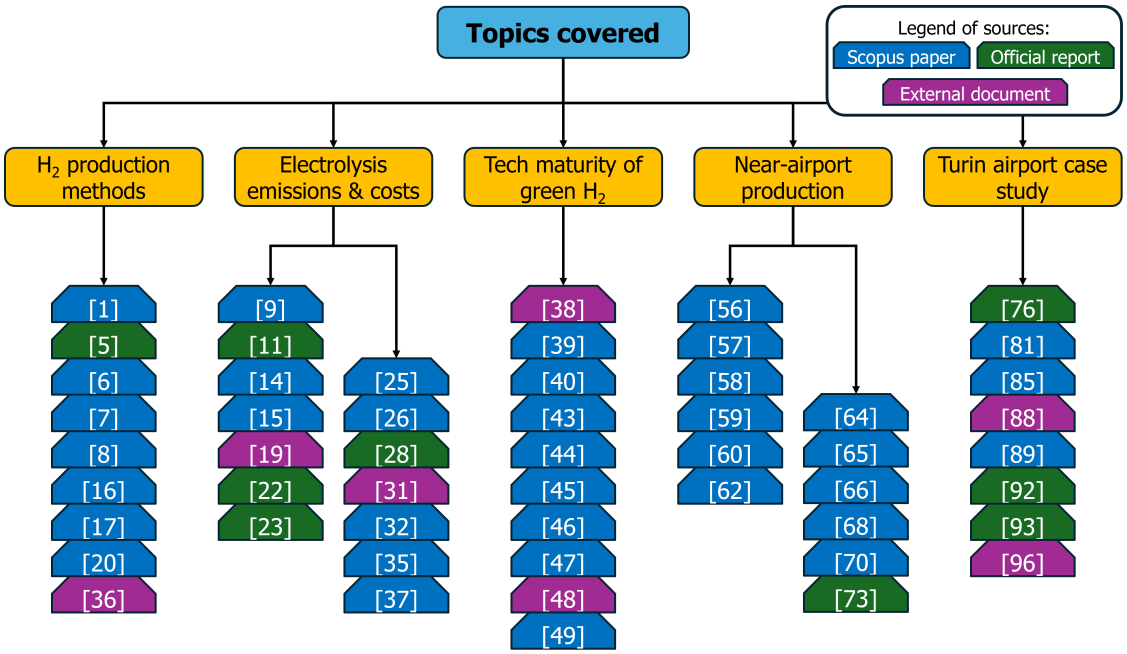

Figure 1.4: bibliographic index of sources by topic

Hydrogen production methods:

1. Factors affecting the production cost of green hydrogen and its challenge for sustainable development [1]
2. Global Hydrogen Review 2024 [5]
3. State of art of hydrogen usage as a fuel on aviation [6]
4. Catalytic decomposition of methane to produce hydrogen: A review [7]
5. Hydrogen combustion, production, and applications: A review [8]
6. Comparing hydrogen fuel cost of production from various sources - a competitive analysis [16]
7. A comprehensive review on environmental and economic impacts of hydrogen production from traditional and cleaner resources [17]
8. Technical and economic assessment of cryogenic fuels for future aviation [20]
9. Path to Hydrogen competitiveness - A cost perspective [36]

Electrolysis emissions & costs:

1. Economic and environmental sustainability of liquid hydrogen fuel for hypersonic transportation systems [9]
2. The Future of Hydrogen [11]
3. Comparative Analysis of Different Hydrogen Production Methods and Their Environmental Impact [14]
4. A review of water electrolysis-based systems for hydrogen production using hybrid/-solar/wind energy systems [15]

5. How to evaluate the cost of the green hydrogen business case? - Assessing green hydrogen production costs [19]
6. Renewable Power Generation Costs in 2018 [22]
7. Projected costs of generating electricity 2020 [23]
8. A review on the role, cost and value of hydrogen energy systems for deep decarbonisation [25]
9. Economics of converting renewable power to hydrogen [26]
10. Green Hydrogen Cost Reduction: Scaling up Electrolysers to Meet the 1.5 °C Climate Goal [28]
11. Fukushima Hydrogen Energy Research Field in Japan ready for green hydrogen production [31]
12. Life-cycle analysis of hydrogen production from water electrolyzers [32]
13. Resource requirements for the implementation of a global H2-powered aviation [35]
14. Evaluation of approaches used for optimization of stand-alone hybrid renewable energy systems [37]

Technological maturity of green hydrogen:

1. Technology Trends Outlook 2024 [38]
2. Techno-economic assessment of various hydrogen production methods - A review [39]
3. Technology readiness level: guidance principles for renewable energy technologies: final report [40]
4. A review of four case studies assessing the potential for hydrogen penetration of the future energy system [43]
5. Green hydrogen production plants: A techno-economic review [44]
6. Biomass-to-hydrogen: A review of main routes production, processes evaluation and techno-economical assessment [45]
7. Applying System Readiness Levels to Cost Estimates - A Case Study [46]
8. System Readiness Assessment (SRA) an illustrative example [47]
9. Integration Maturity Metrics: Development of an Integration Readiness Level [48]
10. Integration readiness levels [49]

Near airport production:

1. Investigation of a new holistic energy system for a sustainable airport with green fuels [56]
2. Techno-economic evaluation of hydrogen production for airport hubs [57]
3. Challenges of Decarbonizing Aviation via Hydrogen Propulsion: Technology Performance Targets and Energy System Trade-Offs [58]
4. Optimal Design of a Sustainable Hydrogen Supply Chain Network: Application in an Airport Ecosystem [59]
5. Estimating the Energy Demand of a Hydrogen-Based Long-Haul Air Transportation Network [60]
6. Hydrogen liquefaction: a review of the fundamental physics, engineering practice and future opportunities [62]
7. Integrating liquid hydrogen infrastructure at airports: Conclusions from an ecosystem approach at Rotterdam The Hague Airport [64]

8. LH_2 supply for the initial development phase of H_2-powered aviation [65]
9. Strategies for decarbonizing the aviation sector: Evaluating economic competitiveness of green hydrogen value chains - A case study in France [66]
10. Challenges, prospects and potential future orientation of hydrogen aviation and the airport hydrogen supply network: A state-of-art review [68]
11. Hydrogen-powered aviation and its reliance on green hydrogen infrastructure - Review and research gaps [70]
12. Eco-Airport Toolkit - A Focus on the production of renewable energy at the Airport site [73]

Turin Caselle Airport analysis:

1. Land cover classification gridded maps from 1992 to present derived from satellite observations [76]
2. Application of Array-Oriented Scientific Data Formats (NetCDF) to Genotype Data, GWASpi as an Example [81]
3. A suite of global, cross-scale topographic variables for environmental and biodiversity modeling [85]
4. Export Potentials of Green Hydrogen - Methodology for a Techno-Economic Assessment [88]
5. Spatial concentration of renewables in energy system optimization models [89]
6. Evolution of hydrogen aircraft fleet to 2050: A "regional first" strategy [92]
7. Aviation Outlook 2050 - main report [93]
8. Aqueduct 4.0: Updated decision-relevant global water risk indicators [96]

Of the 53 papers listed above, 37 come from Scopus, 9 are institutional reports (published by ICAO, IEA, IRENA and others) and 7 are from other sources (some have DOIs but are not listed on Scopus, some others are reports from private institutes).

1.5.2 Analysis of the papers from Scopus

The Scopus research tool enables users to perform analyses directly on the papers among the results. By creating a list of the documents used as sources in this thesis and available in the Scopus catalogue, it was possible to examine their shared features.

A notable classification is by **country of origin**, shown in Figure 1.5. The data analysis presents a clear prevalence of papers from the United States, reflecting intense investment in hydrogen research and innovation, both academically and industrially. In the US, the interest in the topic is not only linked to the energy transition but also to technological leadership and competitiveness goals on a global scale.
The next most prominent countries are Germany and the United Kingdom, the main European hubs in this sector. In the German case, its prominence can be attributed to well-established political and industrial support, expressed in particular through an advanced National Hydrogen Strategy aimed at decarbonising energy-intensive sectors and transport.
The remaining countries reflect global interest in hydrogen technologies, with both Western and Asian countries represented. China's relatively marginal position, with only two

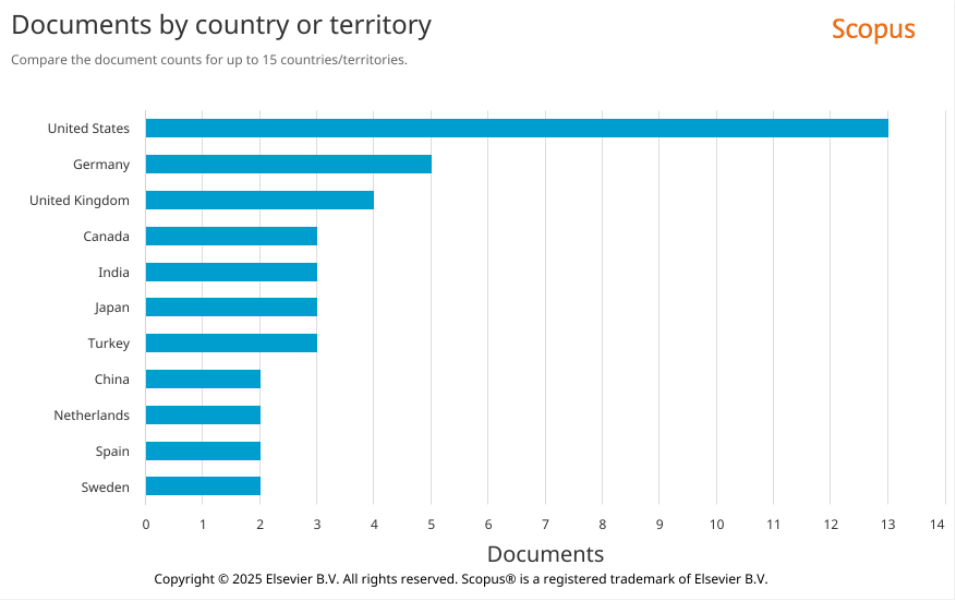

Figure 1.5: Scopus analysis by country of origin

contributions, contrasts with the leading role of the country in global hydrogen development. This discrepancy could originate from a probable bias in Scopus indexing, which tends to under-represent Chinese scientific publications because they are either published in local journals or in non-English languages. The result is therefore a partial picture, which does not fully reflect the intensity of investment and research activities conducted in this country.

Figure 1.6 shows the graphical distribution of the documents by year of publication. All papers published before 2018 concern topics that are not central to this thesis (e.g. small-scale wind turbines, LCOE definition, topographic variables). The only exceptions are those on technological maturity scales, as this tool has existed since the last century and was therefore already present in scientific debate. Since 2019, there has been a significant increase in the number of papers, with the emergence of those related to hydrogen production. The absolute peak is represented by the year 2024, with 11 papers dealing with hydrogen production methods and costs, or the integration of hydrogen into the airport environment.

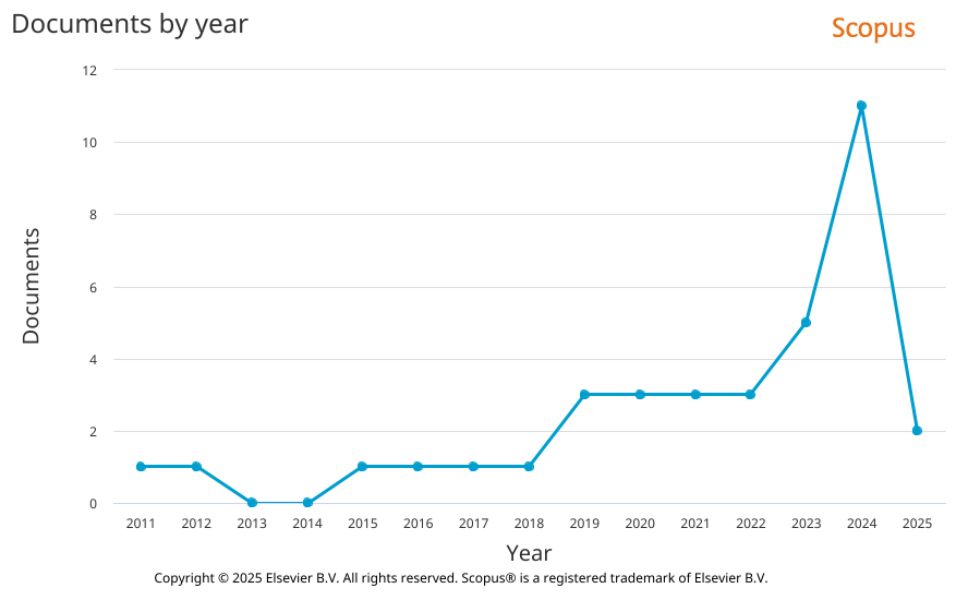

Figure 1.6: Scopus analysis by year of publication

Chapter 2

Hydrogen production routes

2.1 Hydrogen life cycle

A summary of the hydrogen life-cycle can be represented by the following production steps:

1. Feedstock procurement
    - Extraction of coal, oil or natural gas
    - Electricity generation from renewables or from other sources
    - Nuclear fission
    - Storage of biomass
2. Transportation
3. Production
    - With COx emission: Syngas (SMR, POx, ATR, Gasification)
    - With CCUS technologies (Carbon Capture, Utilisation & Storage)
    - Without COx: Electrolysis, photo-/thermo-chemical water splitting
4. Distribution
    - long-distance transmission (LH_2,NH_3,LOHC)
    - last-mile (gaseous/liquid trucking, pipelines)

In the following paragraphs, each step will be explained in detail.

Feedstock procurement Different kinds of feedstock are used depending on the source of hydrogen (mainly fossil sources or renewables) and the production technology. The most used *fossil sources* are natural gas, coal, and oil. Coal is extracted in mines and is usually found in a solid state, while oil and natural gas are naturally accumulated in underground deposits, the former in a liquid form and the latter in a gaseous state. Both these types of deposits have to be drilled during the extraction process.
On the other hand, *renewable feedstocks* are used as a source of energy to electrolyse and split water molecules, obtaining hydrogen and oxygen. Their procurement varies

from source to source, but most of them need the conversion into electricity to be used. Solar energy is collected through photovoltaic panels, wind energy through wind turbines, and energy from watercourses is stored by specific power plants. A different kind of renewable source is represented by nuclear energy, obtained by fission of the atomic nucleus; this energy is then converted into electricity through a thermodynamic cycle. The last example is biomass, which is stacked in piles and then converted into electricity through its combustion.

Transportation Depending on the type of energy source, a first transportation phase may be necessary to move the feedstock or electricity from its procurement site to the hydrogen production location. For this reason, it is preferable to have the two kinds of production sites close to each other to reduce the transportation losses and the carbon footprint of the produced hydrogen.

Production There are two types of production pathways, one involving carbon emissions and the other avoiding them. The first route includes all the processes that involve the transformation of methane or solid carbon into *syngas* (a mixture of carbon monoxide and hydrogen). The latter represents all the processes, mainly from renewable sources, which consist of splitting water molecules into hydrogen and oxygen, through an energy source that is usually electricity or heat.
There's also a third option that stays in between them and is CCUS (Carbon Capture, Utilisation, and Storage). This method goes along with hydrogen production from fossil fuels and allows for reducing their carbon footprint by capturing part of the emissions from the production process.
The aspects related to hydrogen production will be further analysed in section 2.2.

Distribution This thesis will cover most of the positive aspects that make on-site hydrogen production preferable to other systemic choices. Avoiding (or reducing to the minimum) the transportation phase is the simplest way to reduce indirect emissions. However, many papers have shown how this solution is ideal only for small airports. Larger airports take a major advantage in importing hydrogen from off-site plants, both for economic and efficiency reasons. This matter will be further analysed in section 5.1.2.
Hydrogen can be transported in various ways, including trucks, pipelines and ships. The optimal transport method depends on factors such as the distance between the production facility and the airport or the amount of hydrogen required. The main obstacle in moving hydrogen is its low volumetric density. One existing solution is to compress and liquefy it, transporting pure hydrogen but in a liquid state (LH_2). Another way to increase its volumetric energy density is by converting it into carriers (i.e. chemical compounds containing hydrogen): the two main carriers available are ammonia (NH_3) and LOHC (Liquid Organic Hydrogen Carriers).
The main division between transportation methods is based on distance. For long-distance transport, the three main options are the above-mentioned liquid hydrogen, ammonia, and LOHC. Last-mile distribution instead can take place through pipelines or trucking (liquid or gaseous) [5].

2.2 Production routes

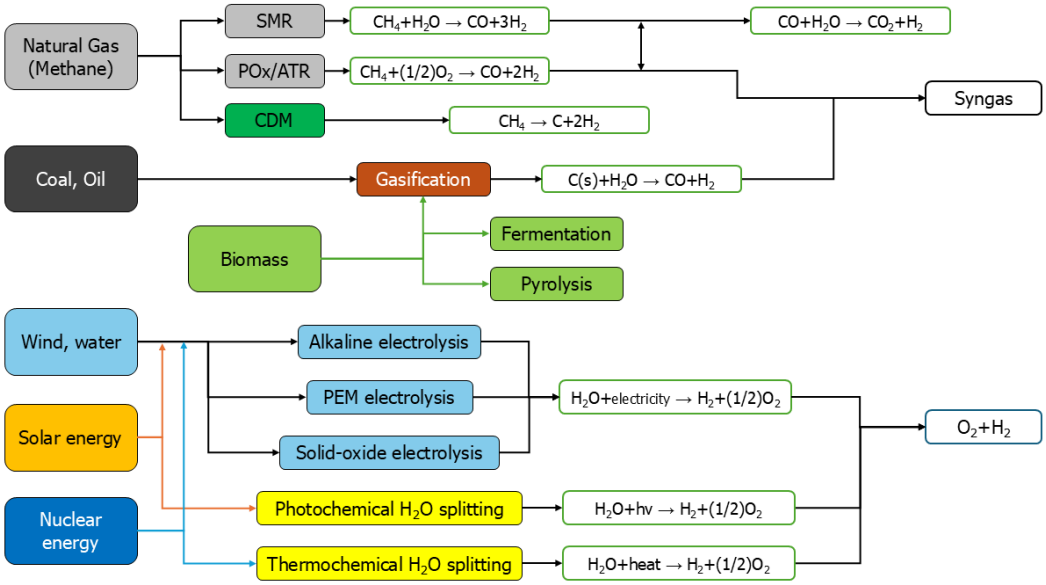

Figure 2.1: Hydrogen production routes

Some of the most common hydrogen production routes are represented in figure 2.1. Hydrogen colours are based on the following distinctions:

- **Black hydrogen** → H_2 from coal and oil gasification
- **Grey hydrogen** → H_2 from:
  - natural gas with SoA[1] technology (POx, SMR)
  - electrolysis with SoA electric grid
- **Blue hydrogen** → H_2 from fossil sources, with the addition of CCUS technologies to reduce carbon footprint
- **Green hydrogen** → H_2 from electrolysis with electricity completely from renewable sources

Hydrogen production technologies might be grouped into two different families [9]:

- Hydrogen separation from hydrocarbons (Natural gas, coal, oil)
- Hydrogen obtained from water splitting (through electricity, heat, photons)

[1] State of the Art

2.2.1 Feedstocks

In this section the different typologies of H_2 feedstocks will be debated.

Natural gas The higher part of figure 2.1 shows the various ways to produce hydrogen from natural gas, with **Steam Methane Reforming** (SMR) being the most widespread method. This process involves the endothermic reaction of methane (CH_4) with steam (H_2O) to form a gaseous compound of carbon monoxide (CO) and molecular hydrogen, called *synthesis gas* or just *syngas* [8]. The secondary reaction of the so-formed carbon monoxide with the remaining steam could lead to the formation of carbon dioxide (CO_2) and additional hydrogen, in a process known as a *water-gas shift reaction* [6].

The exothermic reaction of **Partial Oxidation** (POx) generates similar products. During this process, a mixture of methane, steam, and oxygen is converted into carbon monoxide and hydrogen (syngas) [6]. The *water-gas shift reaction* may happen as well. The oxygen used in this process is only a portion of the amount needed for the complete combustion of the feedstock [8].

A combination of these two processes is the **Auto-Thermal Reforming** (ATR). The process involves an initial thermal zone where a *partial oxidation* happens, while in the subsequent catalytic zone, a reaction of *steam reforming* produces hydrogen. The heat of the exothermic partial oxidation is reused during endothermic steam reforming, to avoid the requirement of external heat sources [8]. This process has many advantages compared to the previous two, but its application hasn't reached a large scale yet [1].

The last process involving natural gas is the Catalytic Decomposition of Methane (CDM). This method relies on multiple steps, with a progressive absorption of methane on a metal-based catalyst. The reaction divides methane molecules into atomic carbon, which diffuses in the metal, and hydrogen atoms, which then gather to form molecules of gaseous hydrogen [7]. This technology is still in an experimental phase but provides a useful example of processes that produce hydrogen from natural gas without carbon oxides (CO or CO_2) as a by-product.

Coal/oil The other fossil feedstocks with a significant share in worldwide production are coal and oil. The most used process in which they're involved is **gasification**, which happens at high temperatures (>700 °C) and without combustion. When the reaction starts from the coil, solid carbon and steam react to form syngas.

Biomass Biomass is not a renewable source; its quantities available without damaging forests, soils, or wildlife are limited. For this reason, in the coming decades, it's reasonable to believe that its employment will be in areas where electrification is more complicated, such as domestic heating, high-temperature industrial sectors, and the production of biofuels for heavy transport. Its use in the production of hydrogen via gasification is not a priority since it is a relatively low-efficiency process and contravenes more direct uses of biomass.

In support of this forecast comes the European *Renewable Energy Directive* 2023/2413 [61]. The act establishes the principle of *cascading use of biomass*, seeking resource efficiency in using biomass to maximise its amount in the system. For this purpose,

it states that its use for energy recovery (bioenergy) is acceptable only when no other economically justifiable or environmentally viable use of biomass exists. The order of priority constituting the cascade is as follows:

- Wood-based products
- Life extension of wood-based products
- Re-use
- Recycling
- Bioenergy
- Disposal

Since the use of biomass to generate hydrogen is a bioenergy process, it would be positioned close to the bottom of the cascading use hierarchy as an energy option when higher value-added uses are not available.

Concerning figure 2.1, **gasification** is an available option to produce H_2 from biomass, but has a huge environmental impact if compared to other processes involving fossil feedstock (e.g. gasification is 3 to 4 times more emissive than SMR) and has polluting by-products like tar. Other alternatives are **pyrolysis**, which happens in anaerobic conditions, and **fermentation**, but both of them require significant technological developments to become cost-effective.

Renewables Water splitting is the best way to produce hydrogen from renewable feedstocks; this **hydrolysis** process needs a lot of energy, usually in the form of electricity, heat, or light. Of these three options, electricity is by far the most widespread, covering about 4% of worldwide hydrogen production in 2024. Electrolysis can achieve production without carbon emissions under specific conditions (depending on the sources of electricity supply). The main problem is related to water consumption: to produce 1 kg of hydrogen and 8 kilograms of oxygen, around 9 litres of distilled water are necessary [1]. As stated in Schenke et al. (2023), water stress is particularly relevant for H_2 production through electrolysis. Fresh water availability is already a serious concern in many regions, and even in those where the water stress is low or medium, locally it can be high, especially in metropolitan areas (where airports are usually located). However, a viable alternative could be represented by desalinated seawater, given the extremely low cost of desalination if compared to the cost of electrolysis [35].

2.2.2 Electrolysers

From a chemical point of view, during hydrolysis processes, water molecules are split into pure oxygen and hydrogen molecules. There are three electrolyser typologies to achieve this reaction: **Alkaline**, **PEM** (Proton Exchange Membrane), and **SOECs** (Solid-Oxide Electrolysis Cells).
Alkaline and PEM electrolysis are the currently leading technologies in terms of H_2 produced worldwide. The main difference between these two processes is that the electrolyte is liquid and alkaline in the first one, while it's a solid polymer membrane (improving conductivity) in the latter [9]. Solid-oxide electrolysis is quite different because it runs

Parameter	Alkaline	PEM	SOEC
Electrolyte	KOH/NaOH (5 M)	Solid polymer electrolyte	Yttria stabilised Zirconia
Separator	Asbestos/Zirfon/Ni	Nafion	Solid electrolyte YSZ
Nominal current density	$0.2 - 0.8\ A/cm^2$	$1 - 2\ A/cm^2$	$0.3 - 1\ A/cm^2$
Voltage range (limits)	1.4-3 V	1.4-2.5 V	1.0-1.5 V
Operating temperature	70-90 °C	50-80 °C	700-850 °C
Cell pressure	<30 bar	<70 bar	1 bar
Efficiency	50-78%	50-83%	89% (laboratory)
Lifetime (stack)	60,000 h	50,000-80,000 h	20,000 h
Development status	Mature	Commercialised	R & D
Capital costs (1 MW)	270 USD/kW	400 USD/kW	>2000 USD/kW
Stack specific costs	262-419 USD/kW	415-1158 USD/kW	1100-1300 USD/kW

Table 2.1: electrolysers technologies comparison [10]

at higher temperatures and reaches better efficiencies, but its implementation still needs to scale up.

The four main sources of electricity are wind, water, solar, and nuclear energy. Solar energy can also be used to split water through a process slightly different from electrolysis, that is **Photochemical water splitting**. According to Athia et al. (2024), «Photo-electrolysis is the term used in this technology when a heterogeneous photo-catalyst is applied to either one or both electrodes. In this technology, both photonic and electrical energy are used to convert into chemical energy to produce hydrogen» [1]. **Thermo-chemical water splitting** instead substitutes electricity with high heat sources like nuclear energy or solar energy concentrators [6]. While it could be a low-cost alternative, it's still far from a commercial production scale.

2.3 Emissions comparison

The production of H_2 through the exposed routes can lead to emissions of various kinds. The SMR and gasification methods use energy to move materials through the plant, heat feedstocks of the desired reaction, and compress and store gaseous components. Similar sources of emissions can be related to H_2 production from biomass, while electrolysis could be emissive only in the upstream production of electricity, whereas the downstream process is emission-free [14].

Not all the cited emissions are equal because the greenhouse gases released depend on the selected process. A common metric to compare them effectively is the *Carbon Dioxide equivalent* (abbreviated as CO_2e). Adopting its definition from the European Commission, this comparison happens «by converting amounts of other gases to the equivalent amount of carbon dioxide with the same global warming potential» [12]. The conversion factor is called Global Warming Potential (GWP) and refers to how long a greenhouse gas remains active in the atmosphere. All the GWPs are compared to carbon dioxide, which has a GWP of 1 on a 100-year basis [13].

Figure 2.2 compares the various methods based on their CO_2e emission to produce 1 kg_{H_2}. Most of the data originate from Nnabuife et al. (2023) and validated in the IEA

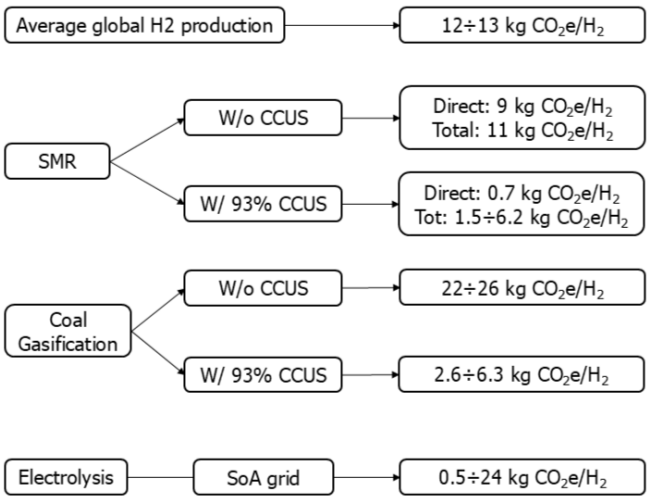

Figure 2.2: CO_2 equivalent emissions of the main H_2 production routes [14]

report *The Future of Hydrogen* (2019) [14] [11]. The first line of the graph displays the current emissions of H_2, to an equal extent of $12 \div 13\ kg_{CO_2e}/kg_{H_2}$. This esteem is based on the average global mix, as shown in figure 2.3.

Moving to the individual processes, it's easy to notice how CCUS has a huge impact on the resulting emissions. Without CCUS, natural gas processes have emissions close to the global average, while coal/oil gasification almost doubles that amount. It's also

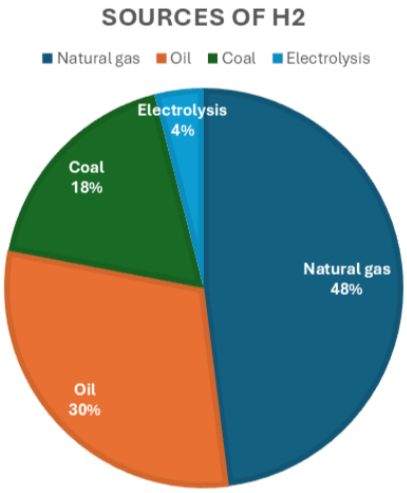

Figure 2.3: Market share of the main hydrogen feedstocks [15]

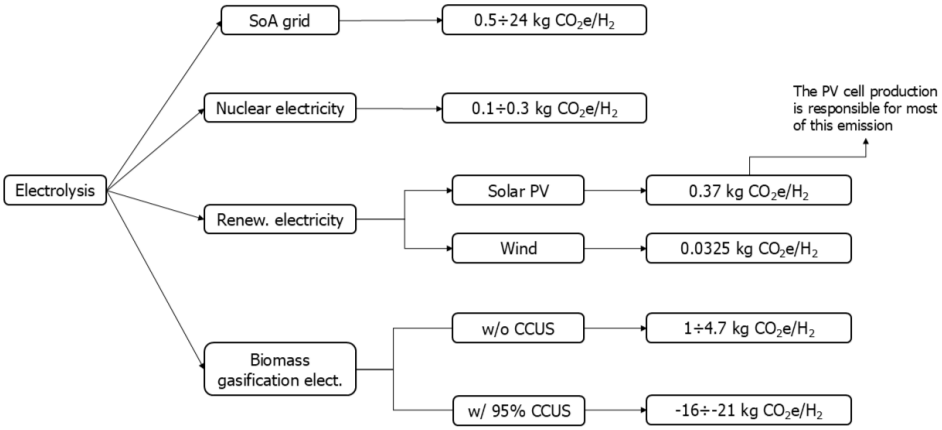

Figure 2.4: CO_2 equivalent emissions of different types of electrolysis

possible to notice how much indirect emissions influence the total quantity; these account for the greenhouse gases produced during the extraction, refining, and transportation of the feedstock (phases that are usually called upstream and midstream). Introducing CCUS technologies can reduce by a factor of 10 the CO_2e emissions, but only with an extremely high percentage of carbon capture (over 90%).
The esteem referring to water electrolysis is far more uncertain, because of its high dependence on the source of electricity. The worldwide average emission of electricity production is 460 g_{CO_2e}/kWh, but in the best-case scenario (represented by the Swedish national grid), it can reach a figure of 10 g_{CO_2e}/kWh. From the last value, an emission of just 0.5 kg_{CO_2e}/kg_{H_2} is obtained, achieving a better result than SMR with 93% of CCUS.

Focusing on the different types of electricity sources for electrolysis, figure 2.4 exhibits their relative emissions. The total is low compared to the fossil feedstocks, with wind energy representing the best-case scenario. Solar energy instead results in slightly higher emissions because of the manufacturing of photovoltaic panels. Biomass could be a valid solution, with even the chance to absorb more greenhouse gases than the emitted total, but it isn't highly accounted for the concerns defined in section 2.2 [61].

Figure 2.5 displays data from the International Energy Agency (IEA), comparable to the previously presented. In this graph, it's even easier to notice how the use of electrolysis with the *world average electricity mix* would be unsustainable; only renewable electricity could compete with fossil sources on the emissions field. Capture rate of 56% for natural gas with CCUS refers to capturing only the feedstock-related CO_2, whereas for a 90% capture rate CCUS is also applied to the fuel-related CO_2 emissions.

2.4 Costs comparison

Cost comparison between different production routes is similar to what was seen for emissions. The diagram in figure 2.6 outlines some preliminary price ranges, as reported in

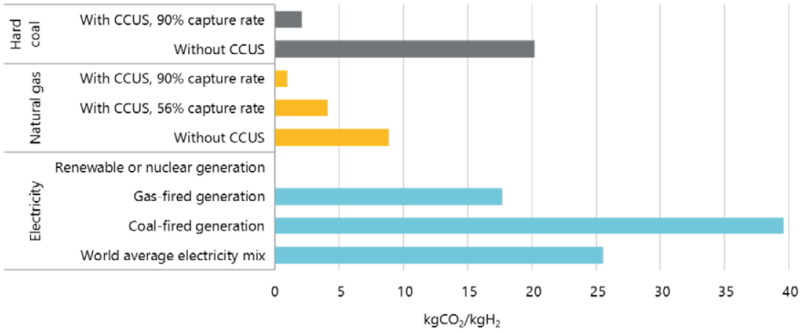

Figure 2.5: CO_2 intensity of hydrogen production [11]

Farhana et al. (2024) [16]. The costs displayed have a reference production capacity[2] of 1000 Nm^3/h, corresponding to a small industrial plant and consistent with the current technological development.
The cheapest process is Steam Methane Reforming without carbon capture technologies, with a lower estimate of 0.7 USD/kg; the introduction of CCUS doubles its cost. Electrolysis with renewable feedstocks for electricity could be cheaper than that from the SoA grid, but in both cases it is more expensive than hydrogen from fossil feedstocks.

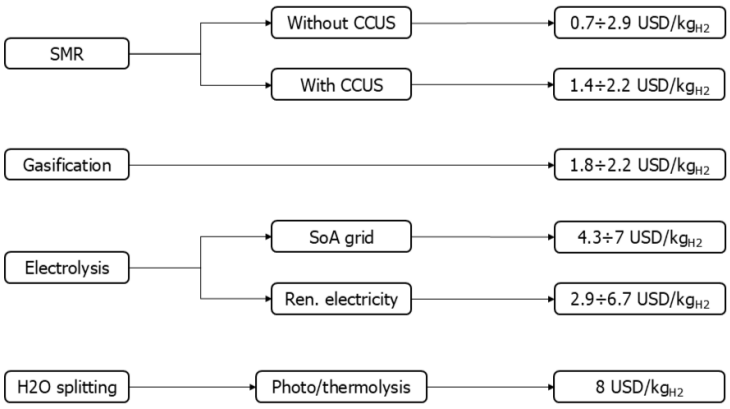

Figure 2.6: Cost comparison between possible production routes

As mentioned in the report *Path to hydrogen cost competitiveness*, published by The Hydrogen Council, the biggest driver of H_2 cost reduction would be scaling up production

[2]Normal Cubic Meters Per Hour (Nm^3/h) is the SI unit for volumetric flow rate of air or gas at a temperature of 0 °C and pressure of 101.3 kPa, expressed in cubic metres per hour.
Source: API STD 2000, *Venting Atmospheric and Low-pressure Storage Tanks*, Sixth Edition, November 2009

and distribution infrastructures [36]. About the latter, last-mile distribution is the major cost driver, accounting for over 50% of the final H_2 price.

2.4.1 Cost of electrolysis

In the subsequent chapter, a simple computation process for the cost of electrolysis will be shown, expressed in terms of the Levelized Cost Of Hydrogen (LCOH). As defined by Fusaro et al. (2020), LCOH is «the present value of the price of the produced hydrogen, considering the economic life of the plant and the costs incurred in the construction, operation and maintenance, and the fuel» [9].

$$\textbf{LCOH} = \text{CAPEX} + \text{OPEX} + \text{EEX} \qquad [€/kg] \tag{2.1}$$

$$\text{OPEX} = 2\% \div 4\% \text{ of CAPEX} \qquad [€/kg]$$

Equation 2.1 displays the items that contribute to the cost of hydrogen production via electrolysis. Capital Expenditures (CAPEX, fig. 2.7) represent the first addend and are directly linked to the investment cost. CAPEX could be divided into direct and indirect costs: direct expenditures are related to the acquisition of plant and equipment, while personnel and energy costs are part of the indirect CAPEX. It is significant to underline how many reports focus only on direct CAPEX. Indirect CAPEX can represent a substantial share of the total Capital Expenditures, but is frequently ignored in industry analyses; besides, economy of scale is mostly related to indirect costs [19].

Direct costs	Indirect costs	
Electrolysers (stacks)	Engineering	Grid fees
Civil, structural & architectural	Project management	Owner project management
Power supply and electronics	Construction supervision and management	Site supervisory teams
Balance of plants(1)	Commissioning	Electricity consumption and lease during construction
Utilities & process automation	Operators training	Contingency(2)
	Insurance	

1) Balance of plants are various supporting components to the system to produce hydrogen
2) Contingency is a budget saved in advance in case unexpected costs occur

Figure 2.7: CAPEX cost components [19]

Operational and Electricity Expenditures (respectively OPEX and EEX) are the remaining part of LCOH. OPEX is the cost of operating and maintaining the infrastructure: it is often estimated at $2\% \div 4\%$ of direct CAPEX, depending on whether stack replacement is included. EEX consists mainly of power purchase costs and costs for purified water (to a minor extent). Therefore, power procurement is essential in assessing the overall feasibility of the business case [19]. The final step of this comprehensive cost estimate is to add liquefaction, storage and distribution costs to the LCOH.

Chapter 3

Cost of electrolysis

The following chapter focuses on an illustrative estimation of the cost of electrolysis, differentiating between an Italian and a European scenario. As shown at the end of the previous chapter, the cost of hydrogen is expressed in terms of LCOH and broken down into three price components: EEX, CAPEX and OPEX.

3.1 Cost of Energy: EEX

The first step in the EEX estimation requires calculating the kWh of energy needed to produce 1 kg of H_2.

Production efficiency The following calculations are needed to figure out the liquefied hydrogen production efficiency in terms of specific electricity consumption. The minimum energy required to achieve the water molecule splitting reaction (eq. 3.1) is the enthalpy of formation $\Delta_f H$. The reaction has on the right side two chemical elements (which by definition do not have an enthalpy of formation), so the total $\Delta_f H$ of the process corresponds to the opposite of the enthalpy of water formation. This figure corresponds to 285.8 kJ/mol under standard conditions [102].

$$\text{Desired reaction: } H_2O \rightarrow H_2 + \tfrac{1}{2}\, O_2 \tag{3.1}$$

$$\text{Liquid water } \Delta_f H\text{: } -285.8\ kJ/mol \text{ (standard conditions)} \tag{3.2}$$

The molar mass of H_2 is 2.016 g/mol circa; therefore, 496 moles must form to obtain 1 kg of H_2.

$$H_2 \text{ molar mass: } 2{,}01568\ g/mol \tag{3.3}$$

$$\frac{1\ kg_{H_2}}{2{,}01568\ g/mol} = 496\ mol \tag{3.4}$$

Multiplying the number of moles by the enthalpy of formation gives the required energy. Converting kJ to kWh then brings the minimum energy to produce 1 kg_{H_2} from 1 kg of liquid water, i.e. 39.4 kWh/kg (of electrical energy in an electrolysis scenario). This

number corresponds to a minimum value as losses are not in the calculation, and the reference atmospheric conditions are standard.

$$496\ mol_{H_2} * \Delta_f H\ [kJ/mol] = 141'856\ kJ \tag{3.5}$$

$$\frac{141'856\ kJ}{3600\ kJ/kWh} = 39{,}4\ kWh \tag{3.6}$$

A more realistic estimate can consider a conversion efficiency of 80%; in this case, the production efficiency rises to 50 kWh/kg_{H_2}. The liquefaction energy, on the other hand, is 12 kWh [20]. The total process, hence, uses 62 kWh.

$$39{,}4\ kWh * 80\%\ [\text{efficiency}] = 50\ kWh \tag{3.7}$$

$$\text{Liquefaction energy: } 43{,}2\ MJ/kg_{H_2} = 12\ kWh \tag{3.8}$$

$$\text{Total energy required for } LH_2 \text{ production: } 62\ kWh \tag{3.9}$$

Levelized Cost Of Electricity Once the production efficiency is known, two further parameters are needed to calculate the EEX. The first one is the Levelized cost of electricity (LCOE), defined as «the rate of the total energy output of the energy system to build and operate it over its lifetime to the average total cost of the system over that lifetime» [37]. The calculation of the LCOE involves a set of financial and energetic inputs that are not of interest for this study. Despite this, it is possible to find LCOE values in the literature that allow the EEX calculation.
Nevertheless, it would be pointless to define a univocal value for each energy source since it fluctuates substantially depending on the method of electricity production. Conversely, as shown in figure 3.1a, a range of values is defined; the width of this range is broader for renewables than for fossil sources, as the production technologies for renewables are less established. The source in figure 3.1b provides narrower ranges for renewables and thus was used for the following calculations.

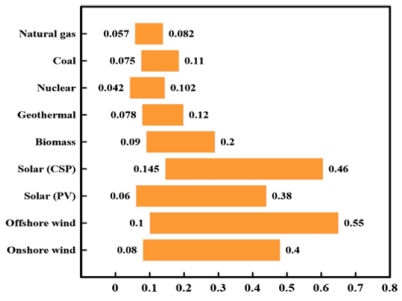

(a) General LCOE overview [15]

	GLOBAL WEIGHTED-AVERAGE COST OF ELECTRICITY (USD/KWH) 2018	COST OF ELECTRICITY: 5TH AND 95TH PERCENTILES (USD/KWH) 2018
Bioenergy	0.062	0.048-0.243
Geothermal	0.072	0.060-0.143
Hydro	0.047	0.030-0.136
Solar photovoltaics	0.085	0.058-0.219
Concentrating solar power	0.185	0.109-0.272
Offshore wind	0.127	0.102-0.198
Onshore wind	0.056	0.044-0.100

(b) LCOE for renewables only [22]

Figure 3.1: Range of LCOE [$/kWh] from different energy sources

Grid share The second one is the percentage breakdown of the electricity grid by sources. Multiplying the LCOE of every energy source by its grid share gives the contribution of that source to the total EEX. Figure 3.2 depicts the share of each electricity source in the Italian national grid in 2022. The graph on the left refers to the total electricity production, showing how fossil sources own over 60% of the gross generation, with a contribution of almost 50% coming from natural gas. About 36% of this production is from renewable sources, with the graph on the right showing their percentage breakdown. Italy has a predominance of hydroelectric and solar energy, both accounting for 34% circa of the production from renewables. Wind energy also plays a significant role, representing around 25% of the total.

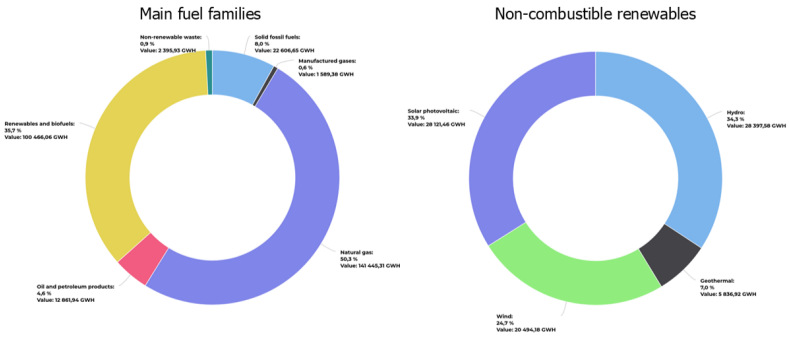

Figure 3.2: Gross electricity production - Italy [21]

Country	Technology	LCOE (USD/MWh)		
		3%	7%	10%
Italy**	Solar PV (residential)	241.73	274.57	302.97
	Solar PV (residential)	114.37	139.73	161.66
	Solar PV (commercial)	76.62	101.58	122.91
	Solar PV (commercial)	53.98	70.98	85.64
	Solar PV (commercial)	70.34	93.74	113.73
	Solar PV (utility scale)	44.53	58.08	69.77
	Solar PV (utility scale)	52.12	62.95	72.29

Figure 3.3: LCOE for photovoltaic solar generators [33]

Discount rate An additional metric that might be considered is the Discount Rate, an economic parameter linked to the private investors' risk perception on a specific project and their preference for immediate returns [27]. A lower discount rate fosters technologies with high initial expenditure but low operational costs. As regards renewable technologies, the discount rate is linked to the initial costs for infrastructures and their life span of production, the availability of low-cost energy and the political support (in terms of subsidies) [26] [24]. Low discount rates are often associated with the H_2 production via electrolysis because it's a case in which the electrolysers' acquisition and the infrastructure investments are far more significant than the cost of operating the plant. Therefore,

it is possible to presume that expectations of hydrogen technologies are quite high and that they could potentially attract substantial investment in the years to come [25]. Despite the relevance of this information, it was chosen to exclude the discount rate as it would further increase the uncertainty of the calculation. In figure 3.3, however, it is possible to see how this parameter influences the value of the LCOE in the example of electricity production from solar energy in Italy in 2020 [23]. Further discussions on the discount rate are in section 3.2.

Having identified all the parameters of interest, the EEX can be estimated through a simple Matlab script. The blue boxes on the left of figure 3.4 show an evaluation flow for the energy cost involving the above-mentioned values. Since the national electricity grid is composed of a mix of different energy sources, it will be necessary to work with data vectors within the Matlab code. On the right, the yellow boxes display the solar energy case, in which the final result corresponds to the contribution of this source to the total EEX. The latter is a more straightforward calculation because it involves only punctual values.

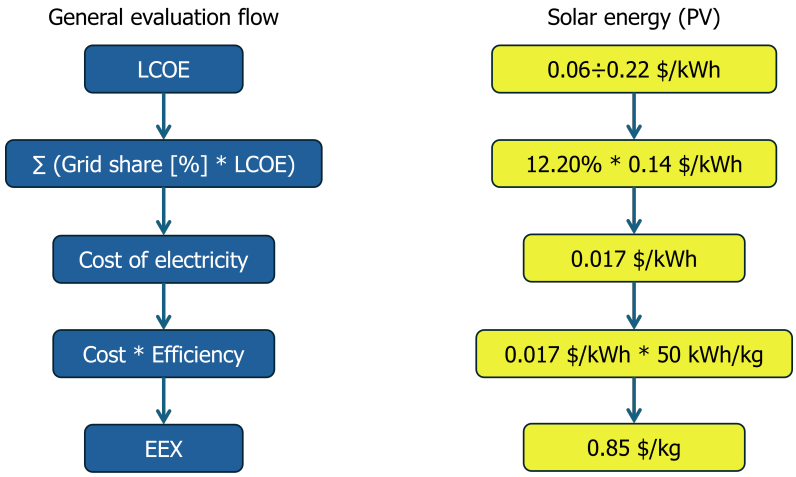

Figure 3.4: EEX evaluation flow

The starting point is the LCOE for each electricity source in the power network. In the instance of solar power, the range is $0.058 \div 0.219$ \$/kWh (see 3.1b): the two data points of interest in this estimate are the lower (best-case scenario) and the mean value (close to a more realistic scenario). Multiplying the LCOE by the grid share gives the cost of electricity. For solar energy, the grid share amounts to 12% circa (figure 3.2), while the average LCOE is 0.14 \$/kWh; therefore, the cost of electricity in a full-solar grid would be 0.017 \$/kWh. Taking into account the efficiency of gaseous H_2 production (50 kWh/kg, see eq. 3.7), the cost of energy to produce 1 kg of hydrogen is obtained.

Following this evaluation flow, the EEX of hydrogen production in Italy can be estimated from data about the national electricity grid and the LCOE of each present source. Figure 3.5 depicts the results for the current composition of the power network, divided

Energy source	LCOE*eff [$/kg]	Grid share [%]	Partial EEX [$/kg]
Natural Gas	3,48	0,51	1,77
Coal	4,63	0,13	0,58
Nuclear	3,60	0,00	0,00
Geothermal	5,08	0,02	0,13
Biomass	7,28	0,01	0,07
Solar PV	6,93	0,12	0,84
Onshore wind	3,60	0,09	0,32
Hydroelectric	4,15	0,12	0,51
Total			**4,20**

(a) Average scenario - current grid (IT)

Energy source	LCOE*eff [$/kg]	Grid share [%]	Partial EEX [$/kg]
Natural Gas	2,85	0,51	1,45
Coal	3,75	0,13	0,47
Nuclear	2,10	0,00	0,00
Geothermal	3,00	0,02	0,07
Biomass	2,40	0,01	0,02
Solar PV	2,90	0,12	0,35
Onshore wind	2,20	0,09	0,19
Hydroelectric	1,50	0,12	0,18
Total			**2,75**

(b) Best-case scenario - current grid (IT)

Figure 3.5: EEX results for the current Italian grid composition

into a best-case scenario (adopting the lower values of LCOE from figure 3.1), and an average one (with the mean value of every LCOE range). The first column of each table displays the product of LCOE and production efficiency, while the second column contains the share of electricity in the national grid derived from that specific source. The sum of the values in the third column leads to the figure in the bottom line, i.e. the total energy cost.

The values in table 3.5a refer to an average scenario with the current national grid composition. The higher contribution to the resulting EEX comes from electricity produced from natural gas (1.77 $/kg), followed by solar energy (0.84 $/kg); the contributions from solid fossil fuels (coal and oil) and hydroelectric are also significant. It's also worth noticing how there's no contribution from nuclear energy because of the specific national regulation against the use of this source.
The resulting EEX is quite high (4.20 $/kg) since CAPEX and OPEX still have to be added to this amount. The resulting hydrogen price will be out of the market as the target price is between 2 and 4 $/kg.

The second table (3.5b) reproduces a similar scenario, adopting the lower LCOEs mentioned. Solar and hydroelectric energy face a significant drop in EEX, with a decrease of more than 60%. Natural gas and coal/oil, on the other hand, see a reduction of around 20% compared to the average scenario, thus having a less noticeable impact on

the decrease in total EEX. This trend is directly linked to the uncertainty of the LCOE ranges, which is much higher for renewables. Nevertheless, it may also be interpreted as a reflection of the broader margin for improvement associated with this type of energy source.

Energy source	LCOE*eff [$/kg]	Grid share [%]	Partial EEX [$/kg]
Geothermal	5,08	0,07	0,36
Solar PV	6,93	0,34	2,35
Onshore wind	3,60	0,25	0,89
Hydroelectric	4,15	0,34	1,42
Total			**5,02**

(a) Average scenario - renewables (IT)

Energy source	LCOE*eff [$/kg]	Grid share [%]	Partial EEX [$/kg]
Geothermal	3,00	0,07	0,21
Solar PV	2,90	0,34	0,98
Onshore wind	2,20	0,25	0,55
Hydroelectric	1,50	0,34	0,51
Total			**2,25**

(b) Best-case scenario - renewables (IT)

Figure 3.6: EEX results for a full-renewable Italian grid

Figure 3.6 contains the hypothetical scenario of an electricity grid fully powered by renewable sources. It's a simple projection of the current shares that doesn't involve the actual chance of increasing the electricity production associated with each source. Still, it can be effective to understand how changing the grid composition can impact the EEX (and so the hydrogen price).

Hydropower and solar photovoltaics have the same grid share in table 3.6a; nevertheless, a remarkably higher solar LCOE causes its contribution to the EEX to grow by 40%. Onshore wind also has a relevant impact on the final figure of EEX (18% of the total). The ultimate energy cost is 0,80 $ more expensive than the current grid scenario, highlighting the difficulties still to be faced in adopting a full-renewable grid.

Lastly, table 3.6b highlights the best-case scenario in which the benefits of renewables lead to a significantly lower EEX, close to 2 $/kg. This scenario is 0,50 $ cheaper than the current grid best case, drawing further attention to the benefits of adopting renewables.

A comparison with the average composition of the European electricity grid helps in understanding the sources with the most improvement potential. Figure 3.7 shows the composition of the EU network; it is immediately noticed that the contribution of natural gas is significantly lower (from 50 to 20%) than in the Italian situation, being replaced mainly by solid fossil fuels and nuclear energy. Concerning renewables, the share of wind energy is much higher (from 25% to 46% circa) to the detriment of solar (-10%) and geothermal energy (almost null).

The considerations above bring to an average current scenario (fig. 3.8a) with meaningful differences, in which the highest contribution to the final EEX comes from coal

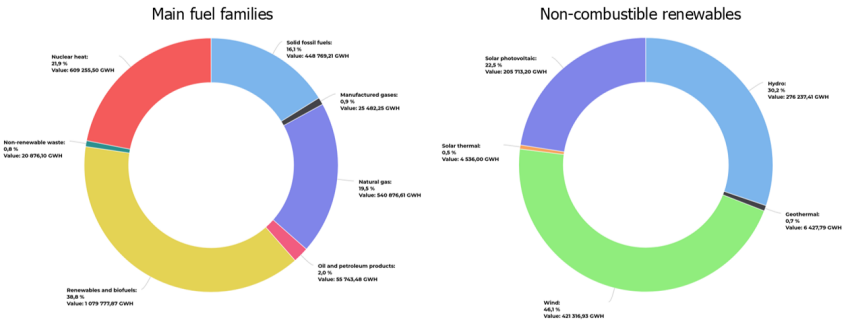

Figure 3.7: Gross electricity production - European Union [21]

Energy source	LCOE*eff [$/kg]	Grid share [%]	Partial EEX [$/kg]
Natural Gas	3,48	0,20	0,71
Coal	4,63	0,18	0,84
Nuclear	3,60	0,22	0,79
Geothermal	5,08	0,00	0,01
Biomass	7,28	0,01	0,06
Solar PV	6,93	0,09	0,62
Onshore wind	3,60	0,18	0,64
Hydroelectric	4,15	0,12	0,49
Total			**4,15**

(a) Average scenario - current grid (EU)

Energy source	LCOE*eff [$/kg]	Grid share [%]	Partial EEX [$/kg]
Natural Gas	2,85	0,20	0,58
Coal	3,75	0,18	0,68
Nuclear	2,10	0,22	0,46
Geothermal	3,00	0,00	0,01
Biomass	2,40	0,01	0,02
Solar PV	2,90	0,09	0,26
Onshore wind	2,20	0,18	0,39
Hydroelectric	1,50	0,12	0,18
Total			**2,58**

(b) Best-case scenario - current grid (EU)

Figure 3.8: EEX results for the current European grid composition

and oil (20% circa). In addition, nuclear and wind energy acquire an increased relevance, covering respectively 18 and 15% of the energy cost. However, the resulting energy cost doesn't change considerably (4,15 $/kg versus 4,20 $/kg of the Italian grid). The best-case scenario (figure 3.8b) displays the increased importance of solid fossil fuels, covering over a quarter of the overall production (26%); moreover, natural gas and coal/oil contribute on aggregate to almost half of the final EEX. The EEX share from nuclear and

wind energy remains almost unvaried (approximately 15%).

The resulting cost of energy is slightly lower compared to the Italian best-case scenario because it benefits from the higher presence in the grid of low-LCOE sources (the median LCOE in the best-case scenario is around 2,59 $/kg), like nuclear energy (from null to 22% with 2,20 $/kg).

Energy source	LCOE*eff [$/kg]	Grid share [%]	Partial EEX [$/kg]
Geothermal	5,08	0,01	0,04
Solar PV	6,93	0,23	1,59
Onshore wind	3,60	0,46	1,66
Hydroelectric	4,15	0,30	1,25
Total			**4,54**

(a) Average scenario - renewables (EU)

Energy source	LCOE*eff [$/kg]	Grid share [%]	Partial EEX [$/kg]
Geothermal	3,00	0,01	0,02
Solar PV	2,90	0,23	0,67
Onshore wind	2,20	0,46	1,01
Hydroelectric	1,50	0,30	0,45
Total			**2,16**

(b) Best-case scenario - renewables (EU)

Figure 3.9: EEX results for a full-renewable European grid

In a hypothetical full-renewable European grid, the scenarios with average and lowest LCOEs have a cheaper energy cost than the equivalent Italian cases. Figure 3.9a displays the costs of a grid with average LCOEs, where the resulting EEX are almost 0,50$/kg lower compared to Italy; the main driver of this reduction is once again wind energy, which has a +20% of grid share than in figure 3.6a and represents 37% of the total EEX. It's also worth noticing how hydroelectric energy becomes the second most relevant source in this scenario, overtaking solar photovoltaics (which is by far the most expensive of the renewables).

The same grid is exhibited in figure 3.9b, considering the lowest LCOE forecasts. The total EEX cost decrease is less relevant, amounting to 0,10 $/kg, with wind energy acquiring an even higher share of the energy cost, reaching 47%. Solar energy covers another 31%, despite being less than a quarter (23%) of the grid composition.

3.2 Cost of investment: CAPEX

The second element to evaluate when calculating the LCOH is the CAPEX, i.e. the initial investment required for hydrogen production. The model adopted in this section is simplified and is only used to give a quantity benchmark. The derived figures help in understanding the different levels of technological maturity between the various types of electrolysers, as well as the impact of economies of scale on the final cost of hydrogen.

Equation 3.10 shows the formula to calculate the CAPEX.

$$\text{CAPEX } [\$/kg] = \frac{\text{Electrolyser Cost } [\$/kW] * \text{Nominal Power } [kW] * \text{CRF}}{\text{Annual Production } [kg]} \tag{3.10}$$

There are four factors to estimate for the calculation. The first two, namely the specific cost and the nominal power of the electrolyser, were found in the literature; the CRF (Capital Recovery Factor) and the annual production, on the other hand, were calculated directly from further data.

The **Specific Electrolyser Cost** is mentioned in the IEA report *The Future of Hydrogen - Seizing today's opportunities* [11]. The cost ranges are broad and reflect the difference in technological maturity between the three types of electrolysers considered in this work:

- *Alkaline* electrolysers are the cheapest (between 500 and 1400 $/kW) due to their greater market penetration and the larger production scale they can achieve.
- The cost of *PEMs* is at least comparable (1100 to 1800 $/kW) with that of alkaline electrolysers, although higher. This is due to the modularity and small size of this type of electrolyser, which makes them very suitable for airport production, but also reduces the benefits of economies of scale.
- In contrast, *SOECs* are the most expensive, as they are not yet commercialised. The minimum cost of a SOEC electrolyser is 2800 $/kW, almost 6 times that of an alkaline one.

As far as the **Nominal Power** is concerned, this was assumed to be 1 MW for all three types of electrolyser. As stated in the report *Green Hydrogen Cost Reduction*, published by IRENA in 2020, the largest electrolysers currently in operation are in the few MW order [28]. The IEA *Hydrogen Production Projects interactive map* [29] provides similar data, where most of the projects currently operational have a production capacity under 5 MW [30]. Although some projects with tenths of MW of power are in advanced development (like the *FH2R* project in Fukushima, with a 10 MW production unit [31]), they represent cutting-edge production scenarios inconsistent with airport systems, where space limitations have high relevance. Thus, the choice of 1 MW of nominal power reflects what is realistically feasible in the short term in an airport scenario. The IRENA publication proves this figure to be the first power goal to achieve with the newly produced electrolysers to take advantage of the economies of scale benefits. This cost reduction would mainly come from the cheaper balance of plant components.

The report also demonstrated that the stacks' dimensions are close to their maximum, so an increase in size doesn't yield a more significant economy of scale. However, a module composed of many stacks can achieve the same result, reducing the balance of plant contribution to the final CAPEX. As shown in figure 3.10 (where the blue and orange lines represent PEM and Alkaline electrolysers, respectively), the investment cost decreases considerably when the nominal power is close to 100 MW.

The third parameter is the **Capital Recovery Factor**, which accounts for the lifespan of the electrolyser stack and the discount rate previously defined. The calculation of

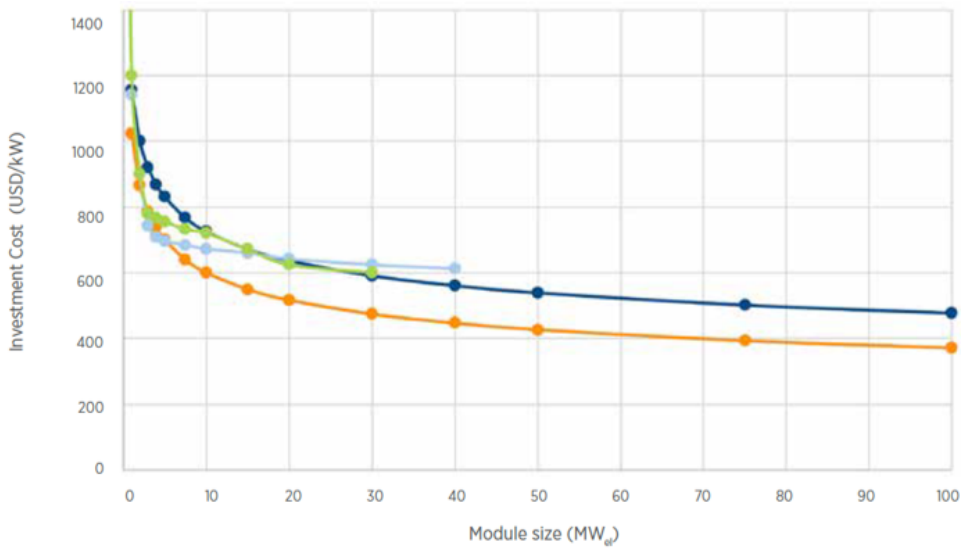

Figure 3.10: Electrolyser investment cost as a function of module size [28]

the CRF resorts to the equation 3.11 [32], where a discount rate of 8% was adopted in conformity to literature [33] [34].

$$\text{CRF} = \frac{\text{discount rate} * (1 + \text{discount rate})^{\text{lifespan}}}{(1 + \text{discount rate})^{\text{lifespan}} - 1} \tag{3.11}$$

Finally, the **Annual Production** for every kind of electrolyser was esteemed, using the equation 3.12.

$$\text{Annual production } [kg/\text{year}] = \frac{\text{Nominal power } [kW] * \text{Capacity Factor } [h/\text{year}]}{\text{Production efficiency } [kWh/kg]} \tag{3.12}$$

The Capacity Factor expresses the percentage of yearly hours during which the electrolyser could be operational. As stated by Machado et al. (2024), PEM electrolysers have the most dynamic technology; therefore, they have a higher Capacity Factor due to shorter switch-on times and response to load changes [10].
Above, the esteem of Production Efficiency was at around 50 kWh/kg (equation 3.7). In contrast, a more precise figure from the literature is adopted here to calculate the annual hydrogen production to distinguish between the various electrolyser types. The remarkable potential of SOECs dictates this choice since their efficiency is 42 kWh/kg circa. The data for the other two electrolyser types is just over 50 kWh/kg, with PEMs being the least efficient.

Table 3.1 displays the results obtained from the calculations previously described. The first calculation step concerns the CRF, which is significantly lower for alkaline electrolysers due to their durability. SOECs have a very high CRF since their stack lifespan is only 4 years. Conversely, SOECs have the best result in the annual production evaluation

	Alkaline		**PEM**		**SOEC**		**Source**
Specific electrolyser cost [$/kW]	500-1400		1100-1800		2800-5600		IEA [11]
Discount rate [%]	8		8		8		
Nominal Power [MW]	1		1		1		
Lifespan [years]	10		7		4		Iyer [32]
Capacity Factor [%]	90		97		90		
Capital Recovery Factor	0,149		0,192		0,302		Eq. 3.11
Operating hours [h/year]	7884		8497		7884		Iyer [32]
Efficiency [kWh/kg]	52		56		42		Iyer [32]
Annual production [kg/year]	151.615		151.736		187.714		Eq. 3.12
scenario	*best*	*mean*	*best*	*mean*	*best*	*mean*	
CAPEX [$/kg]	0,491	0,934	1,392	1,836	4,504	6,755	Eq. 3.10

Table 3.1: CAPEX evaluation for the three type of electrolyser

due to their high production efficiency. On the other hand, the outputs of alkaline and PEM electrolysers are quite comparable, demonstrating the relative balance between the pros and cons of each variety. While the former are slightly more efficient, the higher operating hours of the latter even out the final figure.
The last line of the table shows the results obtained for CAPEX. There are two columns for every result, the first calculated using the lowest figure of specific electrolyser cost and the other one with the mean value of the cost range. **Alkaline** electrolysers have quite low outcomes (even the mean scenario results below 1 $/kg), reflecting the remarkable maturity of this technology and its advanced degree of commercialisation. **PEM** electrolysers are almost 1 $/kg more expensive than the alkalines in both scenarios, presenting room for improvement before reaching an attractive LCOH for the energy market. Lastly, **SOECs'** results are far more expensive, consistent with the recent appearance of the technology. The elevated specific electrolyser cost and the short lifetime of the stack strongly penalise the resulting CAPEX.

3.2.1 Cost of operations: OPEX

The last contribution to LCOH comes from operational expenditures (OPEX). Expressing them as a percentage of CAPEX can simplify their computation, which otherwise could be quite demanding. It is set here at 3% of the total CAPEX to avoid an over-optimistic LCOH forecast. A higher percentage would account for the replacement cost of the stacks, but this has not been considered so far (the electrolysers' lifespan excluded the replacements). The third line of table 3.2 contains the results for the OPEX estimation.

		Alkaline		**PEM**		**SOEC**	
scenario		*best*	*mean*	*best*	*mean*	*best*	*mean*
EEX	*IT*	2,75	4,20	2,75	4,20	2,75	4,20
	EU	2,58	4,15	2,58	4,15	2,58	4,15
CAPEX		0,49	0,93	1,39	1,84	4,50	6,76
OPEX		0,02	0,03	0,04	0,05	0,14	0,20
LCOH	*IT*	**3,26**	**5,16**	**4,18**	**6,09**	**7,39**	**11,16**
	EU	**3,09**	**5,11**	**4,01**	**6,04**	**7,22**	**11,11**

Table 3.2: LCOH results for the current Italian and European grid

3.3 Levelized Cost Of Hydrogen: LCOH

Combining the results obtained so far gives a rough estimate of the LCOH. As previously shown in equation 2.1, it is sufficient to sum the values obtained so far of EEX, CAPEX and OPEX to obtain the levelized cost of hydrogen. Table 3.2 contains the EEX results divided into Italian and European grids; the figures selected are only those referred to the current grids because they're more realistic than the full-renewable scenario results.

Assuming a figure of around 4 $/kg as the target cost of hydrogen in the short term for it to be suitable for the energy market, we see how only **Alkaline** electrolysers can achieve an LCOH below this mark. Their intermediate scenario stands at around 5 $/kg, an acceptable price considering the margins for technological improvement on both the electrolyser and the electricity grid (and thus on the energy cost).
PEM electrolysers have a higher LCOH, but the result is still close enough to the price target in the best scenario; in the average one instead, the LCOH is almost 2 $/kg over the goal, mostly because of their elevated CAPEX.
Lastly, **SOECs** have completely out-of-scale outcomes since their CAPEX exceeds 4 $/kg. The intermediate scenario also surpasses 10 $/kg but is still acceptable when considering the commercialisation yet to take place for this electrolyser technology.

Chapter 4

Technological maturity

Another way to compare the production routes, besides emissions and costs, is their degree of technological maturity. The chart in Figure 4.1 shows the stage of maturity of some of the most popular hydrogen production pathways [1] [14].

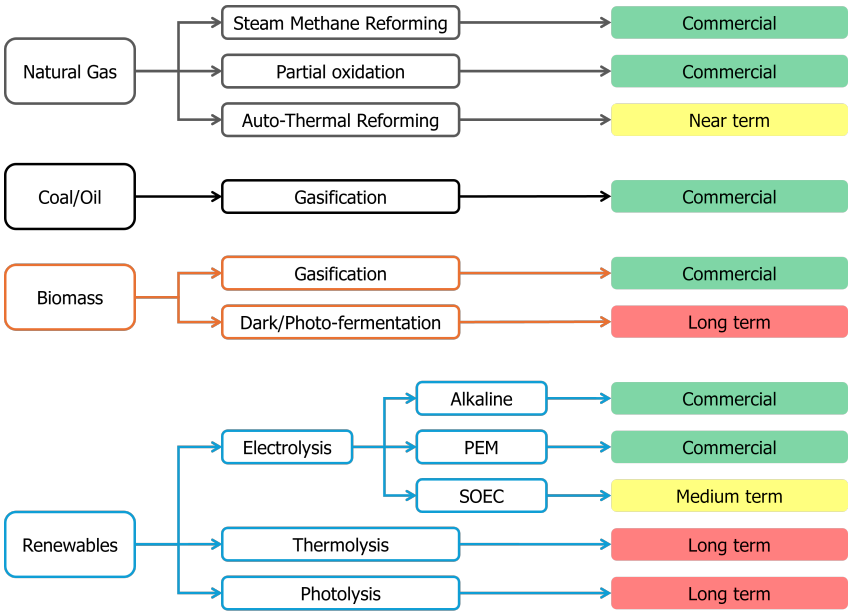

Figure 4.1: Technological maturity overview

Many of the technologies described in the previous chapters are labelled as *commercial*, as they are the only ones whose costs and emissions can be quantitatively analysed. The already mentioned technologies for natural gas (SMR and POx), the gasification of carbon fossil sources (coal and oil), and alkaline and PEM electrolysis belong to this category. On the other hand, the Autothermal Reforming of natural gas, which, as previously mentioned, lies halfway between the benefits of Steam Methane Reforming and those of Partial Oxidation, is indicated as *near term* (i.e. available in less than 5 years).

By *medium term*, referred to SOECs in the chart, is meant instead a technology commercially available within 10 years. Finally, *long term* applies to production methods with a time-to-market of more than 10 years, which cannot therefore be relied upon for the early stages of the transition to green hydrogen.

It is relevant to notice that the only route involving renewable sources with commercial maturity is electrolysis; none of the others could be available before ten years. This is the reason why the focus on electrolysis' cost reduction is fundamental to achieving a significant green hydrogen market before 2035.

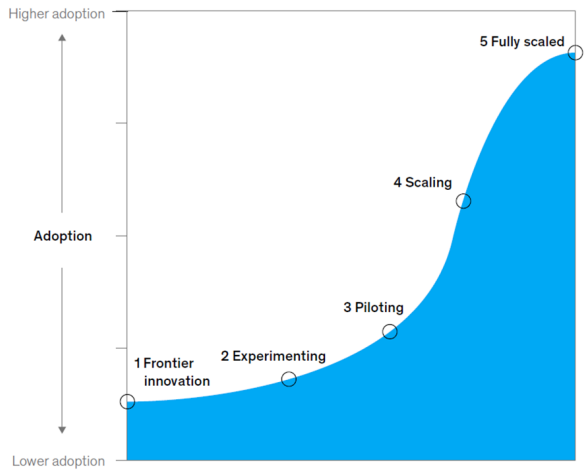

Figure 4.2: Technologies progress through different stages [38]

The availability in the literature of predefined assessment scales allows the comparison of different degrees of technological maturity. Figure 4.2 shows a qualitative example of the functioning of these scales, as defined by McKinsley & Company (2024) [38]. In this grading system, the lower evaluation level is assigned to technologies with a low to null adoption level, often representing a breakthrough discovery in their field. It is, for instance, the case of thermolysis, where economic and technological constraints (high capital costs, hazardous materials, corrosion issues) considerably delay the commercialisation of the technology [39].
Levels 2 and 3 of the scale represent the emerging technologies undergoing experimentation or trial, respectively. At these stages are found technologies like Auto-Thermal Reforming and Solid-Oxide Electrolysis. Level 4 presents a significant increase in the degree of adoption, where the benefits of economies of scale begin to reveal; the already commercialised electrolysers (Alkalines and PEMs) are approximately in this phase. The last step of the system involves the full commercialisation and scaling of the technology. The worldwide adopted production routes, like Steam Methane Reforming and Gasification, can be considered at this stage because of their competitive hydrogen price and capability to meet the global H_2 demand.

TRL	Description
1	basic principles observed
2	technology concept formulated
3	experimental proof of concept
4	technology validated in lab
5	technology validated in relevant environment
6	technology demonstrated in relevant environment
7	system prototype demonstration in operational environment
8	system complete and qualified
9	actual system proven in operational environment

Table 4.1: Technology Readiness Level scale [40]

4.1 Technology Readiness Level (TRL)

Based on this qualitative scale, it is possible to define some quantitative models used in academic research. The most widely adopted system in this respect is the Technology Readiness Level, proposed by NASA in 1974 and developed into its current form in the 1990s [41]. Table 4.1 shows the TRL defined by the European Commission [40]. This scale consists of 9 rating levels, each associated with a brief description of the degree of technological maturity it represents. In the application of this scale to a H_2 production technology, the aspects to consider are divided into two categories [43]:

- Quantitative: cost of production, storage and transportation
- Qualitative: technological progress, automated production and market penetration

In the study conducted by Abdelsalam et al. (2024), the TRL was used to rank the three types of water electrolysers [44], with Alkaline and PEM electrolysers rated at 9, while SOECs are considered in the demonstration stage, ranking between 6 and 7 on the scale. The Alkaline technology is more mature and suitable for large-scale operations than PEM, while the latter is more adequate for renewable sources due to faster response times with intermittent power supplies. Concerns about the economy of scale lead to higher costs and lower applicability of electrolysis if compared to other fossil-based production techniques (similarly having a TRL of 9 but larger production scales) [43]. TRL can't point out these differences because it limits the analysis to the research and development process, leaving out the advancements that follow the commercialisation.

Lepage et al. (2021) draw attention to the same matter (see table 4.2), comparing TRL and production scale of the most common production routes. There's no distinction between different technologies when mentioning water electrolysis in the table, and its TRL rank is again 9, levelling off with SMR and gasification results. Nevertheless, in the third column, it is emphasised that the production scale of electrolysis plants is small, in contrast to the large scale achieved by fossil fuel technologies. By production scale, electrolysis is also inferior to two methods involving biomass, like gasification and pyrolysis, although both have a TRL of 7.

Resource	Process	TRL	Production scale
Fossil	SMR	9	Large/Available
	Coal gasification	9	Large/Available
Water	Water electrolysis	9	Small/Available
Vegetal/algal biomass	Gasification	7	Mid-size/Available
	Steam reforming	8	Small/Available
	Pyrolysis	7	Mid-size/Available
	ScWG	4	Pilot plant
Other	APR	4–5	Pilot plant
	Dark fermentation	5	Pilot plant
	Photo-fermentation	4	Under research
	MEC	2–4	Under research

Table 4.2: Comparison of TRL and production scale of different processes [45]

A further weakness of the scale was pointed out by Malone (2020), stating that «it was demonstrated that a Technology Readiness Assessment (TRA) applied to a large complex system provides optimistic results with the actual Technology Readiness Level (TRL) being much lower when including system integrations». The issue of integration between subsystems is indeed a priority to establish the maturity level of a complex and innovative technology. For this reason, other scales have been developed that complement the TRL; among these is the System Readiness Level.

4.2 System Readiness Level (SRL)

IRL	Description
0	No integration
1	High-level concept for integration
2	Some level of specificity of requirements for components' interaction
3	Detailed integration design (including interface details)
4	Validation of components' integration in a laboratory environment
5	Validation of components' integration in a relevant environment
6	Validation of components' integration in a relevant end-to-end env.
7	Prototype integration demonstrated in an operational high-fidelity env.
8	System integration and mission readiness confirmed in operational env.
9	System integration validated through proven operational capabilities

Table 4.3: Integration Readiness Levels' description [47]

The SRL scale relies on the TRL values associated with each component of a system and on an auxiliary scale called Integration Readiness Level (IRL). The latter represents

a systematic assessment of the interrelation between different components, providing also a consistent comparison of maturity between interfaces. Ultimately, the IRL serves as a means of risk reduction when integrating new elements into a system [47]. While the levels of Technology Readiness extend from 1 to 9, Integration Readiness also presents a level of 0, representing the complete absence of integration between subsystems.

IRL	Definition by Gove (2007)	Definition by Long (2011)
0	No integration at all	Supplier has access to the necessary technology, but no experience
1	Selection of a medium for integration	Supplier has some experience with the technology for different applications
2	Medium has been defined, but there's no interaction over it yet	Supplier has developed similar items for different applications
3	Initial integration successfully achieved, with basic interaction and influence	Supplier has developed a similar item for a related application, but major changes are needed
4	Data exchange improved with checks on quality and assurance of the integration	Supplier has developed a very similar item for a closely related application, only moderate changes are needed
5	Sufficient control between technologies to establish, manage, and terminate the integration	Supplier has developed a very similar item for a very similar application, and only minor changes are needed
6	The technologies can process, translate and structure information for their application (highest technical level)	Supplier has developed a representative prototype, but it hasn't undergone environmental testing
7	Performance and reliability requirements satisfied	Supplier has developed a representative prototype with some testing
8	Actual integration completed and validated in the system environment	Supplier has already integrated the item into another system with similar requirements, with some positive results
9	Successful use of the technologies in the final operation environment (requires TRL 9)	Supplier has integrated the item into a mature system with similar requirements

Table 4.4: Alternative definitions for the IRLs [48] [49]

Table 4.3 shows the definition of every Integration Readiness Level. Tiers range from no integration at all between components to demonstrated integration through proven and successful operational capabilities. The intermediate levels are characterised initially by the design of interfaces and then by progressive experimentation in environments increasingly conforming to the operational.

However, the definition of these levels is not unique, but can vary according to necessity. Two kind of definitions that differ from Austin's are shown in Table 4.4: in the first one, provided by Gove et al. (2007), there is a more detailed description of the integration modalities, with the first six levels focusing on technical aspects and the following ones introducing the performance requirements point of view [48]. In the right-hand column, instead, is the definition by Long (2011), which is devoted to hardware components (where CI stands for *Configuration Item*) and refers to the technical expertise of the suppliers [49].

The complete definition of IRL involves the construction of a square matrix with $m\,x\,m$ dimensions, where m represents the number of components in the system. The matrix is shown in the centre of table 4.5. It is important to note that the main diagonal shows the integration of each component with itself, which is equal to the maximum value of the scale by convention.

Once the IRL matrix is obtained, it is possible to proceed to the calculation of the SRL of the overall system. There are three types of SRL, which must be calculated in sequence to obtain a definitive value.

- The first step is the **component SRL**, which is associated with each element according to its TRL and the IRLs that connect it to other parts. The table 4.5 shows the matrix formula by which this value is calculated as a vector of m elements, as many as the components in the system. An essential final step is the normalisation of the Component SRL by the number of integrations it has within the system (i.e. by its number of non-zero IRLs). In this way, the user obtains a decimal value that allows the comparison of components with different interfaces' amounts within the same system.

$$\begin{vmatrix} SRL_1 \\ SRL_2 \\ SRL_3 \\ \dots \\ SRL_m \end{vmatrix} / m_i \quad = \quad \begin{vmatrix} IRL_{1,1} & IRL_{1,2} & IRL_{1,3} & \dots & IRL_{1,m} \\ IRL_{2,1} & IRL_{2,2} & \dots & \dots & IRL_{2,m} \\ IRL_{3,1} & \dots & IRL_{3,3} & \dots & \dots \\ \dots & \dots & \dots & \dots & \dots \\ IRL_{m,1} & IRL_{m,2} & \dots & \dots & IRL_{m,m} \end{vmatrix} \; x \; \begin{vmatrix} TRL_1 \\ TRL_2 \\ TRL_3 \\ \dots \\ TRL_m \end{vmatrix}$$

Table 4.5: Component SRL calculation

  Component SRL is used to identify which system components are lagging or may be too far ahead in terms of readiness and, therefore, require attention, as they pose a risk to uniform system development.

- The second type is the **Composite SRL**, which measures the system readiness by considering how well the individual components fit together and how effectively they work as a whole. The SRA method calculates this value by averaging the Component SRLs and presenting the result as a decimal. However, being an average value, it may mask substantial differences between components, as in the case where one element is significantly further behind or ahead in development than the others.

- Lastly, the ultimate **System Readiness Level** can be determined by converting

the Composite SRL into a 1-9 integer scale, with nine representing maximum readiness. The transition to this kind of scale is facilitative to the adequate presentation and evaluation of results.

This definition of SRL refers to a significant distinction from TRL. While TRL is, in fact, a key element in the development of SRL, the two indicators serve different purposes. As previously discussed, the TRL scale enables the comparison of disparate technologies' maturity states through the measurement of their levels of testing and development (beyond the limitations expressed).
Conversely, the SRL scale tracks the progress of one system over time; it cannot give a helpful comparison between several systems because the specific architecture of each system determines its translation model. Lastly, the number of parts considered has a notable impact on the reliability of the SRL measurement: this number cannot be too small (fewer than five) or excessive (higher than fifteen), as either extreme may significantly distort the resulting average.

4.3 A case study: Rotterdam The Hague Airport

To illustrate the application of technology readiness levels to hydrogen production and employment, Rotterdam The Hague Airport (RTHA) will be used as a model below. There, projects aimed at introducing hydrogen technologies into the airport environment have been underway for several years. These programmes are led by the *Rotterdam The Hague Innovation Airport Foundation* (RHIA), established in 2019 from an agreement between the airport and the city of Rotterdam with the aim of "tackling the economic, social and sectoral challenges of aviation through a holistic approach" [50].

Project	**Description**	**TRL**	**Date**
TULIPS	LH_2 refuelling and turnaround on a drone	6	2024
	Small-scale storage tank to dispense LH_2 at the airport	7	2024
GH_2 leakage detection	Gas leakage sensors at the LH_2 storage facility	7	2025
Hydrogen Refuelling Station	HRS for heavy-duty vehicles and aircraft	9	2026
HAPPS	Hydrogen Aircraft Powertrain and Storage System via fuel cells	3	2029
AeroDelft	GH2 & LH_2 refuelling and ground tests on a Sling 4 aircraft	6	2026
ZeroAvia	GH_2 refuelling and flight demonstration on a Cessna	7	2026

Table 4.6: Ongoing hydrogen programmes at RHIA [64]

Table 4.6 lists some of the projects currently underway at Rotterdam Airport involving hydrogen technologies, as presented by Van Dijk et al. (2024) [64]. Many of

the technologies listed in the table are classified at a TRL between 6 and 7, as they have been demonstrated in relevant or operational environments (often the airport itself). This further emphasises how hydrogen technologies are currently close to the certification and commercialisation phase, making it essential to prepare the ground for an increase in their economy of scale.

TULIPS

TULIPS is a consortium of various European airport authorities, led by the Dutch *Royal Schiphol Group*, which manages the airports of Amsterdam Schiphol (AMS) and Rotterdam The Hague (RTM). The consortium also includes the Norwegian group *Avinor*, the Cypriot group *Hermes*, and the Italian group *Sagat*, which manages the Turin Caselle Airport (TRN) [51]. This cooperative seeks to lead the shift towards low-carbon air transport.

The TULIPS project aims to demonstrate the operability of a hydrogen-powered *HYDRA-II* drone, developed by the Netherlands Aerospace Centre (NLR). This test flight could facilitate the analysis of operational aspects related to LH_2 refuelling and turnaround operations. To assist this demonstration, RTHA is simultaneously developing a storage facility for liquid hydrogen. The infrastructure helps the understanding of safety and regulatory aspects of LH_2 storage and dispensation [52].

The demonstration flight of the *HYDRA-II* drone is classified under level 6 of the TRL scale: "technology demonstrated in a relevant environment". So far, this aircraft has only flown at the NLR site in Marknesse (Netherlands), inaugurating its outdoor flight [53]. The flight at Rotterdam Airport will bring this technology up to TRL 7, as the airport is a full-scale operational environment.

One step higher on the TRL scale is small-scale hydrogen tank storage, as it has already been demonstrated at Rotterdam Airport [64].

Hydrogen Refuelling Station (HRS)

The only programme classified at the highest TRL level among those listed in Table 4.6 is the hydrogen refuelling station for heavy-duty vehicles at RTHA. The HRS is currently under construction, but is expected to be operational by the end of 2025. The existence of identical stations already in operation means that the actual system can be considered as already tested in operational environments. This type of station allows both the recharge of electric vehicles and the refuelling of hydrogen ones. Furthermore, the presence of a supply line directed towards the airside offers the possibility of refuelling hydrogen aircraft as well [54]. Section 5.1.5 will further discuss the operation of this type of station.

Hydrogen powertrain

The programme with the lowest TRL classification is HAPPS (Hydrogen Aircraft Powertrain and Storage System), with a rating of 3: "experimental proof of concept". The project by *Concept Aerospace* involves the development of an electric powertrain powered by hydrogen fuel-cells and designed for regional aircraft. RTHA will host the preliminary

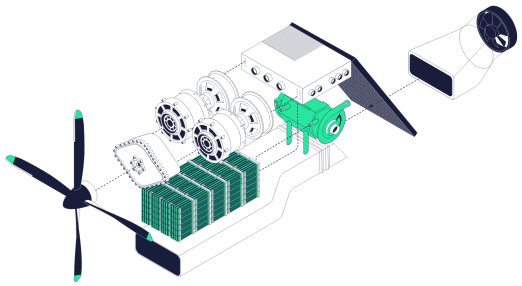

Figure 4.3: Fuel Cell System (highlighted) of the CA2000 powertrain [55]

engine development operations, which will last until 2029 (the year of expected certification). The successful outcome of the programme should lead to the retrofitting to electric propulsion of the DHC Dash 8-300 fleet of Air New Zealand. Inside the engine are PEM fuel cells that produce electricity from the reaction between hydrogen and oxygen. Cryogenic tanks will be located at the rear of the aircraft to supply hydrogen to these cells. As stated on the manufacturer's website, the goal for 2025 is «confirming that our designs are on track to operate safely and effectively», indicating that the project is still in its preliminary stages and therefore justifying the attribution of a low TRL [55].

Chapter 5

Hydrogen production for airport use

5.1 Production scenarios

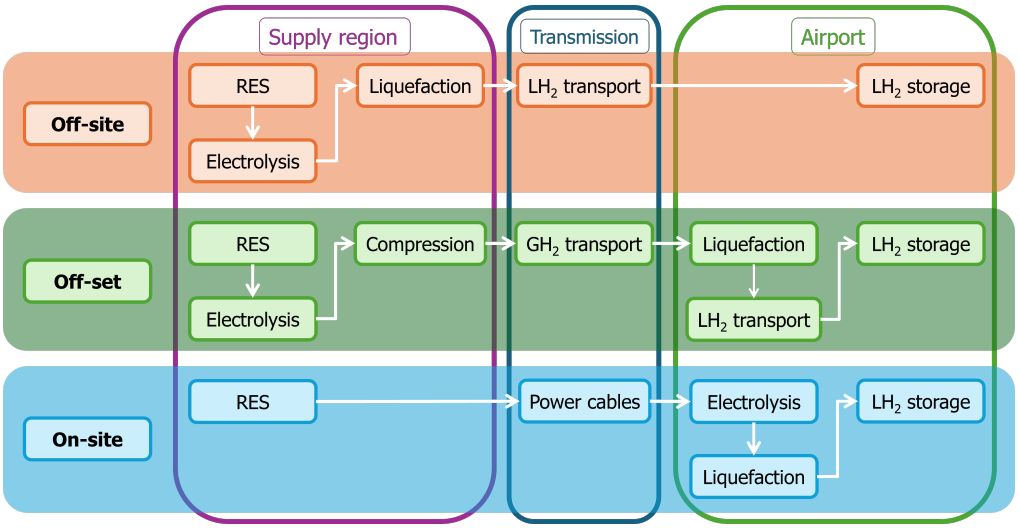

Figure 5.1: Scenarios outline [64]

The three scenarios analysed in this chapter are:

- **On-site**: H_2 production and liquefaction inside or next to the airport
- **Off-set**: H_2 production off-site, then transported as a gas and compressed/liquefied on-site
- **Off-site**: H_2 production and compression/liquefaction off-site, with subsequent transport and storage in the airport

What emerges from the papers taken into considerations considered is the greater feasibility of on-site production in small airports. That production would have to make

use of renewable sources, which highly influence the competitiveness of the proposed solution. Renewable sources are also subject to a certain seasonality, making some case-by-case estimates necessary to determine the feasibility of the selected scenario.

Talking about large airports, the solution is hardly feasible, as their electricity and hydrogen demand is too high to be entirely met by on-site production. Space constraints are one of the worst issues, especially in the case of airports located near urban centres (see section 5.1.2).

The following sections will show some case studies concerning the three scenarios.

5.1.1 On-site scenario

The production of hydrogen on site can be described according to the logic flow in the last line of figure 5.1. The first requirement is **electricity**, which can be supplied from the national grid or generated in the airport surroundings. Under the assumption that green hydrogen is to be produced, only the second alternative is taken into account since no national grid is currently composed of renewable sources alone. The most widespread solutions are wind and photovoltaic solar energy, often used in conjunction to absorb the seasonality of both. Among the currently viable alternatives, it is worth mentioning geothermal and biomass energy. Some examples of the use of these sources are provided in the following paragraphs.

Once the electricity is transported and stored within the airport, it is used for the **electrolysis** process. The characteristics of the various types of electrolyser available have already been discussed in detail above; however, the size of the plant to be used overlaps almost entirely with land availability issues [65]. With regard to the percentage of the total amount electricity used for hydrogen production, it is reasonable to argue that hydrogen is produced using only the surplus electricity left after meeting the demand from all other airport users [58].

The hydrogen produced through electrolysis must then be liquefied, increasing the gravimetric energy density to levels that make it competitive with other fuels used in aviation. **Liquefaction** requires considerable amounts of energy, having an efficiency close to 12 kWh/kg [60]. The capital cost of the plant is also a relevant factor in the sizing of the airport hydrogen production facility. Liquid hydrogen requires very low storage temperatures (around $-253\,^{\circ}\mathrm{C}$ or 21 K, achieving a volumetric density of up to $70.8\,\mathrm{kg/m^3}$), achieved by insulated cryogenic tanks [57]. The volume density of LH_2 is more than four times lower than that of jet fuel, which implies the need for much larger storage tanks [64]. Hydrogen **storage** is essential to balance hourly fuel demand with fluctuating production and to take advantage of periods of lower electricity prices. For this reason, the tanks should be sized to meet the airport needs for at least two to three operating days [60].

The **distribution** of liquid hydrogen from the storage tanks to the aircraft gates can take place via a pipeline system within the airport. Refuelling takes place by pumping hydrogen from the pipeline system directly into the aircraft tanks. Hydrogen losses along the entire supply chain (storage, distribution, refuelling) are estimated to be very low [60].

5.1.2 Issues concerning the airport size

To demonstrate the unsolvable problems that, as things stand, make on-site production in large airports unfeasible, here there are some case studies dealing with this issue.

The first one is the report "Estimating the energy demand of a Hydrogen-based long-haul air transportation network" by Gaubatz et al. (2023). The paper asserts that the transition of air transport to hydrogen should start with long-haul flights and focus on a small network of airports. It proves how the creation of a hydrogen network involving top 100 airports in the world (by passenger traffic) would be sufficient to make 83.3% of long-haul flights hydrogen-powered. This solution has the advantage of limiting the necessary structural changes to this small network without impacting the rest of the world airports. The effectiveness of the proposed solution increases if the transition to electric for short-haul flights takes place at the same time [60].

To explain this theory, the paper analyses the energy requirements of Chicago O'Hare Airport (IATA code: ORD), the 20th largest airport by daily long-haul departing pax-km[1] volume in 2019. The results of this case study, shown in Table 5.1, are a numerical example of the problems (in terms of space and energy requirements) mentioned above for on-site hydrogen production at large airports.

	Required daily capacity	**Space/Volume requirements**	**Additional notes**
Electricity	44.5 GWh	105 km^2 (SPV)	The space required is 3.5 times the current airport area (31 km^2)
Electrolysis	1.5 GW	0.075 km^2	15 electrolysers required (each one supplying 100 MW)
Liquefaction	719 tonnes	*not provided*	26.5 times the capacity of the largest existing facility
Storage	1500 tonnes	22 000 m^3	5 times the volume of the largest existing LH_2 tank (NASA)

Table 5.1: Energy demand of Chicago airport for a H_2-based air transportation [60]

The first line of the table shows the electricity demand, amounting to 44.5 GWh/day. The authors calculated that supplying this energy during December (the month with the lowest solar irradiance in terms of kWh/m^2/day) would require about 105 km^2 of solar cells. This area almost equals 3.5 times the current airport area; adding up the size of the current airport and that planned for the photovoltaic panels gives a total area of 136 km^2, equal to that of Denver International Airport (DEN), the second largest airport in

[1]The unit of measurement pax-km (passenger-kilometre) is used in the aviation sector to quantify transport demand in joint terms of people and distance. 1 pax-km means one passenger transported over 1 kilometre of distance; in the example of 200 passengers transported over 500 kilometres, this would result in 200 pax × 500 km = 100 000 pax-km.

the world[2].

Moving to the second line, the necessary installed electrolysis capacity is estimated at 1.5 GW, corresponding to the installation of 15 electrolysers of 100 MW each. The global water electrolysis installed capacity is about 1.4 GW currently, according to the International Energy Agency [5].

Liquefaction and Storage requirements raise further questions about the technological maturity of the infrastructure involved. The amount of LH_2 required to propel long-haul aircraft is equivalent to 720 tonnes per day; the maximum capacity currently achieved is just under 30 tonnes/day at the SK E&S Co. facilities in Incheon, South Korea [62]. Chicago airport would need a plant more than 25 times larger. The storage capacity would have to be at least double the daily demand for LH_2, thus amounting to 1500 tonnes per day (or 22 000 m^3). The world's largest tank for LH_2 storage has a capacity of less than 5000 m^3 [3], so Chicago airport would need at least five equivalent tanks to store its long-haul demand.
These and other considerations are of fundamental importance in understanding the low feasibility of on-site hydrogen production for large airports at this stage.

Concerning the production in small hubs, Taha et al. (2024) conducted a comparative analysis between two Stockholm airports, Skavsta (NYO, 365 000 passengers in 2024 [63]) and Arlanda (ARN, 22 million passengers [63]). In the case of Skavsta Airport, the study examines the production of hydrogen using electricity generated from on-site renewable sources. What emerges is the insufficiency of currently available resources (mainly solar and wind) and the need for further technological advancement for them to become so; despite this, the study considers the solution viable in the years to come. In contrast, the proposed solution for Arlanda Airport involves offshore hydrogen production and subsequent transport to the airport facility.
Nevertheless, the Swedish energy market, where the national electricity grid is one of the least emissive in the world (10 g_{CO_2e}/kWh [14]), has a non-negligible influence on the results of this report.

To demonstrate this, Cybulsky et al. (2024) conducted a study to make some predictions about the Western European energy infrastructure in the coming decades, using the open-source energy system optimisation model DOLPHYN (Decision Optimisation of Low-carbon Power and Hydrogen Networks). This study shows that on-site production is a viable solution only in areas where renewable resources are abundant (such as in Italy, coastal Spain and the UK). On the other hand, the paper shows that in many northern European regions (above all, France and Germany), hydrogen production from fossil sources with the implementation of CCUS is more cost-effective.

Khalil and Dincer (2024) proposed a holistic system to develop a self-sufficient airport with on-site production of green fuels [56]. This study is based on data from the Vancouver Airport (YVR) in British Columbia (Canada), where an innovative geothermal system

[2]The first is King Fahd International Airport (DMM) in Dammam, Saudi Arabia, which is located in a completely desert region and has an area of 776 km^2.

[3]located at NASA Kennedy Space Center, Florida.

is already in function. The three energy sources are geothermal, solar PV and biomass, with five outputs: electricity, heat, hot water, hydrogen and kerosene. Differentiating the sources is helpful to face their seasonality, with solar PV being dominant during summer and biomass meeting most of the demand in winter.

5.1.3 Off-set scenario

The off-set scenario envisages the off-site production of H_2, with transport in a gaseous state (as GH_2) and subsequent on-site liquefaction to LH_2. The main difference between this scenario and the previous one is the longer residence time of hydrogen in gaseous form. This phase requires the use of technologies that provide proper storage and transport of GH_2 before its liquefaction.

There are two main **storage** techniques for gaseous hydrogen [57]:

- Compressed hydrogen (CH_2), so a high-pressure gas stored in cylindrical tanks at pressures of up to 80 MPa (reaching a volumetric density of 36 kg/m^3). The process has an energy efficiency of 2.85 kWh/kg_{H_2}.
- Cryo-compression (CcH_2), a form between CH_2 and LH_2: it is stored in cryogenic tanks that require auxiliary equipment to maintain around 35 MPa of pressure and a temperature of 70 K. The energy efficiency of CcH_2 production is 3.47 kWh/kg_{H_2}.

Both technologies have far better energy efficiency than the liquefaction process, which is about 12 kWh/kg_{H_2}. Despite this, the higher fuel tank gravimetric efficiency[4] of LH_2 makes it a more suitable choice [60]. It is also worth mentioning that CcH_2 has a higher LCOH than the other two forms of storage, a factor that makes it a poorly considered alternative nowadays [57].

Concerning GH2 **transport**, among the various alternatives, currently it makes sense to take pipelines and truck transport into consideration. As stated by Cybulsky et al. (2024), pipelines have «practically non-existent operating and maintenance costs»; moreover, they have the advantage that the pipeline itself can serve as a storage medium [58]. For larger airports and higher demand, pipeline transport is considered the only viable option because its cost decreases rapidly with growing demand [66].

As far as the supply network is concerned, there are three viable options in Europe: retrofitting pre-existing pipelines (currently dedicated to natural gas transport), construction of new pipelines, or the *European Hydrogen Backbone* (EHB, shown in figure 5.2) [65]. The latter is a strategic pipeline hydrogen transport network planned across European countries, designed to connect hydrogen production sites (including import hubs) with demand centres across Europe. A similar project is crucial for the transition to a hydrogen-based economy and achieving net-zero emissions targets, reducing dependence on expensive and inefficient long-distance hydrogen transport. The EHB will integrate with national pipeline networks and serve as a primary source for last-mile distribution pipelines to end users, such as airports [65] [64].

[4] ratio of the mass of stored fuel to the total mass of the full tank (mass of fuel and mass of empty tank)

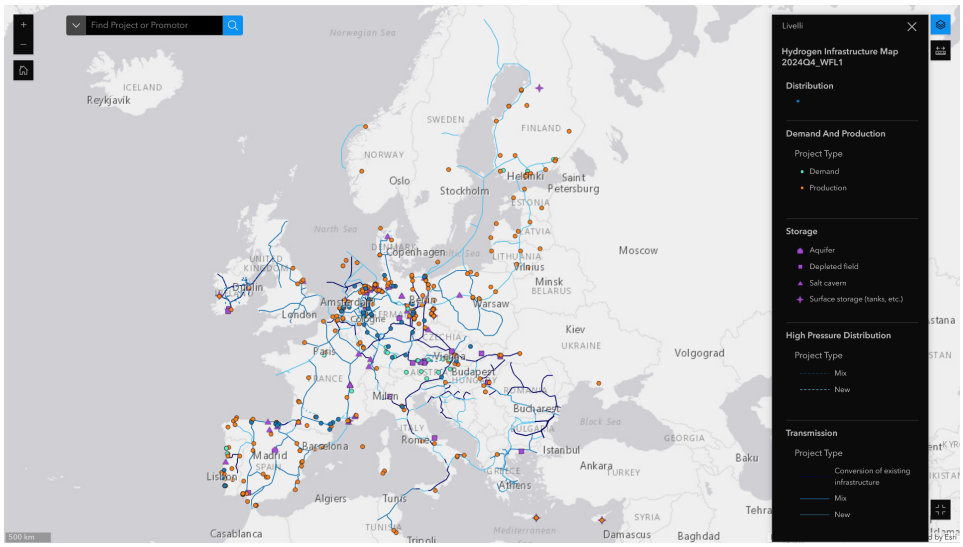

Figure 5.2: European Hydrogen Backbone [67]

5.1.4 Off-site scenario

The off-site scenario involves the production and liquefaction of hydrogen away from the airport, where it is then transported in a liquid state. Off-site production is vital in large airports, considering the points made in section 5.1.2, where land availability around the airport and proximity to urban areas emerged as considerable obstacles to on-site production.

The **regional hub** concept is vital for the development of a large-scale hydrogen economy. In order to maximize the use of electrolysers and liquefiers it is necessary to concentrate the production in large clusters; if located in the airport, they would be switched on/off according to the demand fluctuations [58] [64].

Pipelines are not suitable to transport liquid hydrogen because of the very low temperatures at which it must be maintained. Therefore, the solution is truck transport, which may feature cryogenic trailers or conventional trucks which transport LH2 capsules (a commercially deployed sample[5] is shown in figure 5.3). For low hydrogen demands (<150 tonnes per day), **cryogenic trailers** are more cost-effective than pipelines, as they also have the advantage of being used as mobile storage tanks [66].

LH2 capsules are a competitive solution when demand is low, but they can only operate with aircraft that use them to replace conventional tanks. This solution would streamline refuelling procedures and make it possible to use regular trucks for transport. The main obstacle to their use lies in the high cost of the capsules, which feature technology similar to cryogenic fuel tanks [65].

Dilip and Stathis (2025) propose the development of Europe's hydrogen economy

[5]https://www.cryoworld.com/wp-content/uploads/Flyer-liquid-hydrogen-storage.pdf

Figure 5.3: LH_2 storage capsules produced by the Dutch manufacturer Cryoworld

through a combined approach, using trucks for the initial stages of hydrogen deployment at airports, then moving to pipelines when demand grows and EHB development is sufficient to provide the required supply [66].

5.1.5 H_2 hubs

Airport hubs are among the innovations worth mentioning regarding the hydrogen economy. They are multifunctional hubs for green hydrogen, serving as demonstration and operational platforms for the integration of H_2 into the airport and territorial ecosystem. These strategic initiatives aim to turn airports into driving forces for energy transition beyond direct aeronautical applications. To this end, hubs are in the proximity of major airports, with the latter acting as the centre of an ecosystem that brings together multiple users and enables the sharing of production and storage costs. The purposes of these hubs are refuelling for terrestrial mobility and energy uses for facilities (electrification, heating), pending the technological development of hydrogen aviation to enable its conversion to aircraft refuelling as well.

H2BER - Berlin (Germany)

The *H2BER project* aims to construct and operate a carbon-neutral hydrogen production plant and refuelling station. The refuelling station is located near Berlin Brandenburg Airport (BER) in Germany [72].

Hydrogen is produced on-site by electrolysis, using electric energy from a farm with 40 wind turbines [59]. Production takes place via a 0.5 MW alkaline electrolyser (with a capacity of 250 kg of hydrogen per day) with a modular capacity that can expand up to 1 tonne of hydrogen per day. The station is designed to supply mainly fuel cell buses and cars, aiming to promote public acceptance of these technologies. The last element of the system is a cogeneration plant that uses the stored hydrogen to provide electricity or heat flexibly and to absorb fluctuations in demand [71].

Figure 5.4: Hydrogen ecosystem at Berlin Brandeburg airport [71]

The project seeks to identify and evaluate the technological, economic and organisational requirements for the commercial operation of hydrogen-wind systems in the medium term [72].

HYPORT - Toulouse (France)

Figure 5.5: H_2 distribution station at the Toulouse-Blagnac Airport [69]

The *HYPORT project* aims at a sustainable hydrogen supply chain network in an airport ecosystem. The airport is the centre of a hydrogen ecosystem, around which several users can cluster, allowing the sharing of hydrogen production and storage costs [59]. The project is located in the Hautes-Pyreneés department (France) and targets two

specific airports: the international airport of Toulouse-Blagnac and the regional airport of Tarbes-Lourdes-Pyreneés [68].

HYPORT requires the implementation of a 1 MW alkaline electrolysis platform to produce green hydrogen, with a daily production of 400 kg. The installed stations will be two: a smaller one (capacity of 20 kg per day) intended exclusively for airport services and a high-capacity one (400 kg per day) distributed in a public area and intended for refuelling all types of vehicles [69]. Although the project aims to support the aviation sector, the initial focus is on ground-based airport applications, such as airport vehicles, general electrification and building heating, rather than on hydrogen aircraft propulsion [70].

5.2 Qualitative analysis

The following section will attempt to summarise and integrate the analysis of the three airport production scenarios. In particular, it will focus on the technological, economic, and geopolitical/regulatory aspects.

5.2.1 Technical analysis: scenarios

	Pros	Cons
On-site scenario	▸ Minimized transport losses and associated risks ▸ Direct integration with local RES (e.g. solar PV, wind) ▸ Greater flexibility and control over the production process	▸ Need for complex infrastructure (electrolysers, compression or liquefaction systems, storage) ▸ High space and safety requirements ▸ Requires stability and continuity in energy supply ▸ Risk of conflict with demand from other airport users
Off-set scenario	▸ Lower infrastructure requirements for production ▸ On-site liquefaction allows more flexibility in demand management ▸ Gaseous transport is easier than cryogenic transport ▸ Good balance between control and reliability	▸ Hydrogen liquefaction is energy-intensive and technically complex ▸ Requires advanced cooling facilities ▸ Higher energy losses than off-site liquefaction ▸ Safety issues in the handling of pressurised gas and liquefaction equipment
Off-site scenario	▸ Higher industrial efficiency (centralized production and liquefaction) ▸ Reduced technical complexity on airport site ▸ Cryogenic transport technology is already developed and available in other sectors (e.g. space)	▸ Complex cryogenic transport: risk of evaporation (boil-off), delicate thermal management ▸ Requires specialised, well-insulated cryogenic tanks ▸ Dependence on external logistics chains and continuous carrier availability

Figure 5.6: Technical aspects

Figure 5.6 shows an analysis of the pros and cons of the three scenarios from a technical point of view.

On-site scenario has lower losses due to the absence of long-distance transport and the greater flexibility in production management. On the other hand, the complexity and bulk of the infrastructure required for on-site production cannot be overlooked, considering the

aforementioned issues of land availability and the compulsory safety distances between the production site and the rest of the airport facilities.

Off-set scenario reduces the amount of infrastructure required, limiting it to facilities needed for liquefaction. Transporting GH_2 is also technically easier than LH_2, as it can rely on pipelines, thus leading to a good balance between technical simplicity and control over production. The downsides are limited to the technological difficulties of liquefaction procedures, notably in relation to cooling and storage at 21 K.

Off-site scenario benefits from the advantages of centralised production on an industrial scale, while at the same time reducing the infrastructural complexity of the airport site (on which only minor adaptation to hydrogen use would be required). On the other hand, the disadvantages are linked to the difficulties of LH_2 transport (in particular the risk of leakage) and dependence on a supply logistics chain beyond the airport administration.

5.2.2 Technical analysis: renewable energy sources

	Pros	Cons
Solar PV	▸ Exploits all the large available areas of the airport (terminal roofs, open spaces and green belts)	▸ Highly intermittent, both on a daily and annual basis (seasonality) ▸ Risks related to solar glare on panels, which may limit installation areas
Wind	▸ High power output from a single wind turbine (2 or 3 are already adequate for a small airport)	▸ Severe safety issues due to the large size of the turbines ▸ Interference with navigation, communication and surveillance facilities.
Biomass	▸ Easy availability from various sources ▸ Versatility of use	▸ Need to assess ethical and sustainability issues (e.g. biosystem management problems)
Geothermal	▸ Low interference with aircraft operations as the infrastructure is mostly underground ▸ Versatility: hot/cold water can be used for space heating/cooling and steam for power generation	▸ Available for a very limited number of airports ▸ Complexity of infrastructure installation makes it mostly suitable for newly built airports
Hydropower	▸ Easy implementation	▸ High dependence on the presence of watercourses in the airport vicinity, only suitable for specific airports

Figure 5.7: Technical considerations for different renewable sources [73]

It is worthwhile to conduct a similar analysis by focusing on the various types of renewable resources, as done to some extent in the previous chapters. Accordingly, the pros and cons of the most popular types of renewable resources are assessed below, including some case studies of existing airport implementations. The primary source for these considerations is the eco-airport toolkit distributed by ICAO, particularly the publication "A Focus on the Production of Renewable Energy at the Airport site" [73].

Solar PV is one the most widely used in airports, as it makes an effective use of the many free surfaces. however, solar energy is linked to seasonality: both over the day (no

production at night) and over the year (reduced performance in winter). Another issue is linked to sunlight reflection: it could trigger pilots while manoeuvring. So, picking where to put the installation site and the degree of inclination is a critical choice.

Wind is of considerable interest due to the high power that can be generated from a small number of turbine units. Despite this, the vertical spread of the structure makes it a poor solution for airports, given the great danger of disturbing take-off/landing procedures and the risk of interference with navigation and communication systems. This point makes it a viable option only at small airports or possibly by resorting to unconventional solutions such as vertical axis turbines.

Biomass is a technically attractive solution, as it is readily available from many different sources (almost all plant matter and also animal waste) and has great versatility of use. However, as already mentioned in section 2.2.1, the exploitation of biomass as a source of bioenergy is regulated within the European Union by the European Renewable Energy Directive 2023/2413, which restricts its use to contexts where no form of reuse or recycling is possible (especially in the case of woody biomass) [61].

Geothermal has the advantage of being a constant source of heat, which can be exploited in the thermal regulation of the airport indoor areas. The resulting steam can also be used for energy production. Another positive aspect is related to infrastructure, as the bulk of the necessary facilities are located underground and, therefore, do not interfere with airport operations. On the other hand, the drawbacks include the small number of airports for which this solution is feasible and the complexity of installing the equipment in existing airports.

Hydropower is (like geothermal power) a source available only for a limited number of airports since the proximity of a suitable watercourse for its generation is a crucial factor. Where exploitable, however, it is a source of easy implementation and constant supply, thus resulting in an attractive choice.

Case study: solar PV

Airport sites around the world resort widely to photovoltaic solar energy due to its ease of handling and the wide availability of empty flat surfaces suitable for its installation. A few examples that can be mentioned are Zurich Airport (ZRH) in Switzerland, Narita (NRT) and Kansai (KIX) International Airports in Japan, Kuala Lumpur International Airport (KUL) in Malaysia, and San Diego International Airport (SAN) in the USA.

Figure 5.8 shows the case study of **Darwin International Airport (DRW)**, located in northern Australia. The project of interest is the construction of a 4 MW solar array aimed at providing approximately 25% of the airport energy needs. As stated by Rhett Nothling, head of the project for Northern Territory Airports, «this project enables to hedge the exposure of the airport to fluctuations in electricity prices thus providing greater certainty for the broader airport community» [73].

Figure 5.8: Solar panel installations at Darwin International Airport

The project required special care to comply with regulations on orientation and reflection produced by the solar panels. For this purpose, a specific software was developed to monitor the glare and glint of the array. The two images above explain how the study on the panels' orientation helped in placing them near the runway. This short distance (below 200 metres) allowed the exploitation of the land that would not otherwise have found a use, thus identifying a solution that can help to resolve the already raised issue of land availability in airports.

Case study: Wind

Below are two case studies in which wind turbines were installed near the runways of the airport, in order to show the feasibility of this solution in specific cases.

Figure 5.9: Wind turbines at the East Midlands Airport, close to Nottingham (UK)

The first example is the **East Midlands Airport (EMA)** (figure 5.9), located in the UK. The project involves the deployment of two 45-metre high wind turbines with a power output of 225 kW each. The two turbines generate about 5% of the airport electricity requirements, reducing annual emissions by 150 tonnes of CO2. Some issues raised by the programme include compatibility with electrical networks, adverse impacts on radar or communications and obstruction to safe aircraft operations (the location of the turbines is far enough away from the runway to be considered safe, as shown in figure

Figure 5.10: Exact location of the turbines in relation to the runway

5.10).

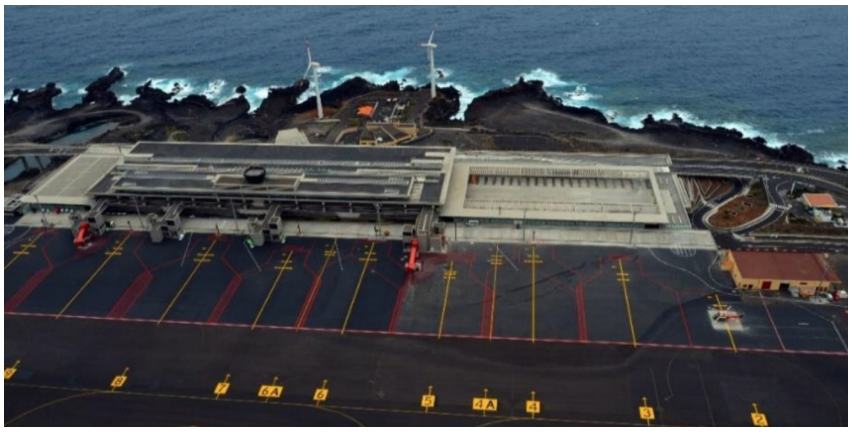

Figure 5.11: La Palma Airport, located in the Canary Islands (Spain)

La Palma Airport (SPC) (figure 5.11) installed two 66-metre high wind turbines in 2003. The power of the two turbines combined is 1320 kW, which is almost 50% of the airport energy requirements. According to data provided by the ICAO *Eco-airport toolkit* in fact, during the period from 2003 to 2016, the facility covered 46.5% of the electricity consumed by the airport.

The airport also has a contract with the energy suppliers of the island, thanks to which it sells the surplus produced at times of lower demand, thus generating an economic return for the operating company. Thanks to this agreement in the same period (2003-2016), about 20% of the energy produced by the two turbines was sold to the public electricity grid.

The turbines are placed in the Eastern zone of the airport (figure 5.12), at a safe

Figure 5.12: Location of the turbines in the outermost area of the airport

distance from the runway and the other operating areas. The chosen location is close to the Atlantic Ocean, exposing the turbines to trade winds that are constant in intensity and direction, thus limiting the fluctuations in energy production.

The two cases presented refer to airports where specific conditions allow the use of conventional turbines without interfering with aircraft operations. In other airports, where the same favourable conditions do not apply, a viable solution for using wind energy are **vertical-axis turbines**.

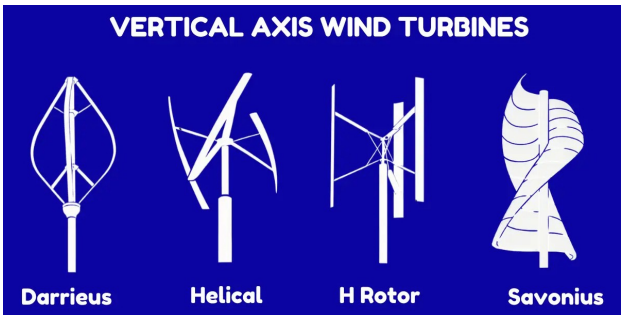

Figure 5.13: Categories of vertical-axis wind turbines [75]

These turbines feature an alternative design with less impact on air traffic, as they are much lower. The reduced height, which facilitates maintenance operations, and the higher efficiency (about 70% compared to $50 \div 60\%$ of conventional turbines) mean that this design is an attractive alternative for applications other than the airport scenario [74].

Case study: Geothermal

An illustrative case of the integration of geothermal energy systems in airport facilities is the **Montreal Pierre Elliott Trudeau International Airport (YUL)**. The project consists of four heat pumps, each with a well just under 200 metres deep. The pumps

are closed-loop and provide a nominal cooling load of 12 tonnes each (about 42.2 kW). Although the initial investment is far higher than for other renewable sources suitable for the airport scenario, the economics of the project lead to the conclusion that, in the long term, geothermal energy is highly competitive due to much lower operating costs.

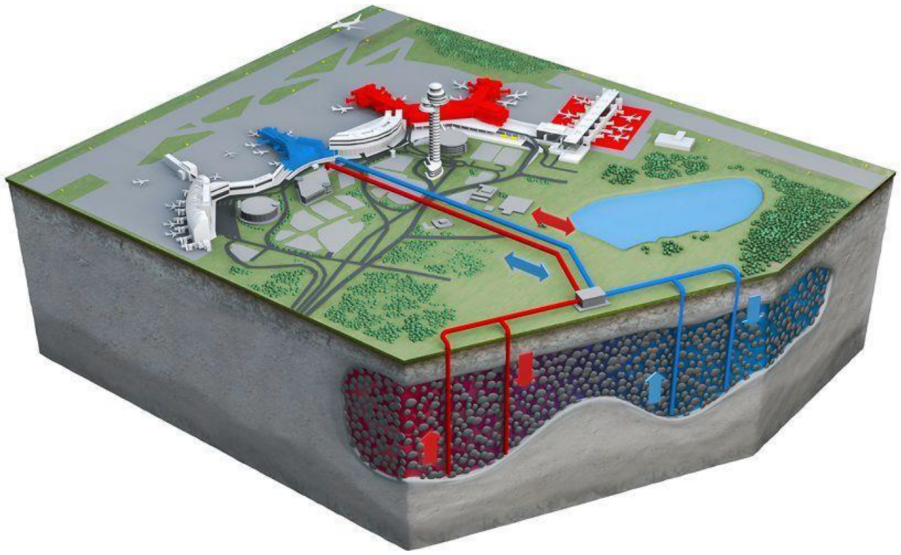

Figure 5.14: Stockholm Arlanda Airport aquifer (Sweden)

Stockholm Arlanda Airport (ARN) is an atypical case because of its thermal regulation of indoor spaces due to the explotation of an aquifer. The difference between the two energy sources is that geothermal energy relies on heat naturally produced within the earth, while groundwater stores heat in the form of hot or cold water. Generally, aquifers consist of sediments or porous rocks which retain water underground.

As shown in figure 5.14, the aquifer in the Arlanda airport has two zones, a hot area and a cold one. This system aims to decrease production peaks and avoid the need for cooling machines. The direct payback time corresponds to approximately 8 years, making this solution of considerable economic interest where available [73].

5.2.3 Economic analysis

The pros and cons of the three scenarios are analysed from an economic point of view in figure 5.15.

On-site scenario The benefits of nearby production include the avoidance of costs for hydrogen transport and the reduced logistical effort, as well as the possibility of generating profits by selling the surplus energy. A huge disadvantage is the elevated initial investment and the operation and maintenance costs related to the production plants. Moreover, as already demonstrated, the solution is hardly feasible for large airports.

	Pros	Cons
On-site scenario	▸ Avoids costs for transport and logistics ▸ Independence from energy price fluctuations ▸ Possibility of selling the surplus energy produced, generating profits for the facility ▸ Competitive H2 cost in the long term	▸ Very high initial investment (CAPEX for electrolysers, liquefaction, storage) ▸ Operating costs related to maintenance and internal plant management ▸ Advantages limited to small airports; implementation of the solution at large airports very difficult
Off-set scenario	▸ Potentially lower production costs in optimised sites ▸ Cost distribution among several actors (external production, internal liquefaction)	▸ Duplication of plants (production vs. liquefaction) ▸ High costs of on-site liquefaction ▸ Cost of transporting compressed gas
Off-site scenario	▸ Economies of scale in centralised production and liquefaction ▸ Similar model to the supply of other fuels (jet fuel, LNG)	▸ High costs of cryogenic transport and specialised logistics ▸ Dependency on price fluctuations in the external liquid hydrogen market

Figure 5.15: Economic aspects

Off-set scenario This solution makes it possible to optimise the distance between the hydrogen production site and the airport, and, as a consequence, to minimise the costs of both electrolysis and GH_2 transport. The offset scenario also provides a convenient distribution of risk among several actors, so that the airport administration is not required to bear too much responsibility for procurement (as in the on-site scenario) or depend excessively on the logistics of external suppliers (off-site scenario). Negative aspects include the duplication of production facilities, which is likely to increase the CAPEX and OPEX of the plants, and the high costs of on-site liquefaction, which may be unaffordable for some airports.

Off-site scenario Outsourcing production and liquefaction can benefit from the greater economies of scale associated with centralised plant management (with far greater demand than at the individual airport due to the higher number of energy users). It is also a solution of quick implementation, as it does not require structural upgrades to the airport and can replicate the existing supply chain of other energy sources. The disadvantages are the currently high cost of transporting LH_2 and the dependence of the cost of hydrogen on fluctuations in the energy market. These concerns result in the off-site strategy being economically suitable for the first stage of the hydrogen transition, but also less cost-effective in the long term.

5.2.4 Geopolitical & regulatory analysis

Figure 5.16 shows an evaluation of the pros and cons of the three scenarios from a geopolitical and regulatory point of view.

On-site scenario Local production increases the resilience to external adversities that could interrupt the airport operation and affect the nearby communities. In addition,

	Pros	Cons
On-site scenario	▸ Less exposure to external instabilities (conflicts, energy crises) ▸ Increases resilience of communities living in the vicinity of the airport ▸ Easier control over local regulatory compliance	▸ Requires complex authorisations for airport industrial facilities ▸ Stringent safety regulations for on-site management of H_2 and critical facilities
Off-set scenario	▸ Possibility of locating production in areas with more flexible regulations or state incentives	▸ Need for coordination between several legal and regulatory entities ▸ Increased regulatory complexity on transport and intermediate storage
Off-site scenario	▸ Fosters international supply partnerships (e.g. MENA countries, Australia, Chile) ▸ Potential alignment to major energy corridors (e.g. European H_2 projects)	▸ High geopolitical dependence and risk of instability in supplier countries ▸ Complex transnational regulations for transport and certification of green H_2

Figure 5.16: Geopolitical & regulatory aspects

it implies easier management of compliance with regulations, but also involves stringent requirements for the construction of facilities and potential safety issues.

Off-set scenario Off-set production has the advantage of being able to be located where there are greater economic or regulatory benefits; at the same time, this means that the production site and the liquefaction site at the airport may have to comply with different legislation. In addition there is the possibility that the areas through which hydrogen is transported introduce additional regulatory limits not foreseen in the on-site scenario.

Off-site scenario Externalising both H_2 production and liquefaction could benefit from the future energy corridors (as the aforementioned *European Hydrogen Backbone*), but also share the drawbacks of the off-set scenario in tying the certainty of supply to regulations and potential geopolitical instabilities of the territories crossed during transport.

Chapter 6

Case study: Turin-Caselle Airport

In this chapter, an assessment of the area surrounding the Turin Caselle airport will be carried out to determine the feasibility of on-site hydrogen production. The purpose of the analysis is to determine whether the areas surrounding the airport are suitable for the installation of photovoltaic solar panels and/or wind turbines, to supply renewable energy to the airport internal production plant. The analysis requires the use of specific maps of the area surrounding the airport, divided into three categories: soil type, slope and protected areas.

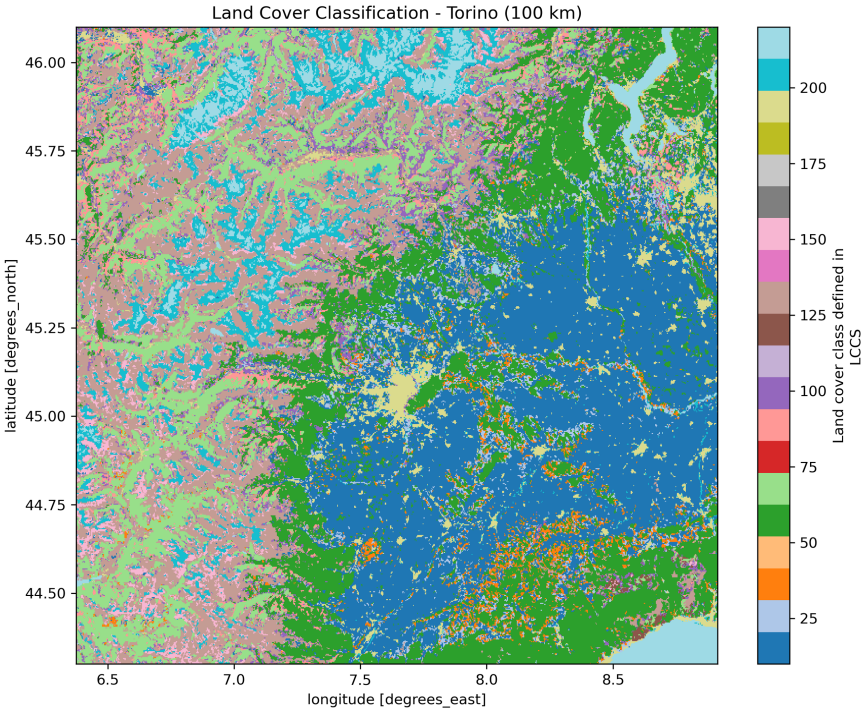

Figure 6.1: Land cover classification map of Piedmont [76]

6.1 Soil type

The soil type is determined using the *Land Cover Classification System* (LCCS) standard defined by the FAO (Food and Agriculture Organisation of the United Nations). This standard defines 22 distinct soil classes, associated with a colour scale, which are applied to satellite images to describe the land coverage of the study area.

The satellite imagery presented in this research comes from the dataset of global land cover maps called *Climate Data Store*, part of the Copernicus project. By its official definition, Copernicus is the «Earth observation component of the European Union's Space programme [...]. It offers information services that draw from satellite Earth Observation and in-situ (non-space) data» [77]. The programme relies on a satellite constellation consisting of 6 different families, whose data is supplemented by ground measurement stations.

Figure 6.1 shows a satellite image of Piedmont from the *Climate Data Store*, in which the soil classes are represented according to the LCCS colour scale. The map depicts the terrain conformation in 2022 and has a horizontal resolution of 300 metres [76]. Obtaining the image from the *Climate Data Store* requires selecting a year of interest and defining a sub-region in terms of latitude and longitude. For this instance, the isolated area corresponds roughly to the entire Piedmont region, bounded between the latitudes of $44° N$ to $46° N$ and the longitudes of $6° E$ to $9° E$. The coordinates of Turin Caselle Airport correspond to $45.20° N$, $7.65° E$.

In the figure, the urban area of Turin can be recognised, corresponding to the pale yellow region (determining class 190: urban areas) in the centre. Other relevant soil classes are cultivated fields in blue (classes 10 and 20), woodlands in green (classes 50 and 60) and sparse vegetation in pink (classes 130 and 150).

Table 6.1 provides a detailed description of the land classification scale, as well as the soil types considered suitable or unsuitable for solar or wind energy production, according to a similar research conducted by Schenke et al. (2024) [65]. it is noteworthy that, in addition to the 22 main classes, there are 5 subclasses (with a code not multiple of 10), which are used to make internal distinctions within classes 10, 60 and 200. Among the soil classes of the LCCS, the following subgroups may be distinguished:

- 10-40: Cultivated terrestrial areas and managed lands
- 50-150: Natural and semi-natural terrestrial vegetation
- 160-180: Natural and semi-natural aquatic vegetation
- 190: Artificial surfaces (settlements)
- 200: Bare areas
- 210, 220: Inland water bodies, snow and ice

As displayed in the third column of the table, the only areas excluded from Schenke's paper are those where there are cultivated fields, woodlands, urban settlements and water bodies. This initial skimming is not exhaustive enough and leaves room for further narrowing of exploitable land.

Class	Description	Suitable for RES
10 11 12	Cropland, rainfed	✓
20	Cropland, irrigated or post-flooding	
30	Mosaic cropland (>50%) / natural vegetation	✓
40	Mosaic natural vegetation (>50%) / cropland	✓
50	Tree cover, broadleaved, evergreen (>15%)	
60 61	Tree cover, broadleaved, deciduous (>15%)	
70	Tree cover, needleleaved, evergreen (>15%)	
80	Tree cover, needleleaved, deciduous (>15%)	
90	Tree cover, mixed leaf type	
100	Mosaic tree and shrub (>50%) / herbaceous cover	✓
110	Mosaic herbaceous cover (>50%) / tree and shrub	✓
120	Shrubland	✓
130	Grassland	✓
140	Lichens and mosses	✓
150	Sparse vegetation (tree, shrub, herbaceous cover)	✓
160	Tree cover, flooded, fresh or brackish water	
170	Tree cover, flooded, saline water	
180	Shrub or herbaceous cover, flooded	✓
190	Urban areas	
200 201 202	Bare areas	✓
210	Water bodies	
220	Permanent snow and ice	✓

Table 6.1: Codification of soil classes along with their suitability for RES [65]

The source file for image 6.1 is in the format NetCDF (*Network Common Data Form*, shortened as NC), a set of software libraries and a file format for storing array-oriented[1]

[1]Array-Oriented Scientific Data Formats are methods of storing and manipulating scientific data using

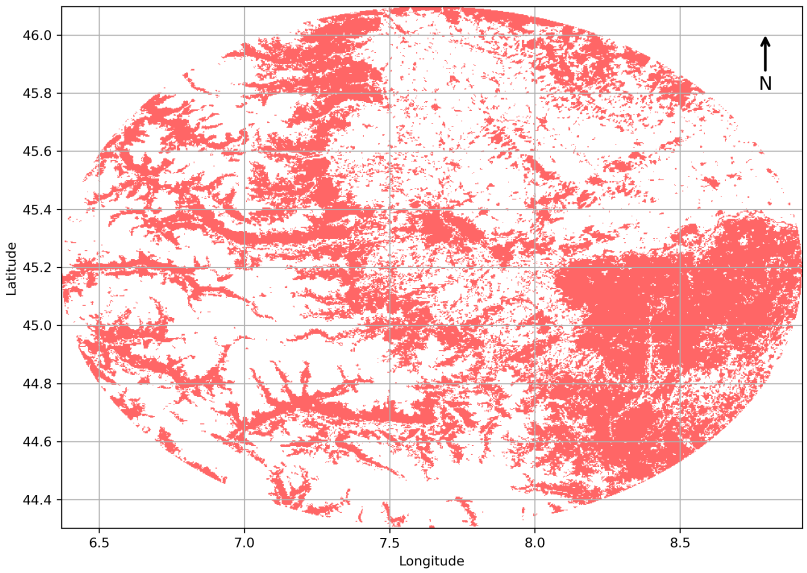

Figure 6.2: Unusable soil within 100 km of Turin-Caselle Airport

scientific data (such as temperature, humidity, pressure, and wind speed) [79] [80]. By using a dedicated Python code (see appendix A), the image 6.1 can be extracted from the NC file, and the matrices containing the scientific data associated with each pixel can be manipulated. The aim is to obtain a picture in which a circular mask centred on Turin Caselle Airport with a radius of 100 km is defined. Furthermore, each pixel associated with a type of soil unsuitable for renewable energy production needs to be highlighted in red.

The result of this analysis is shown in figure 6.2, which appears elliptical because of the adopted projection. The standard used in cartography is the WGS84, defined by the *US Office of Geomatics* as: «World Geodetic System 1984 (WGS 84) is a 3-dimensional coordinate reference frame for establishing latitude, longitude and heights [...] for practical applications of mapping, charting, geopositioning, and navigation.» [82]. WGS84 is the basis for many of the spatial reference systems in the EPSG public registry, with EPSG:3857 and EPSG:4326 being the two most widespread systems [84]. While the first one is based on the *Web Mercator Projection*, which projects the Earth onto a two-dimensional flat surface, the latter represents the Earth as a three-dimensional ellipsoid. Figure 6.2 was generated using EPSG:4326, which allows an accurate representation of the true distances on the Earth surface, but appears elliptical when drawing nearer to the poles. Since the Turin metropolitan area is located at a latitude of 45°, the map flattening is still acceptable. If the EPSG:3857 projection had been used, the map would have been circular, but distances would have been distorted (as it always happens with

a multidimensional array structure [81].

the Mercator projections) [83].

Class	Description	Pixels	Share [%]
10		33.992	7,27
11	Cropland, rainfed	56.885	12,17
12		13.801	2,95
20	Cropland, irrigated or post-flooding	34.534	7,39
30	Mosaic cropland (>50%) / natural vegetation (<50%)	14.783	3,16
40	Mosaic natural vegetation (>50%) / cropland (<50%)	11.042	2,36
50	Tree cover, broadleaved, evergreen (>15%)	0	0
60	Tree cover, broadleaved, deciduous (>15%)	77.497	16,58
61		64	0,01
70	Tree cover, needleleaved, evergreen (>15%)	45.590	9,75
80	Tree cover, needleleaved, deciduous (>15%)	31	0,01
90	Tree cover, mixed leaf type (broadleaved and needleleaved)	10.607	2,27
100	Mosaic tree and shrub (>50%) / herbaceous cover (<50%)	19.689	4,21
110	Mosaic herbaceous cover (>50%) / tree and shrub (<50%)	1.006	0,22
120	Shrubland	38	0,01
130	Grassland	77.917	16,67
140	Lichens and mosses	0	0
150	Sparse vegetation (tree, shrub, herbaceous cover) (<15%)	11.719	2,51
160	Tree cover, flooded, fresh or brackish water	0	0
170	Tree cover, flooded, saline water	0	0
180	Shrub or herbaceous cover, flooded, fresh/saline/brackish water	15	0
190	Urban areas	15.860	3,39
200		21.018	4,50
201	Bare areas	9.383	2,01
202		18	0
210	Water bodies	2.004	0,43
220	Permanent snow and ice	9.856	2,11

Table 6.2: Analysis of soil presence in figure 6.2

Table 6.2 provides an analysis of figure 6.2 performed by Python code, to detect how many pixels are present for each land class. Dividing the values of column 3 by the totality of pixels that make up the image gives the share of occurrence of each soil type, listed in column 4. By cross-referencing this data with the classes unsuitable for renewable energy production (see table 6.1), it can be assumed that approximately 40% of the target area is unsuitable. The table also shows how the most common soil types in Piedmont are cropland, deciduous tree cover and grassland, which together account for 45% of the region. Of these three types, only woodlands are unsuitable for the purposes

of this analysis.

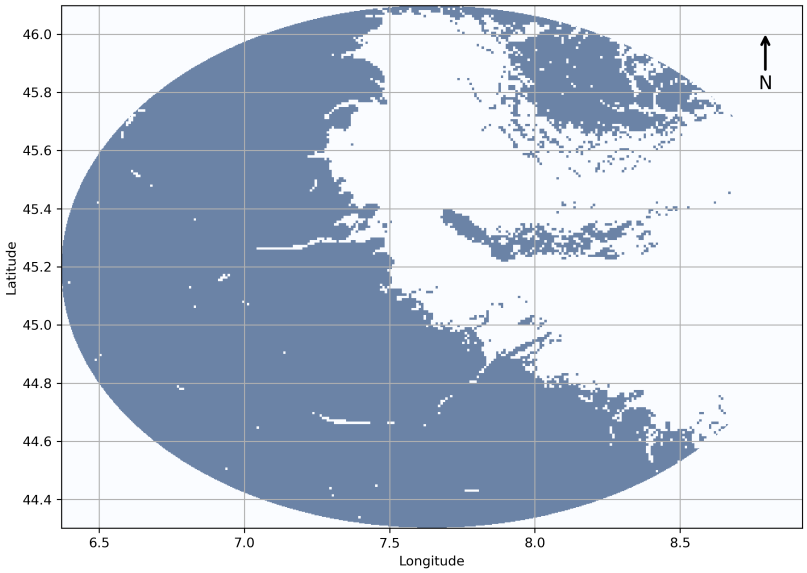

Figure 6.3: Non-flat land (slope>5°) within 100 km of Turin-Caselle Airport

6.2 Terrain slope

The second part of the analysis concerns the slope of the terrain in the study area. The threshold of acceptance for terrain slope was set at 5°, in accordance with the reference paper by Schenke et al. (2024) [65]. With this assumption, terrains with a slope greater than 5° are not deemed suitable for the installation of solar panels or wind turbines. The maps related to the terrain inclination originate from the *EarthEnv* project, which allows the download of a map of global slopes with an accuracy of 1 km [86]. This project is associated with a publication from Amatulli et al. (2018); it is defined as «a collaborative project of biodiversity scientists and remote sensing experts to develop near-global standardised, 1 km resolution layers for monitoring and modelling biodiversity, ecosystems, and climate» [85]. This map was then cropped and modified through Python code to obtain the result shown in figure 6.3. Areas with a slope greater than 5° are marked in blue and therefore excluded.

6.3 Protected areas

The last type of land to exclude are protected areas, where environmental restrictions preclude the installation of the infrastructure needed to produce renewable energy. The protected areas in the region of interest come from the *World Database on Protected Areas* (WDPA) of *Protected Planet*, a joint project between *UN Environment Programme*

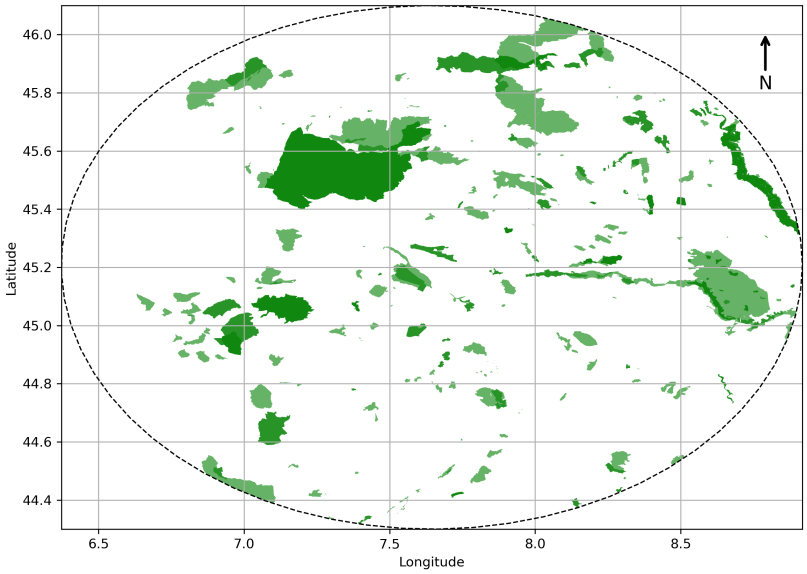

Figure 6.4: Protected areas within 100 km of Turin-Caselle Airport

(UNEP) and the *International Union for Conservation of Nature* (IUCN) [87]. The database provided a complete map of all protected areas in Italy, which was then filtered using Python code to delimitate a circular area with a radius of 100 km around Turin Caselle Airport. In the map shown in figure 6.4, the protected areas are in green. Among these, in the top left can be seen the *Gran Paradiso National Park*, corresponding to the widest and darkest area, and the *Mont Blanc* massif, with an elongated shape and crossing the 7th degree of longitude. It should be noted that this map does not show the protected areas located in French territory, but still within the 100 km range. However, a comparison with figure 6.3 makes clear that they are in steep mountainous regions and would therefore be excluded from the analysis because of the slope criterion.

6.4 Available land for RES production

6.4.1 Overlay of the 3 analysis

The last two maps show the overlap of the three analyses conducted so far on land cover, slope and protected areas. In the first figure (figure 6.5a), the three previous maps are superimposed and left in their original colours. Figure 6.5b, instead, shows a negative of figure 6.5a, in which all the areas that are still available for renewable energy production at the end of the analysis are marked in a dark green colour.

There are two methods to assess the ratio of available land for RES to the total study area. The first one (already applied to the land cover map, see table 6.2) requires the metadata associated with each map: by computing them through Python code, it can be determined how many pixels are suitable or unsuitable according to the criteria used so

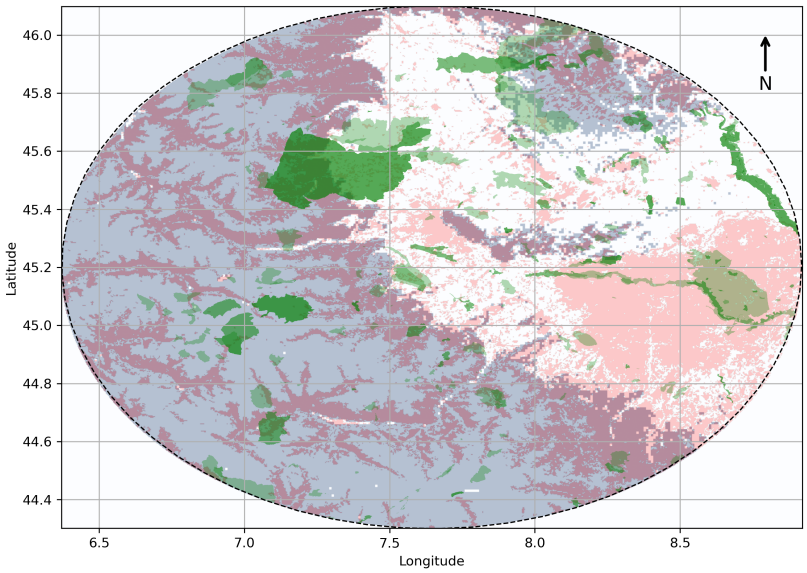

(a) Overall map of unavailable areas within 100 km of Turin-Caselle Airport

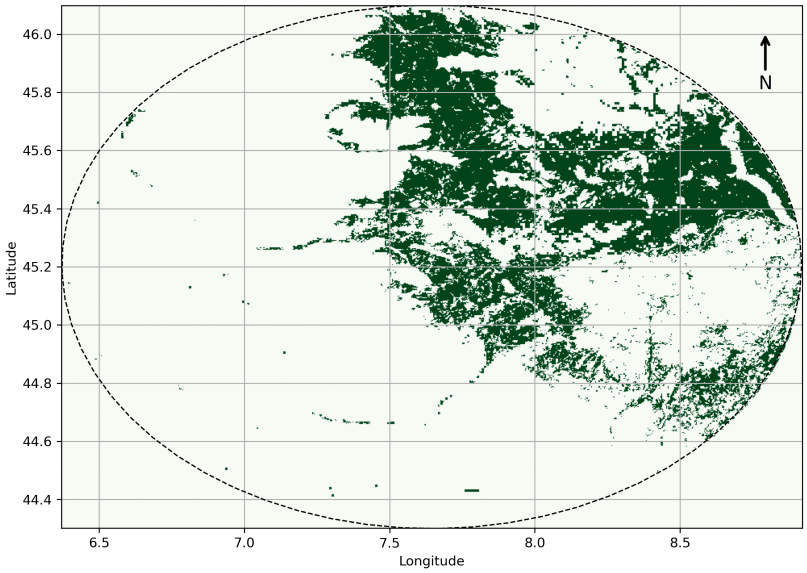

(b) Land available for RES within 100 km of Turin-Caselle Airport

Figure 6.5: Resulting maps of the analysis

far (i.e. slope<5° and unprotected area). This method also requires the elimination of overlaps between pixels, to avoid, for instance, the double count of a pixel both outside protected areas and with a slope below 5°. Following this approach, the number of usable

pixels obtained is 92 882 out of 467 349, i.e. 19.87% of the map.

The second method is the direct count of the coloured pixels in picture 6.5b and is used here to ensure that the result of the first method is correct. The number of green pixels counted corresponds exactly to that of the first method, namely 92 882 pixels.

In a spatial perspective, these results correspond to an available area of 6243.67 km^2 out of 31 415.93 km^2. However, it is logical to assume that the area actually available is consistently smaller, because of the interaction between the RES to be installed and the existing vegetation. For instance, considering a region in class 100 of the LCCS (i.e. characterised by the presence of shrubs and trees alternating with meadows), it could not be entirely overlayed by photovoltaic panels or wind turbines without cutting down the plants that are present on it.

6.4.2 Land-use criteria

In order to take this contingency into account, it is advisable to adopt the *Land utilisation factors* available in the literature. The following analysis will resort to those defined by Pieton et al. (2023), listed in Table 6.3 [88]. The correspondences between the categories

Land-use category	**Utility-scale PV**	**Onshore wind**
Barren	20%	50%
Cropland natural	2%	20%
Croplands	1%	10%
Forest	0%	10%
Grassland	10%	40%
Shrub land	5%	20%

Table 6.3: Land utilisation factors as defined by Pieton et al. (2023)

defined in the table and the LCCS soil classes are as follows:

- Croplands → 10, 11, 12, 20
- Cropland natural → 30, 40
- Forest → 50, 60, 61, 70, 80, 90, 160, 170
- Shrubland → 100, 110, 120, 150, 180
- Grassland → 130, 140
- Barren → 200, 201, 202
- Water → 210

Classes 200 (urban areas) and 220 (permanent snow and ice) are not included in the correspondences as they are intuitively unsuitable for the installation of utility-scale PV or wind turbines.

The implementation of land utilisation factors requires a further map, such that only pixels not excluded from the analyses conducted so far are shown (as in figure 6.5b), but including the soil types associated with each pixel. This map is depicted in figure 6.6, along with a chromatic legend. The last steps are identifying the types of soil depicted

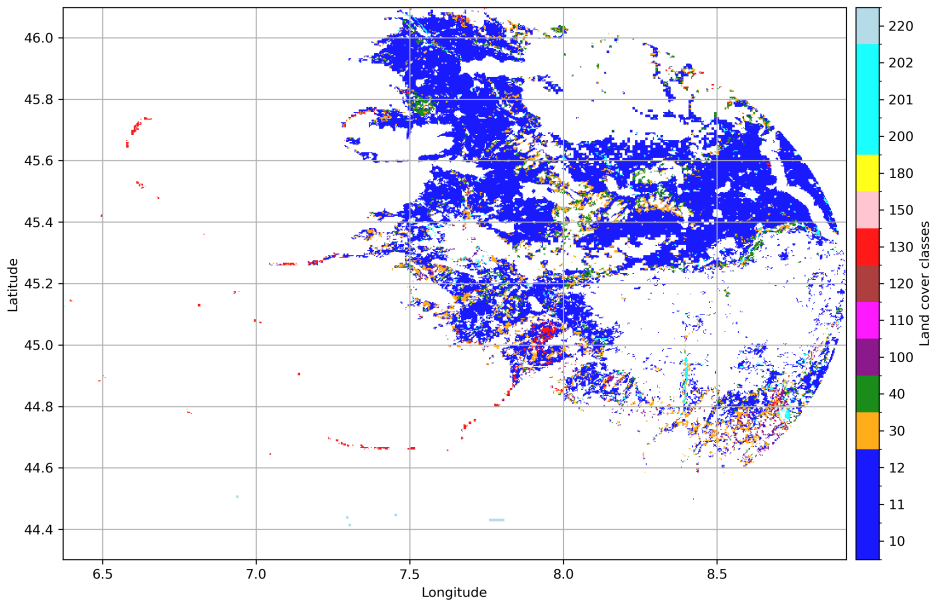

Figure 6.6: Available land for RES showing the type of soil classification

and multiplying the rate of occurrence of each class by the corresponding land utilisation factor. Table 6.4 shows the results, where the two percentages on the right in the last line must be applied to the area obtained from the previous analysis.

6.5 Results

6.5.1 Comparison with other European airports

In the Turin Caselle Airport case, the available area estimated was 6243.67 km^2. The application of appropriate land utilisation factors results in the following final figures:

- **Utility-scale PV**: 1,65% of 6243.67 km^2 $\rightarrow$ 103.02 km^2
- **Onshore Wind**: 12,68% of 6243.67 km^2 $\rightarrow$ 791.70 km^2

To assess the accuracy of this estimate, it is worth comparing it with some of the results obtained by Schenke et al. (2023). The analysis conducted in the benchmark

Class	Description	Share [%]	Utility-scale PV LUF	Utility-scale PV [%]	Onshore Wind LUF	Onshore Wind [%]
10		26,38		0,26		2,64
11	Croplands	46,16	1%	0,46	10%	4,62
12		8,35		0,08		0,84
30	Cropland Natural	9,80	2%	0,20	20%	1,96
40		4,80		0,10		0,96
100	Shrubland	1,33	5%	0,07	20%	0,27
130	Grassland	1,33	10%	0,13	40%	0,53
150	Shrubland	0,02	5%	0,00	20%	0,00
180		0,01		0,00		0,00
200		1,71		0,34		0,85
201	Barren	0,00	20%	0,00	50%	0,00
202		0,02		0,00		0,01
220	Permanent snow/ice	0,09	0%	0,00	0%	0,00
		100		1,65		12,68

Table 6.4: Soil type of the land available for RES surrounding Turin Airport

paper involves seven airport sites; among these, Hamburg Airport and Málaga-Costa del Sol Airport will be used here. This choice is advantageous because the two airports represent two opposite scenarios: the Hamburg region is totally flat, a very favourable condition that leads to a large area available for RES; Málaga, on the other hand, is close to the sea and to mountain ranges, both of which significantly reduce the available area. The same analysis performed for Turin Caselle Airport was conducted on both airports.

Figure 6.7 depicts the resulting available land for the two benchmark airports. It is worth noticing how the map of Málaga Airport is slightly closer to a circle than the Turin one, while the Hamburg map is much more compressed. This effect is caused by the EPSG:4326 reference system, which, as mentioned above, reproduces increasingly elliptical shapes when approaching the poles. Being significantly further north ($+8.4° N$ than Turin and $+17° N$ than Málaga), Hamburg Airport is affected more heavily by this compression.

Table 6.5 shows a comparison between the results obtained.

6.5.2 Energy consumption of H_2 aviation

Table 6.6 presents the steps taken to estimate the potential for exploitation of the land available for RES. The first row shows the available area near Turin Caselle Airport as identified in the previous sections. The second row exhibits the surface area required to produce 1 GW of power, as defined by Lohr et al. (2022) [89]. Solar photovoltaic energy,

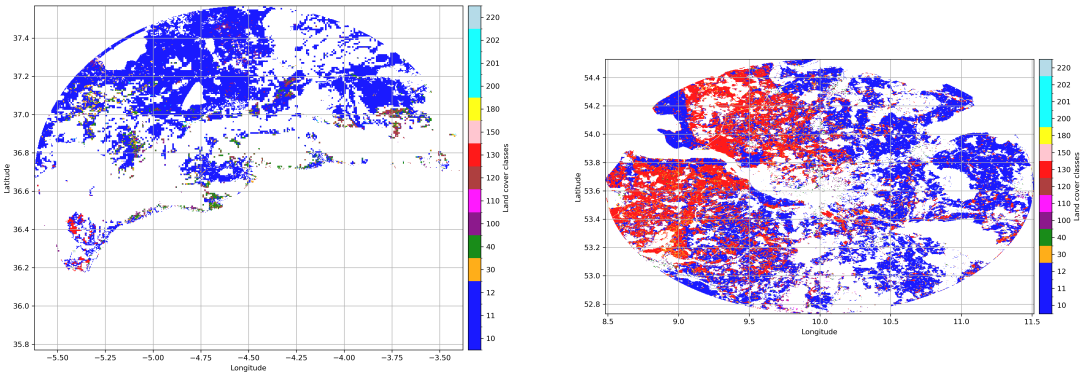

(a) Málaga-Costa del Sol Airport (b) Hamburg Airport

Figure 6.7: Land available for RES in the two benchmark airports

AIRPORT	Current analysis PV	Current analysis onW	Schenke et al. [65] PV	Schenke et al. [65] onW
Turin-Caselle	103,02	791,70	-	-
Málaga-Costa del Sol	93,12	769,56	32,11	238,53
Hamburg	644,33	3295,80	521,85	2348,85

Table 6.5: Comparison between the results obtained here and in the benchmark paper

which has been undervalued so far due to its horizontal extent on the ground, stands out here for its high power intensity per unit area (in fact, 10 km^2 of PV panels are needed to produce 1 GW of electrical power). Wind power, on the other hand, had significantly higher land utilisation factors for all soil types thanks to its vertical spatial configuration. However, here it is disadvantaged by the low power associated with each wind turbine. Hence, 200 km^2 of wind turbines are needed to produce 1 GW of electrical power.

The *Global Solar Atlas*[2] provides data to determine the *Specific Photovoltaic Power Output* (third line of the table) of solar panels installed in the Turin Caselle area. By identifying the same circular area of section 6.1, a power output distribution is supplied (see figure 6.8a) to identify a single suitable value for the studied region. The median result is 3.82 $kWh/kWp * \text{day}$ and represents the daily production in kWh of electricity for each kWp (peak kW) installed.

Just as the Specific PV Power Output provides a conversion factor for solar energy, Capacity Factor (fourth line) does likewise for wind energy. This value is obtained from

[2] *Global Solar Atlas 2.0, a free, web-based application is developed and operated by the company Solargis s.r.o. on behalf of the World Bank Group, utilizing Solargis data, with funding provided by the Energy Sector Management Assistance Program (ESMAP)*

data	Solar	Wind	source
Space available [km^2]	103.02	791.07	
Space requirement [km^2/GW]	10	200	[89]
Specific PV power output [KWh/KWp*day]	3.82	-	[90]
Capacity factor	-	0.10	[91]
Total power [GW]	10.30	3.96	
Annual conversion factor [days] & [h/year]	365	8760	
Annual energy production [GWh/year]	14 364.08	3464.89	
Total energy production [GWh/year]	17 828.97		

Table 6.6: Annual energy production calculation

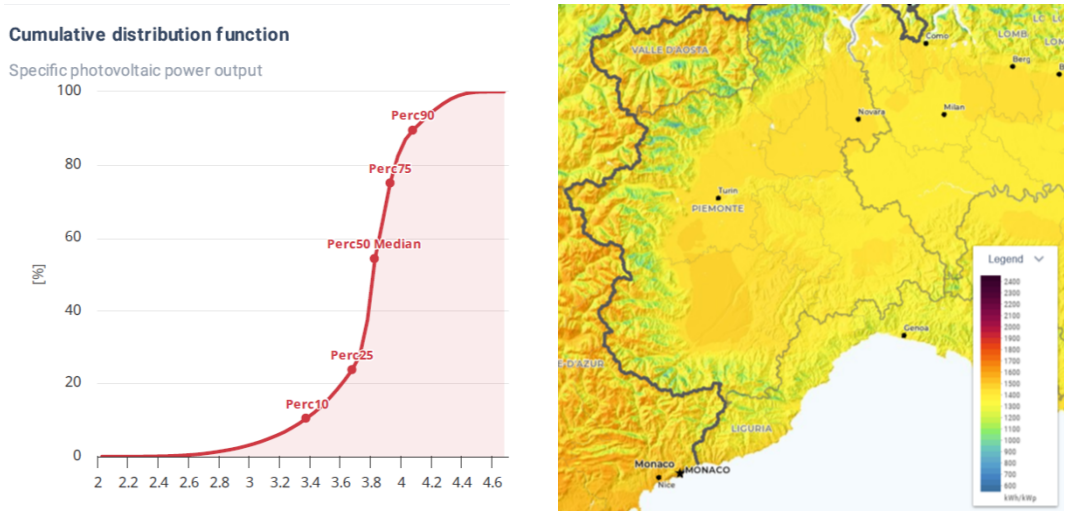

(a) Specific PV Power Output distribution

(b) Piedmont Specific PV Power Output

Figure 6.8: Data by the Global Solar Atlas [90]

the *Global Wind Atlas*[3], a tool that works in exactly the same way as the *Global Solar Atlas*. Figure 6.9b shows the capacity factor in Piedmont, measured at a 100-metre altitude above ground to simulate the wind speed at which a generic turbine would operate. The colour scale in the legend indicates that Piedmont is not a suitable region for wind energy, as the average wind speed is low, resulting in a correspondingly poor

[3] *Global Wind Atlas version 4.0, a free, web-based application developed, owned and operated by the Technical University of Denmark (DTU). The Global Wind Atlas version 4.0 is released in partnership with the World Bank Group, utilizing data provided by Vortex, using funding provided by the Energy Sector Management Assistance Program (ESMAP)*

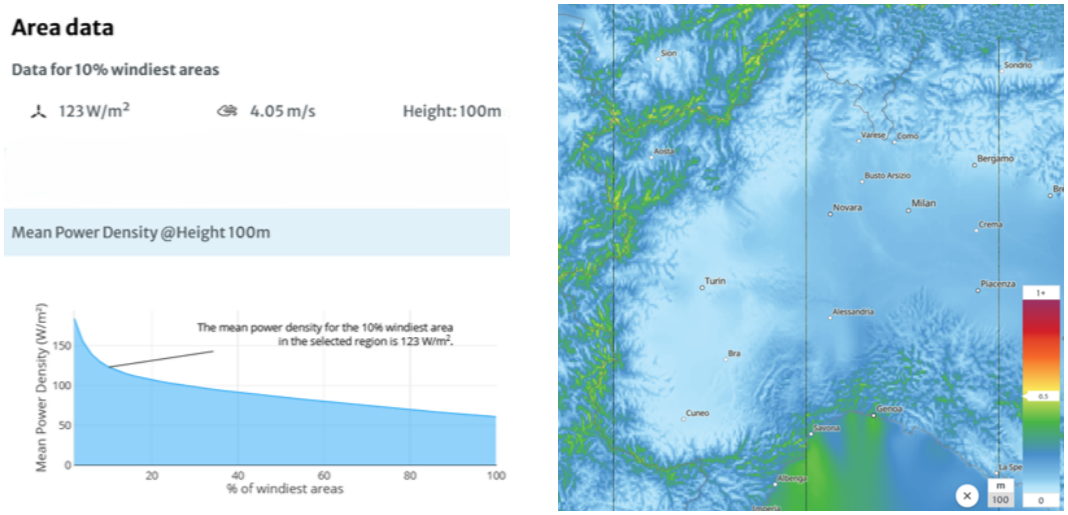

(a) Wind power density distribution

(b) Piedmont Capacity Factor

Figure 6.9: Data by the Global Wind Atlas [91]

capacity factor. Mountainous areas could achieve better yields, but the analysis doesn't consider them due to the slope criteria. Figure 6.9a displays the average power density and average wind speed values in the windiest 10% of the region under consideration. These are low values, as a speed of around 4 m/s is barely enough to start the turbine, and a well-functioning turbine should reach a power density of 300 W/m^2.

The fifth line of table 6.6 calculates the total power produced by the hypothetical RES infrastructures presented, obtained by dividing their available space by their space requirement.

Once all this information has been gathered, the amount of energy annually produced by each energy source is calculated according to the following operation:

$$\text{Solar energy} : (3.82\ \frac{kWh}{kWp} * day) * (365\ \frac{day}{year}) * (10.30\ GW) = 14\,364.08\ \frac{GWh}{year}$$

$$\text{Wind energy} : 0.10 * (8760\ \frac{h}{year}) * (3.96\ GW) = 3464.89\ \frac{GWh}{year}$$

Assuming that the two RES technologies can coexist on the identified land, adding up the resulting electrical energy figure can return an estimate of the maximum energy that can be produced. The last line of table 6.6 shows this value, equal to 17 828.97 $GWh/year$.

6.5.3 Traffic projections for 2050

Once the maximum amount of energy available has been determined, it is necessary to estimate the volume of hydrogen-powered aircraft traffic. Table 6.7 provides this forecast, based on official IATA and EUROCONTROL data. The first three rows of the table show IATA projections for the global aircraft fleet in 2050 [92]. According to the association, the number of aircraft in service will more than double the 2019 figure. Of these, about

Region	data	2019	2050	comments	source
World	Total fleet [n° of aircraft]	30 172	66 812	+221% growth	[92]
	H_2 fleet	-	12 151	18% of total	[92]
	H_2 regional fleet	-	6560	54% of H_2 fleet	[92]
Europe	Yearly traffic [flights/year]	11 100 000	16 000 000	+144% growth	[93]
Italy	Yearly traffic [flights/year]	1 643 852	2 367 147		[94]
Turin	Yearly traffic [flights/year]	43 655	62 966	2.66% of Italian traffic	[94]
	Daily traffic [flights/day]	120	173	Yearly traffic/365 days	
	H_2 traffic [flights/day]	-	17	daily traffic $*$ 54% $*$ 18%	

Table 6.7: Traffic estimate for 2050

one in five will be powered by hydrogen technologies; in half of these cases, they will be regional transport aircraft, i.e. with a limited number of passengers ($<$ 100 pax) and a short operating range ($<$ 1500 km).

EUROCONTROL additionally provides estimates on European air traffic (line four of the table), assuming a 44% increase between 2019 and 2050, when there could be 16 million flights per year [93]. These figures can be supplemented with data from *Assaeroporti*, the association of Italian airport operators, which reports that domestic air traffic in 2019 amounted to over 1,5 million flights. Of this total, 43 655 flights were to and from Turin Caselle Airport, corresponding to a share of 2.66% [94]. A preliminary estimate can therefore be made, projecting the +144% growth of European flights to the Italian domestic traffic. Maintaining the same percentage ratio as in 2019, this gives a total of 62 966 flights at Turin Airport in 2050. The final estimate requested is that of annual and daily hydrogen-powered flights at Turin Caselle Airport, to determine the amount of electricity needed to produce the hydrogen that would power them. In this analysis, only hydrogen aircraft dedicated to regional transport were considered, for which the liquid hydrogen demand per flight is available in the literature. Hydrogen-powered aircraft dedicated to medium or long-haul flights would require large amounts of hydrogen to be produced, which would necessitate massive and complex infrastructure that would be difficult for a small airport to manage in the short term. According to IATA projections for 2050, regional H_2 flights will account for approximately 10% of total flights. This translates into an average of 17 hydrogen flights per day at Turin Airport (last line of the table).

6.5.4 Energy requirements of Turin airport

By combining energy production data (table 6.6) and traffic forecasts (table 6.7), it is possible to obtain a rough estimate of hydrogen consumption at Turin Caselle Airport in the near future. The assessment consists of two scenarios: the more conservative one envisages five H_2-powered flights per day, referring to an initial penetration phase of this new technology (hypothetically referring to 2040, when the first commercial hydrogen-powered aircraft could enter service); the second scenario assumes 17 flights per day,

data	5 flights per day	17 flights per day	source
LH_2 production efficiency [kWh/kg]	62.00	62.00	
LH_2 demand per flight [kg]	336.25	336.25	[65]
Energy demand per flight [kWh]	20 847.50	20 847.50	
Turin flights per year [n° of aircraft]	1825	6205	
Turin energy demand per year [GWh/year]	38.05	129.36	
Share of total energy produced [%]	0.21	0.73	

Table 6.8: Energy consumption of Turin Caselle Airport

according to the result obtained in table 6.7. This second scenario refers to 2050, when hydrogen technologies could be sufficiently established to triple the number of flights with respect to the first scenario.

Table 6.8 reports the assessment conducted. The first line value is the same as that calculated to compute the cost of electrolysis, shown in the equation 3.9. The second line figure comes from the benchmark paper by Schenke et al. (2023) and represents the liquid hydrogen required to fly a turboprop regional aircraft over a 500 km mission [65]. By multiplying this value and the production efficiency of LH_2, the result of the third line is obtained, i.e. the electrical energy requirement of a single flight.

The results of the fifth line, so the electrical energy demands of Turin airport to produce H_2, are obtained by multiplying the previous two lines (energy demand per flight and number of flights per year). By comparing these two figures with the total energy production of the Turin Caselle area (last line of table 6.6), it is possible to express the share percentage of land required.

By comparing these two values with the total energy that can be produced in the airport area (last line of table 6.6), it is obtained the percentage of land available in the Turin Caselle area that must be used for RES in order to meet the airport needs. The values obtained are very low, less than 1% in both scenarios. This means that of the total usable land around the airport, less than 1% would be used to install solar panels and/or wind turbines.

These results seem quite viable, but it should be noted that over time the percentage is set to grow rapidly as hydrogen-powered aircraft replace traditional ones. Furthermore, this estimate only considers the electricity needed to produce hydrogen, to which should be added that required to power all other airport facilities (e.g. heating, lighting, electronic devices and others). The other notable limitation concerns the availability of space at the airport for electrolysis and liquefaction facilities (as already mentioned in section 5.1.2), which requires an in-depth analysis of the airport site.

6.5.5 Water stress issues in Piedmont

The last eventual constraint on on-site hydrogen production at Turin Caselle Airport comes from *water scarcity*. The evaluation of this parameter happened through the Water Risk Atlas (similar to the Global Solar/Wind Atlas) [95]. The metric selected to assess water availability is *water stress*, defined as the ratio between total water demand

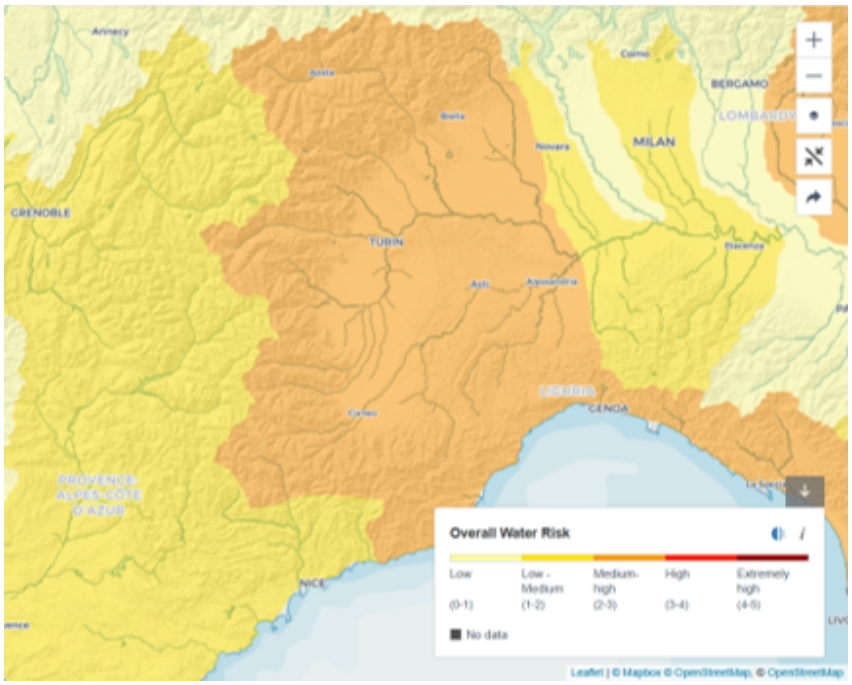

Figure 6.10: Current water stress levels in Piedmont (2025) [95]

and available renewable water supplies [96]. Water stress, therefore, does not directly measure the amount of water available, but rather the level of competition for it among potential users. Its advantage lies in the distinction between upstream and downstream users, with the former's water consumption clearly influencing the availability for the latter.

Figure 6.10 shows the water stress map of the Piedmont region. A label in the centre of the map indicates the location of the city of Turin; Turin Caselle Airport is located in the immediate vicinity (about 15 km away). The map also shows the main rivers of Piedmont, including the basins of the rivers Po (which passes through Turin) and Tanaro (running through Asti).

Most of the region is coloured in orange, which indicates a medium-high overall water risk, i.e. a water stress ratio between 20 and 40%. Since this figure represents an annual average, it is worthwhile identifying the seasonality of water stress. Figure 6.11 shows the water stress ratios for the months of December (Figure 6.11a, month of maximum water availability) and August (Figure 6.11b, month of peak shortage). It can be seen from the figures that the seasonality of water stress is quite remarkable: in December, the entire region is subject to minimal stress (less than 10%), while less than half of the renewable supplies remain unused in August (water stress between 40 and 80%). The August map also shows that water stress decreases along the course of the Po River, as numerous tributaries increase the flow rate of the river.

The forecast displayed in figure 6.12 shows how, according to the Water Risk Atlas, the overall scenario is set to worsen significantly, with the breach of the 20% threshold of mean annual stress already predicted for 2030 (Figure 6.12a). By 2050, moreover,

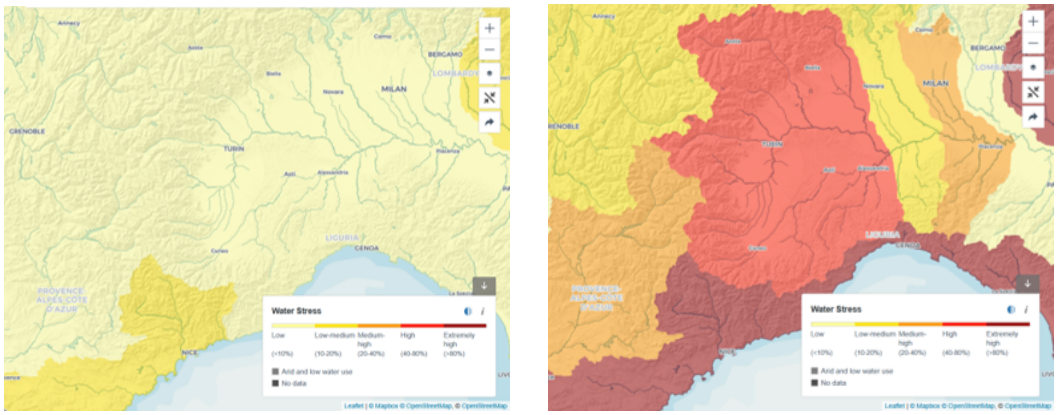

(a) December (b) August

Figure 6.11: Water stress during sensible month in Piedmont (2025) [95]

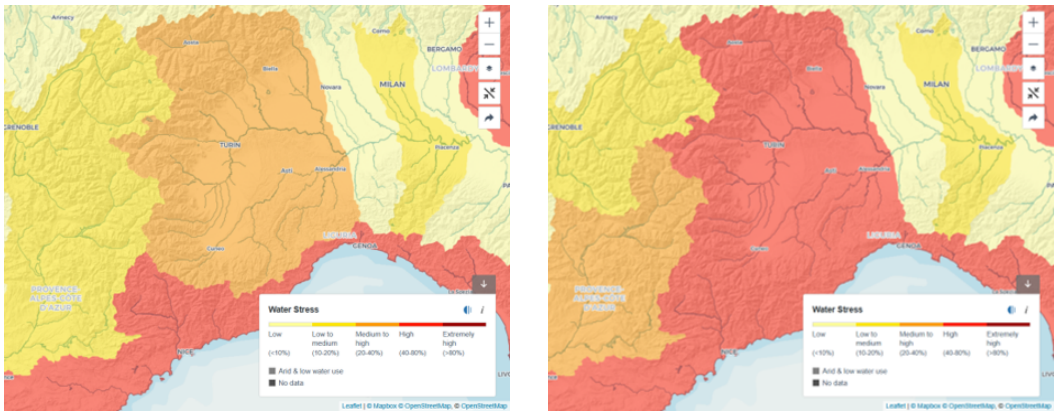

(a) 2030 (b) 2050

Figure 6.12: Future water stress in Piedmont [95]

the 40% mark should be exceeded for the entire Piedmont and Liguria territory (figure 6.12b). Meanwhile, stress levels will rise in the Alpine arc surrounding Piedmont towards the French border. It should also be noted that this figure represents the annual average, meaning that stress levels closer to the maximum value can be expected during the summer months.

Combining the considerations from the previous chapters on the seasonality of renewable energy sources (solar energy above all) with the above-mentioned water scarcity, the logical outcome is the necessity of a shrewd management of resources to allow the breakthrough of hydrogen at Turin Airport. Assuming that hydrogen production will be entirely on-site, there are three main pathways to consider:

- Collecting water in dedicated reservoirs during the winter months to increase its availability in the summer months

- Storage of the surplus electricity generated during summer, when solar PV systems have maximum efficiency, to increase its availability during the winter months
- Replacement or integration of solar energy with renewable resources with lower seasonality or higher yields in the winter months

The first two options aim to transfer surplus resources (water or electricity) from one season to the other, thereby attempting to level out the amount of hydrogen produced at different times of the year. This type of solution relies on the assumption that there is an actual production surplus in either summer or winter. The third option, on the other hand, seeks to maximise hydrogen production during the winter months, when water shortages are less likely to be an issue. In this way, storage directly concerns the produced hydrogen.

All three solutions share problems related to the storage of resources or energy. In particular, hydrogen storage facilities have already been discussed in the previous chapters: gaseous hydrogen requires a considerable amount of space because of its low volumetric density; liquid hydrogen storage, on the other hand, faces technological difficulties related to cryo-compression processes.

Conclusion

The research conducted in this thesis aims to investigate the feasibility of employing green hydrogen as an energy carrier on a large scale, specifically in the aviation industry. Therefore, chapter 2 begins with an examination of the early stages of the hydrogen life cycle. By comparing the emissions of each production pathway, it became clear that electrolysis is the only way to produce clean hydrogen. However, this is only possible under fairly stringent conditions, by supplying the production plant with electricity generated entirely from renewable sources. Yet, national electricity grids are still lagging far behind in the energy transition, with a few exceptions in the Scandinavian region. Electrolysis using existing national electricity grids emits amounts of CO_2e comparable to (or higher than) traditional methods. This statement means that green hydrogen production is necessarily subordinate to the national energy transition.

Chapter 3 carries out an estimate of the cost of electrolysis in Italy and Europe. This assessment requires calculating the LCOH, based on cost of energy, capital expenditures, and cost of operations. The results are divided into an average scenario, estimated with the state-of-the-art grid, and a best-case scenario, corresponding to a full renewable electricity grid. The resulting LCOH is slightly lower for the European scenario than for the Italian one. However, even in the best-case scenario, the LCOH of green hydrogen produced from Alkaline electrolysers stands around 3 \$/kg, over 1\$ more expensive than the target cost to be competitive on the market. Since hydrogen derived from fossil sources has comparable costs to the fuels currently used in aviation, many efforts are required before green hydrogen becomes an economically sustainable alternative.

Chapter 4 faces the matter of technological maturity. While the electrolysis is considered a mature technology, it still needs to progress in terms of economy of scale to become fully established in the hydrogen production market. Concerning the adoption of hydrogen as an aviation fuel, significant improvements are necessary before hydrogen aircraft can replace traditional ones. This progress is fundamental in particular for airport turnaround operations, because there are still many uncertainties on the H_2 storage and refuelling methods.

The issue of hydrogen integration into airport facilities is debated in chapter 5. The initial focus is on three production scenarios, differing by the location of H_2 production and liquefaction plants. The analysis of the pros and cons of each scenario shows that on-site production is currently unfeasible, particularly for large airports. On the other hand, off-site production could benefit from the economies of scale of centralised plants, being a practicable option for the early deployment of hydrogen technologies. However, the LH_2 transport imposes significant technological challenges yet to be overcome.

Finally, chapter 6 analyses how to produce green hydrogen in Turin Caselle Airport. First, a circular region around the airport was defined, from which areas considered unsuitable for renewable energy production were then excluded. Next, it was determined whether the energy produced in this area could be enough to meet the airport requirements for the coming decades. This demand also includes the energy needed to produce green hydrogen through electrolysis. Although the analysis yields positive results (highlighting the availability of land to provide the necessary renewable energy), the issue of water consumption remains open. As a matter of fact, Piedmont is a region subject to significant water stress, which is set to worsen in the coming years; therefore, the use of water for electrolysis could make it even worse.

According to this analysis, it is unlikely that green hydrogen could decarbonise aviation in the short term. Although it may appear an ideal solution, it presents challenges in many respects that are difficult to overcome:

- Emissions → Without electricity produced exclusively from renewable sources, emissions from electrolysis would remain equal to, or higher than, those from traditional methods. The decarbonisation of the electric national grids is a priority: the energy produced from renewables should be used to achieve this goal before any other use, including electrolysis. For this reason, the role of hydrogen risks being counterproductive to the energy transition.

- Costs → As things stand, the price of green hydrogen is far from being competitive with other fuels on the market. For H_2 to become a viable option, institutional incentives are required. What Bardon and Massol said about SAF also applies to hydrogen: «A deregulated market will lead the aviation industry to choose inefficient solutions, ranging from green-washing and the promotion of technological myths to the use of unsustainable feedstock and energy» [97].

- Integration into airport facilities → The deployment of hydrogen requires a set of adjustments to the existing infrastructure that could be challenging to realise. The size of production and liquefaction plants makes on-site production unfeasible in many large airports; similar reasons prevent the production of electricity from RES.

- Water scarcity → The last issue regarding green hydrogen adoption is the lack of water resources in many regions. Most urban areas, where the largest airports are usually located, have an elevated water stress index.

- "Green colonialism" → Since the most developed countries face so many problems in producing hydrogen themselves, some projects are meant to delocalise the production in foreign countries. A relevant example is the *SouthH2Corridor* project, a 3,300-kilometre hydrogen corridor planned to connect Northern Africa with Germany. This project aims to produce in Tunisia and Algeria the green H_2 for the European market. However, the programme lacks guarantees regarding respect for the populations living in the areas designated for hydrogen production [103]. Furthermore, Northern Africa is a region where water scarcity is a priority issue, and

allocating that water to hydrogen production for Europe is a neo-colonial approach that should be avoided at all costs.

To conclude, it is essential to focus on propellants which could really make a difference in decarbonising aviation in the short period. Hyping on dead ends and unreliable energy carriers, such as green hydrogen, could mislead from the crucial issue: climate change. It is essential to act fast to prevent the Earth from collapsing, in order to preserve human life and biodiversity.

Appendix A

Satellite imagery analysis using Python

This appendix will show and explain how to use Python to generate the maps of the analysis conducted in Chapter 6.

A.1 Land cover classification

```
1 ds = xr.open_dataset(r"C:\Users\matti\Tesi\Torino_land_cover.nc")
2 land_cover = ds['lccs_class'].isel(time=0)
3 lat = ds['lat'].values
4 lon = ds['lon'].values
5 data = land_cover.values
```

Listing A.1: LCC part 1

The line `xr.open_dataset(path)` (where *xr* stands for the *xarray* package) allows to open NetCDF datasets (data structures containing multidimensional variables), such as those obtained from the Copernicus Climate Data Store. These datasets contain a series of 2D maps relating to different time frames. The `isel(time=0)` command (line 2) allows to save in `land_cover` only the first map of the time span, thus excluding the time variable from the dataset. The subsequent lines store the latitude and longitude values in dedicated variables, while the generic variable `data` stores all the metadata associated with the image.

```
1  lat0 = np.radians(45.200)
2  lon0 = np.radians(7.645)
3  lat_rad = np.radians(lat)
4  lon_rad = np.radians(lon)
5  lon2d, lat2d = np.meshgrid(lon_rad, lat_rad)
6  dlat = lat2d - lat0
7  dlon = lon2d - lon0
8  a = np.sin(dlat/2)**2 + np.cos(lat0) * np.cos(lat2d) * np.sin(dlon/2)**2
9  c = 2 * np.arcsin(np.sqrt(a))
10 earth_radius_km = 6371
11 dist_km = earth_radius_km * c
12 mask_circle = dist_km <= 100
```

```
masked_land_cover = np.where(mask_circle, data, np.nan)
```

Listing A.2: LCC part 2

NumPy (abbreviated as *np*) is the Python package used to create the desired map. The variables `lat0` and `lon0` store the coordinates (in radians) of Turin Caselle Airport, which is the centre of the circular mask to be delimited. The `np.meshgrid` instruction in line 5 creates a 2D mesh grid based on the latitude and longitude information from the Copernicus dataset.

Starting from line 6, the *haversine formula* is used to determine a 100 km vectorial distance from the central point (Caselle Airport) of the map. This formula allows the calculation of the distance between two points on the surface of a sphere; it takes its name from the trigonometric function defined as $\text{haversine}(\theta) = \sin^2\left(\frac{\theta}{2}\right)$.

Line 12 assigns the variable `mask_circle`, which contains the circular mask of 100 km radius centred on Turin Caselle Airport. The line below defines a new map where everything outside the mask is not considered and overwritten by NaN (*Not a Number*).

```
rows = np.where(mask_circle.any(axis=1))[0]
cols = np.where(mask_circle.any(axis=0))[0]
row_min, row_max = rows.min(), rows.max()
col_min, col_max = cols.min(), cols.max()
masked_cropped = masked_land_cover[row_min:row_max+1, col_min:col_max+1]
mask_cropped = mask_circle[row_min:row_max+1, col_min:col_max+1]
lat_cropped = lat[row_min:row_max+1]
lon_cropped = lon[col_min:col_max+1]
extent_cropped = [lon_cropped.min(), lon_cropped.max(), lat_cropped.min(),
    lat_cropped.max()]
```

Listing A.3: LCC part 3

Lines 1 to 4 define the minimum rectangle that circumscribes the mask. The map processed so far is then cropped to the size of this rectangle, thus eliminating all pixels whose data has been overwritten by NaN (line 5). Lines 7 and 8 cut the information relating to the cartesian grid of the map to the dimensions of the rectangle, combining latitude and longitude in the variable `extent_cropped`.

```
sel_codes = [20, 60, 70, 80, 90, 190, 210]
soil_map = np.where(np.isin(masked_cropped, sel_codes), 1, np.nan)
cmap_red = ListedColormap(['red'])
```

Listing A.4: LCC part 4

The codes listed in line 1 are the soil classes of the Land Cover Classification System that will be excluded from the analysis (see table 6.1). The pixels belonging to these classes are marked with 1 (true) by the command in line 2, while all the other pixels are labelled as NaN. In the resulting map, pixels belonging to soil classes not suitable for RES will be coloured in red, while all others (NaNs) will remain white.

```
fig, ax = plt.subplots(figsize=(10, 8))
plt.imshow(soil_map, cmap=cmap_red, interpolation='nearest',
           extent=extent_cropped, origin='lower', alpha=0.6)
plt.annotate('N', xy=(0.95, 0.95), xytext=(0.95, 0.85), xycoords='axes
    fraction', textcoords='axes fraction',
```

```
5                fontsize=14, ha='center', va='center', arrowprops=dict(
    arrowstyle='->', color='black', lw=2))
6 plt.xlabel('Longitude')
7 plt.ylabel('Latitude')
8 plt.grid(True)
9 plt.show()
```

Listing A.5: LCC part 5

This code produces the image shown in figure A.1, containing the map of excluded soil types.

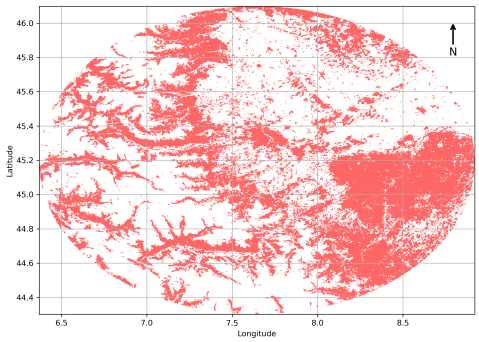

Figure A.1: Excluded soil types map

```
1 valid_values = masked_land_cover[~np.isnan(masked_land_cover)].astype(int)
2 counts = pd.Series(valid_values).value_counts().sort_index()
3 values = masked_land_cover
4 values_clean = values[~np.isnan(values)]
5 unique, counts = np.unique(values_clean, return_counts=True)
6
7 df = pd.DataFrame({
8     "Code": unique.astype(int),
9     "Incidence": counts})
10 df["Share"] = 100 * df["Incidence"] / df["Incidence"].sum()
11 df = df.sort_values("Code").reset_index(drop=True)
```

Listing A.6: LCC part 6

The first two lines of this part of the code count the unusable soils, indicated by pixels marked as **non**-NaN (NumPy's `isnan` function combined with logical negation ~), and save the total number of pixels in the variable `counts`. Lines 3 to 5 remove the NaNs, leaving only the count of usable classes and the pixels associated with each of them.

The variable `df` in line 7 is a dataframe, i.e. a two-dimensional table structure in which the first column contains the code for each soil class, the second column its incidence measured in number of pixels, and the third column the percentage of area relative to the total surface area.

A.2 Terrain slope

```
path_slope = r"C:\Users\matti\Tesi_capitolo_7\slope_1KMmn_GMTEDmd.tif"
slope = rxr.open_rasterio(path_slope, masked=True).squeeze()
boundary_slope = 5 # degrees
slope = slope.rio.write_crs("EPSG:4326")
```

Listing A.7: Slope part 1

These code lines are used to open the slope file, then define the boundary slope at 5 degrees and specify the CRS (Coordinate Reference System) as EPSG:4326.

```
min_lon, max_lon, min_lat, max_lat = extent_cropped
slope_clipped = slope.rio.clip_box(minx=min_lon, miny=min_lat, maxx=
    max_lon, maxy=max_lat)
land_cover = land_cover.rio.write_crs("EPSG:4326")
slope_matched = slope_clipped.rio.reproject_match(land_cover)
slope_matched_cropped = slope_matched.isel(y=slice(row_min, row_max + 1),
    x=slice(col_min, col_max + 1))
```

Listing A.8: Slope part 2

The first two lines extract the geographical limits (min/max longitude and latitude) from the previously defined `extent_cropped` variable, then crop the dataset within the box to fit the slope map into the study area. The coordinate system is then overwritten as EPSG:4326, ensuring that the slope and land cover datasets are in the same CRS. The fourth line reprojects the slope raster onto the *land_cover* coordinate system and grid, using the `reproject_match` command. After the indexing (`isel` command) of the fifth line, a perfectly aligned slope map is obtained with the same geographical area as the land cover.

```
slope_data = slope_matched_cropped.values
slope_data = np.where(slope_data < 0, np.nan, slope_data)
mask_cropped_2 = mask_circle[row_min:row_max+1, col_min:col_max+1]
mask_da = xr.DataArray(mask_cropped_2.astype("float32"), coords={"lat":
    lat_cropped, "lon": lon_cropped}, dims=["lat", "lon"])
mask_da = mask_da.rio.write_crs("EPSG:4326")
mask_da = mask_da.rio.set_spatial_dims(x_dim="lon", y_dim="lat")
```

Listing A.9: Slope part 3

The first line of code extracts the numerical values from the DataArray and saves them in `slope_data`, so that direct mathematical operations can be performed on them. All missing or negative values are then replaced with NaN, since they would not make sense in relation to a slope. The last four lines are preliminary operations on the circular mask (which is cropped and adapted to the dimensions of the slope map), necessary for the subsequent steps of the analysis.

```
mask_resampled = mask_da.rio.reproject_match(slope_matched_cropped)
mask_resampled_np = mask_resampled.values > 0
slope_masked = np.where(mask_resampled_np, slope_data, np.nan)
slope_map = (slope_masked > boundary_slope)
```

Listing A.10: Slope part 4

The first line conducts the resampling of the mask on the slope grid. The second line converts the DataArray into a boolean array where *True* = within 100 km from the

airport. The third line applies the mask to the map, maintaining the `slope_data` values only inside its extent (so that everything outside the mask is defined as NaN). In this way, the slope map is limited to the study area. Lastly, a boolean (true/false) mask is created, with the true value associated with the pixels where the slope is above the 5° limit.

```
fig, ax = plt.subplots(figsize=(10, 8))
plt.imshow(slope_map, cmap='Blues', interpolation='nearest', extent=
    extent_cropped, origin='lower', alpha=0.6)
plt.annotate('N', xy=(0.95, 0.95), xytext=(0.95, 0.85), xycoords='axes
    fraction', textcoords='axes fraction', fontsize=14, ha='center', va='
    center', arrowprops=dict(arrowstyle='->', color='black', lw=2))
plt.xlabel('Longitude')
plt.ylabel('Latitude')
plt.grid(True)
plt.show()
```

Listing A.11: Slope part 5

This code produces the image shown in figure A.2, highlighting the areas with excessive steepness.

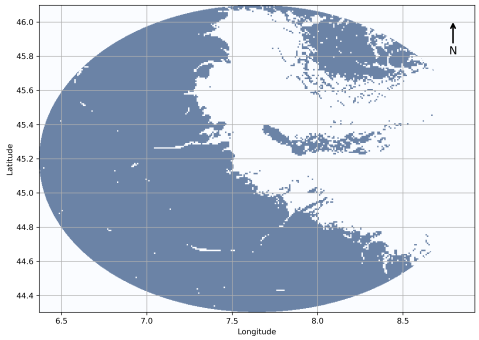

Figure A.2: Map of steep areas

A.3 Protected areas

```
airport_point = Point(7.645, 45.200)
gdf = gpd.GeoDataFrame({'geometry': [airport_point]}, crs="EPSG:4326")
gdf_utm = gdf.to_crs(epsg=32632)
buffer_utm = gdf_utm.geometry.buffer(100000)
buffer_gdf = gpd.GeoDataFrame(geometry=buffer_utm, crs=gdf_utm.crs)
buffer_wgs84 = buffer_gdf.to_crs(epsg=4326)
```

Listing A.12: Protected areas part 1

The first three lines define the location of Caselle airport, create a GeoDataFrame of the point and project it into a metric CRS (saved in the variable `gdf_utm`). The fourth line then generates a 100 km buffer around the point, with the buffer then being inserted

likewise into a GeoDataFrame. The last line transforms the buffer into EPSG:4326, to allow it to be overlaid with other data.

```
part1 = gpd.read_file(r"C:\Users\matti\Tesi_capitolo_7\
    Torino_aree_protette\WDPA_WDOECM_Jun2025_Public_ITA_shp_0\
    WDPA_WDOECM_Jun2025_Public_ITA_shp-polygons.shp")
part2 = gpd.read_file(r"C:\Users\matti\Tesi_capitolo_7\
    Torino_aree_protette\WDPA_WDOECM_Jun2025_Public_ITA_shp_1\
    WDPA_WDOECM_Jun2025_Public_ITA_shp-polygons.shp")
part3 = gpd.read_file(r"C:\Users\matti\Tesi_capitolo_7\
    Torino_aree_protette\WDPA_WDOECM_Jun2025_Public_ITA_shp_2\
    WDPA_WDOECM_Jun2025_Public_ITA_shp-polygons.shp")
protected_areas = gpd.GeoDataFrame(pd.concat([part1, part2, part3],
    ignore_index=True))
protected_areas = protected_areas.to_crs(epsg=4326)
```

Listing A.13: Protected areas part 2

Since the protected areas of Piedmont are obtained from the *WDPA* database in the form of three separate *.shp* files, these are loaded and merged within the `protected_areas` variable. The last line assigns the correct CRS to the variable.

```
protected_clipped = clip(protected_areas, buffer_wgs84.geometry.iloc[0])
fig, ax = plt.subplots(figsize=(10, 8))
buffer_wgs84.boundary.plot(ax=ax, color='black', linestyle='--', linewidth
    =1, label='Buffer 100 km')
minx, miny, maxx, maxy = buffer_wgs84.total_bounds
ax.set_xlim(minx, maxx)
ax.set_ylim(miny, maxy)
protected_clipped.plot(ax=ax, color='green', alpha=0.6, label='Protected
    areas (clip)')
plt.annotate('N', xy=(0.95, 0.95), xytext=(0.95, 0.85), xycoords='axes
    fraction', textcoords='axes fraction', fontsize=14, ha='center', va='
    center', arrowprops=dict(arrowstyle='->', color='black', lw=2))
plt.xlabel("Longitude")
plt.ylabel("Latitude")
plt.grid(True)
ax.set_aspect('equal')
plt.show()
```

Listing A.14: Protected areas part 3

In the first line, the areas represented in the *shape* files are filtered so that only those inside the circular mask are retained. The result `protected_clipped` contains only the protected areas that intersect or fall within the buffer, i.e. the outer boundary of the mask. The command `ax.set\aspect("equal")` is used to set the 1:1 ratio between the X and Y axis units. This ensures that the distances in latitude and longitude appear correctly proportioned, avoiding visual distortions. Without this command, the map would appear circular rather than elliptical like the previous two, preventing the three maps from overlapping and distorting the distances represented.

The plotted figure is showed in picture A.3, where the shapes in green represent the protected areas in the region of interest.

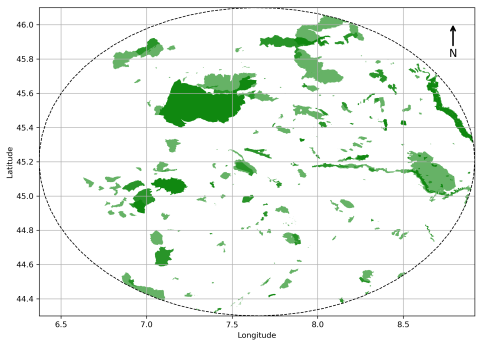

Figure A.3: Map of protected areas

A.4 Overlap & Results

```
1  fig, ax = plt.subplots(figsize=(10, 8))
2  im1 = ax.imshow(soil_map, cmap=cmap_red, extent=extent_cropped, origin='
       lower', alpha=0.3)
3  im2 = ax.imshow(slope_map, cmap='Blues', extent=extent_cropped, origin='
       lower', alpha=0.3)
4  protected_clipped.plot(ax=ax, color='green', alpha=0.3, label='Protected
       areas')
5  buffer_wgs84.boundary.plot(ax=ax, color='black', linestyle='--', linewidth
       =1)
6
7  plt.xlabel("Longitude")
8  plt.ylabel("Latitude")
9  plt.annotate('N', xy=(0.95, 0.95), xytext=(0.95, 0.85), xycoords='axes
       fraction', textcoords='axes fraction', fontsize=14, ha='center', va='
       center', arrowprops=dict(arrowstyle='->', color='black', lw=2))
10 plt.grid(True)
11 plt.xlim(extent_cropped[0], extent_cropped[1])
12 plt.ylim(extent_cropped[2], extent_cropped[3])
13 ax.set_aspect('equal')
14 plt.show()
```

Listing A.15: Results part 1

In this part of the code, all four elements that are to be overlapped in the final map are defined. The variable `im1` plots the unsuitable types of soil; `im2` does the same for the non-flat areas. In line 4 `protected_clipped` is plotted to represent the protected areas, while the following line draws the buffer which surrounds the study region.

The result is represented in figure A.4.

```
1  valid_soil_map = np.isnan(soil_map)
2  valid_slope_map = ~slope_map
3  height, width = soil_map.shape
4  transform = Affine.translation(extent_cropped[0], extent_cropped[2]) *
       Affine.scale((extent_cropped[1] - extent_cropped[0]) / width,(
       extent_cropped[3] - extent_cropped[2]) / height)
```

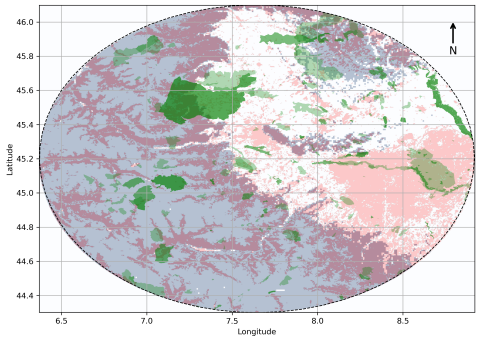

Figure A.4: Final overlap of the 3 maps and the buffer

```
5 Protected_areas_map = rasterize([(geom, 1) for geom in protected_clipped.
      geometry], out_shape=(height, width), transform=transform, fill=0,
      dtype=np.uint8)
6 valid_protareas_map = Protected_areas_map == 0
```

Listing A.16: Results part 2

The first two lines generate the negative of the maps of soil types and slope, colouring the pixels suitable for RES and indicating those to be excluded as NaN (unsuitable soil type and/or slope greater than 5°). A similar reversal occurs for the map of protected areas, where, however, preliminary steps are necessary to define the reference grid (line 4) and to rasterise the map (line 5).

```
1 final_mask = (valid_soil_map & valid_slope_map & valid_protareas_map &
      mask_cropped)
2 pixel_within_circle = np.count_nonzero(mask_cropped)
3 valid_pixel = np.count_nonzero(final_mask)
4 percentage = 100 * valid_pixel / pixel_within_circle
5 total_area_km2 = np.pi * 100**2
6 usable_area_km2 = (percentage / 100) * total_area_km2
7 print(f"1st method - Usable pixels within 100 km: {valid_pixel} out of {
      pixel_within_circle} ({percentage:.2f}%)")
8 print(f"Available area: {usable_area_km2:.2f} km2 out of {total_area_km2
      :.2f} km2")
```

Listing A.17: Results part 3

The variable `final_mask` stores the ensemble of all the desired maps. The following lines calculate the available area in terms of pixels and square kilometres: line 2 counts the pixels within the external buffer, while line 3 counts only the coloured pixels of the overlapped maps. The share percentage of coloured pixels is stored in the variable `percentage`, while line 5 and 6 convert the results from pixels to km^2. These results are then printed in line 7-8.

```
1 fig, ax = plt.subplots(figsize=(10, 8))
2 im = ax.imshow(final_mask, cmap='Greens', extent=extent_cropped, origin='
      lower')
3 buffer_wgs84.boundary.plot(ax=ax, color='black', linestyle='--', linewidth
      =1)
```

```
ax.set_xlabel("Longitude")
ax.set_ylabel("Latitude")
ax.annotate('N', xy=(0.95, 0.95), xytext=(0.95, 0.85), xycoords='axes
    fraction', textcoords='axes fraction', fontsize=14, ha='center', va='
    center', arrowprops=dict(arrowstyle='->', color='black', lw=2))
ax.grid(True)
plt.xlim(extent_cropped[0], extent_cropped[1])
plt.ylim(extent_cropped[2], extent_cropped[3])
ax.set_aspect('equal')
plt.show()

figure_valid_pixel = np.count_nonzero(final_mask)
print(f"2nd Method - Green pixels in the map: {figure_valid_pixel}")
```

Listing A.18: Results part 4

The plot in the first part of the code produces the figure A.5, where all the areas available for RES production within 100 km of Turin Caselle Airport are shown.

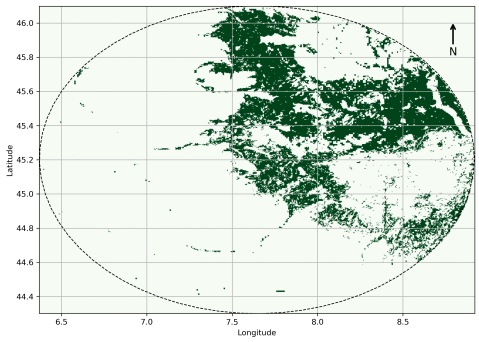

Figure A.5: Land available for RES production

The last two lines count the number of coloured pixels by directly scanning the image: if the result obtained is identical to that of the first method, the success of the analysis is confirmed.

Bibliography

[1] Athia, N., Pandey, M., Sen, M. et al.
Factors affecting the production cost of green hydrogen and its challenge for sustainable development. Environ Dev Sustain (2024).
DOI: 10.1007/s10668-024-04798-w

[2] Lila D Bunch Library (2024).
Research guides: Faculty: Scopus. Last updated on December 17, 2024. Visited on March 12, 2025.

[3] University College London (2025).
Library services: Library skills: Scopus. Last updated on January 30, 2025. Visited on March 12, 2025.

[4] Elsevier (2024).
Scopus Support Center: How can I best use the Advanced search?. Last updated on August 15, 2024. Visited on March 10, 2025.

[5] IEA - International Energy Agency (2024).
Global Hydrogen Review 2024

[6] Surer, M. G., Arat, H. T.
State of art of hydrogen usage as a fuel on aviation. European Mechanical Science, 2(1), 20-30 (2018).
DOI: 10.26701/ems.364286

[7] Fan Z., Weng W., Zhou J., Gu D., Xiao W.
Catalytic decomposition of methane to produce hydrogen: A review, Journal of Energy Chemistry, Volume 58 (2021).
DOI: 10.1016/j.jechem.2020.10.049

[8] Habib M.A., Abdulrahman G.A.Q., Alquaity A.B.S., Qasem N.A.A.
Hydrogen combustion, production, and applications: A review. Alexandria Engineering Journal, Volume 100, Pages 182-207 (2024).
DOI: 10.1016/j.aej.2024.05.030

[9] Fusaro R., Vercella V., Ferretto D. et al.
Economic and environmental sustainability of liquid hydrogen fuel for hypersonic transportation systems. CEAS Space J 12, 441-462 (2020).
DOI: 10.1007/s12567-020-00311-x

[10] Machado, H., Ferreira, A. C., Teixeira, S. F., Teixeira, J. C.
Green Hydrogen Value Chain: Modelling of a PV Power Plant Integrated with H2 Production for Industry Application. Energies, 17(6), 1414 (2024).
DOI: 10.3390/en17061414

[11] IEA (2019).
The Future of Hydrogen.

[12] Eurostat, an official website of the European Union (2025).
Glossary:Carbon dioxide equivalent. Visited on April 14, 2025.

[13] Eurostat, an official website of the European Union (2025).
Glossary:Global-warming potential (GWP). Visited on April 14, 2025.

[14] Nnabuife S.G., Darko C.K., Obiako P.C., Kuang B., Sun X., Jenkins K.A
Comparative Analysis of Different Hydrogen Production Methods and Their Environmental Impact (2023).
DOI: 10.3390/cleantechnol5040067

[15] Nasser M., Megahed T.F., Ookawara S., Hassan H.
A review of water electrolysis-based systems for hydrogen production using hybrid/-solar/wind energy systems (2022).
DOI: 10.1007/s11356-022-23323-y

[16] Farhana K., Shadate Faisal Mahamude A., Kadirgama K.
Comparing hydrogen fuel cost of production from various sources - a competitive analysis (2024).
DOI: 10.1016/j.enconman.2024.118088

[17] Yagmur Goren A., Dincer I., Khalvati A.
A comprehensive review on environmental and economic impacts of hydrogen production from traditional and cleaner resources, Journal of Environmental Chemical Engineering, Volume 11, Issue 6 (2023).
DOI: 10.1016/j.jece.2023.111187

[18] IEA (2023).
Energy Technology Perspectives 2023.

[19] KPMG Advisory N.V. (2022).
How to evaluate the cost of the green hydrogen business case? - Assessing green hydrogen production costs.

[20] Wei C., Undavalli V.K., Perkins C., Heglas K., Oswald E., Gbadamosi-Olatunde O.B., Khandelwal B.
Technical and economic assessment of cryogenic fuels for future aviation (2024).
DOI: 10.1016/j.paerosci.2024.101053

[21] Statistics | Eurostat (2022).
Eurostat Database: Energy balances. Visited on February 14, 2025.

[22] IRENA - International Renewable Energy Agency (2019).
Renewable Power Generation Costs in 2018. Visited on March 10, 2025.

[23] IEA - International Energy Agency (2020).
Projected costs of generating electricity 2020. Visited on March 19, 2025.

[24] IRENA - International Renewable Energy Agency (2020).
Green Hydrogen: A Guide to Policy Making. Visited on May 2, 2025.

[25] Parra D., Patel M. K., Bauer C.
A review on the role, cost and value of hydrogen energy systems for deep decarbonisation, Renewable and Sustainable Energy Reviews, vol. 101, pp. 279-294 (2019).
DOI: 10.1016/j.rser.2018.11.010

[26] Glenk G., Reichelstein S.
Economics of converting renewable power to hydrogen, International Journal of Hydrogen Energy, vol. 45, no. 39, pp. 20736-20746 (2020).
DOI: 10.1016/j.ijhydene.2019.11.081

[27] IEA - International Energy Agency (2019).
The Future of Hydrogen: Seizing Today's Opportunities. Visited on May 9, 2025.

[28] IRENA - International Renewable Energy Agency (2020).
Green Hydrogen Cost Reduction: Scaling up Electrolysers to Meet the 1.5 °C *Climate Goal*. Visited on May 14, 2025.

[29] IEA - International Energy Agency (2024).
Hydrogen Production Projects Interactive Map: Project-level data on low-emissions hydrogen production worldwide. Last updated on November 13, 2024. Visited on May 21, 2025.

[30] IEA - International Energy Agency (2024).
Hydrogen Production and Infrastructure Projects Database. Last updated on October, 2024. Visited on May 21, 2025.

[31] Fuel Cells Bulletin (2020).
Fukushima Hydrogen Energy Research Field in Japan ready for green hydrogen production, Volume 2020, Issue 3, March 2020, Page 1.
DOI: 10.1016/S1464-2859(20)30089-4

[32] Iyer R.K., Prosser J.H., Kelly J.C., James B.D., Elgowainy A.
Life-cycle analysis of hydrogen production from water electrolyzers, International Journal of Hydrogen Energy, Volume 81 (2024).
DOI: 10.1016/j.ijhydene.2024.06.355

[33] IEA - International Energy Agency (2020).
Global average levelised cost of hydrogen production by energy source and technology, 2019 and 2050. Last updated on September 24, 2020. Visited on May 21, 2025.

[34] Taghizadeh-Hesary F. et al.
Financing Solutions for the Economic Feasibility of Hydrogen Projects: Case Study in China, ERIA (Economic Research Institute for ASEAN and East Asia) Research Project Report FY2021 No. 19 (2021).
In Hydrogen Sourced from Renewables and Clean Energy: A Feasibility Study of Achieving Large-scale Demonstration.

[35] Schenke F., Hoelzen J., Minke C., Bensmann A., Hanke-Rauschenbach R.
Resource requirements for the implementation of a global H2-powered aviation, Energy Conversion and Management: X, Volume 20 (2023).
DOI: 10.1016/j.ecmx.2023.100435

[36] The Hydrogen Council (2020).
Path to Hydrogen competitiveness - A cost perspective. Published on January 20, 2020. Visited on May 24, 2025.

[37] Tezer T., Yaman R., Yaman G.
Evaluation of approaches used for optimization of stand-alone hybrid renewable energy systems, Renewable and Sustainable Energy Reviews, Volume 73, (2017).
DOI: 10.1016/j.rser.2017.01.118

[38] McKinsey & Company (2024).
Technology Trends Outlook 2024. Published on July, 2024. Visited on May 26, 2025.

[39] Yukesh Kannah R., Kavitha S., Preethi, Parthiba Karthikeyan O., Gopalakrishnan Kumar, Dai-Viet N. Vo., Rajesh Banu J.
Techno-economic assessment of various hydrogen production methods - A review, Bioresource Technology, Volume 319, (2021).
DOI: 10.1016/j.biortech.2020.124175

[40] Strazza C., Olivieri N., De Rose A., Stevens T., Peeters L., Tawil-Jamault D. et al.
Technology readiness level: guidance principles for renewable energy technologies: final report, Publications Office, European Commission: Directorate-General for Research and Innovation (2017).
DOI: 10.2777/577767

[41] NASA - National Aeronautics and Space Administration (2010).
Technology Readiness Levels Demystified, by Jim Banke. Published on August 20, 2010. Visited on May 26, 2025.

[42] Li Destri A., Conte R., Gregorio A., Enrico R., Bosso L.
Przewodnik po samolotach z całego świata, The Polish Journal of Aviation Medicine, Bioengineering and Psychology (2000).
DOI: 10.14052000/acab.1312

[43] Chapman A., Itaoka K., Hirose K., Davidson F.T., Nagasawa K., Lloyd A.C., Webber M.E., Kurban Z., Managi S., Tamaki T., Lewis M.C., Hebner R.E., Fujii Y.
A review of four case studies assessing the potential for hydrogen penetration of the future energy system (2019).
DOI: 10.1016/j.ijhydene.2019.01.168

[44] Abdelsalam R.A., Mohamed M., Farag H.E.Z., El-Saadany E.F.
Green hydrogen production plants: A techno-economic review (2024).
DOI: 10.1016/j.enconman.2024.118907

[45] Lepage T., Kammoun M., Schmetz Q., Richel
Biomass-to-hydrogen: A review of main routes production, processes evaluation and techno-economical assessment (2021).
DOI: 10.1016/j.biombioe.2020.105920

[46] Malone P.K.
Applying System Readiness Levels to Cost Estimates - A Case Study Part 2 (2020).
DOI: 10.1109/AERO47225.2020.9172591

[47] Austin M.F., York D.M.
System Readiness Assessment (SRA) an illustrative example (2015).
DOI: 10.1016/j.procs.2015.03.031

[48] Gove R., Sauser B., Ramirez-Marquez J.
Integration Maturity Metrics: Development of an Integration Readiness Level (2007).
DOI: 10.3233/IKS-2010-0133

[49] Long J.M.
Integration readiness levels (2011).

DOI: 10.1109/AERO.2011.5747629

[50] RHIA - Rotterdam The Hague Innovation Airport (nd).
About RHIA: Our story..

[51] TULIPS (nd).
Overview of TULIPS projects and demonstrations. Visited on Semptember 4, 2025.

[52] TULIPS (2024).
RTHA advances liquid hydrogen storage for sustainable aviation. Published on April, 2024. Visited on Semptember 5, 2025.

[53] NLR - Netherlands Aerospace Centre (2025).
Maiden flight of a drone on liquid hydrogen, a Dutch first. Published on Semptember 3, 2025. Visited on Semptember 8, 2025.

[54] Fountain Fuel (nd).
Locations in the Netherlands. Visited on Semptember 8, 2025.

[55] Concept Aerospace (nd).
The anatomy of our hydrogen electric powertrain. Visited on Semptember 9, 2025.

[56] Khalil M., Dincer I.
Investigation of a new holistic energy system for a sustainable airport with green fuels (2024).
DOI: 10.1016/j.scs.2024.105624

[57] Taha M., Lundvall N., Kyprianidis K., Salman A., Vouros S., Zaccaria V.
Techno-economic evaluation of hydrogen production for airport hubs (2024).
DOI: 10.46855/energy-proceedings-11088

[58] Cybulsky A., Allroggen F., Shao-Horn Y., Mallapragada D.S.
Challenges of Decarbonizing Aviation via Hydrogen Propulsion: Technology Performance Targets and Energy System Trade-Offs (2024).
DOI: 10.1021/acssuschemeng.4c02868

[59] Ochoa Robles J., Giraud Billoud M., Azzaro-Pantel C., Aguilar-Lasserre A.A.
Optimal Design of a Sustainable Hydrogen Supply Chain Network: Application in an Airport Ecosystem (2019).
DOI: 10.1021/acssuschemeng.9b02620

[60] Gaubatz J., Martin E., Miyamoto A., Murga B., Sharpe P., Travnik M., Tsay A., Wang Z.J., Hansman R.J.
Estimating the Energy Demand of a Hydrogen-Based Long-Haul Air Transportation Network, International Conference on Future Energy Solutions (FES) (2023).
DOI: 10.1109/FES57669.2023.10182543

[61] European Union (2023).
Directive (EU) 2023/2413 of the European Parliament and of the Council of 18 October 2023 amending Directive (EU) 2018/2001, Regulation (EU) 2018/1999 and Directive 98/70/EC as regards the promotion of energy from renewable sources, and repealing Council Directive (EU) 2015/652

[62] Al Ghafri S.Z., Munro S., Cardella U., Funke T., Notardonato W., Trusler J.P.M., Leachman J., Span R., Kamiya S., Pearce G., Swanger A., Rodriguez E.D., Bajada P., Jiao F., Peng K., Siahvashi A., Johns M.L., May E.F.
Hydrogen liquefaction: a review of the fundamental physics, engineering practice

and future opportunities, Energy & Environmental Science, vol. 15 (2022).
DOI: 10.1039/D2EE00099G

[63] Agenzia svedese dei trasporti (2025).
Statistiche nel settore dell'aviazione: statistiche aeroportuali: passeggeri per aeroporto 2024. Last updated on May 15, 2025. Visited on June 11, 2025.

[64] van Dijk D., Ebrahim H., Jooss Y., Bødal E.F., Hjorth I.
Integrating liquid hydrogen infrastructure at airports: Conclusions from an ecosystem approach at Rotterdam The Hague Airport (2024).
DOI: 10.69554/uueu4515

[65] Schenke F., Hoelzen J., Bredemeier D., Schomburg L., Bensmann A., Hanke-Rauschenbach R..
LH_2 supply for the initial development phase of H_2-powered aviation, Energy Conversion and Management: X, Volume 24, (2024) .
DOI: 10.1016/j.ecmx.2024.100797

[66] Stathis A., Dilip K.
Strategies for decarbonizing the aviation sector: Evaluating economic competitiveness of green hydrogen value chains - A case study in France, Energy, Volume 314 (2025).
DOI: 10.1016/j.energy.2024.134111

[67] Hydrogen Infrastructure Map (2024).
Showcasing concrete European hydrogen infrastructure projects and possibilities for transport routes and corridors. Visited on June 28, 2025.

[68] Degirmenci H., Uludag A., Ekici S., Karakoc T.H.
Challenges, prospects and potential future orientation of hydrogen aviation and the airport hydrogen supply network: A state-of-art review, Progress in Aerospace Sciences, Volume 141 (2023).
DOI: 10.1016/j.paerosci.2023.100923

[69] McPhy|Hyport (nd).
A first hydrogen production and distribution system to be implemented in an airport area. Visited on June 29, 2025.

[70] Hoelzen J., Silberhorn D., Zill T., Bensmann B., Hanke-Rauschenbach R.
Hydrogen-powered aviation and its reliance on green hydrogen infrastructure - Review and research gaps, International Journal of Hydrogen Energy, Volume 47 (2022).
DOI: 10.1016/j.ijhydene.2021.10.239

[71] McPhy|H2BER (nd).
La nostra attrezzatura per la produzione e lo stoccaggio dell'idrogeno a Berlino. Visited on June 29, 2025.

[72] NOW GmbH (nd).
H2-BER - Construction and operation of a wind hydrogen production facility and the world's first carbon neutral refuelling station. Visited on June 29, 2025.

[73] ICAO - International Civil Aviation Organization (nd).
Eco-Airport Toolkit - A Focus on the production of renewable energy at the Airport site. Visited on July 1, 2025.

[74] Abhishiktha T., Ratna K.V., Dipankur K.S., Indraja V., Hari Krishna V.
A review on small scale wind turbines (2016).
DOI: 10.1016/j.rser.2015.12.027

[75] Windmills Tech (nd).
Vertical Axis Wind Turbines. Visited on July 3, 2025.

[76] Copernicus Climate Change Service (C3S) - Climate Data Store (2025).
Land cover classification gridded maps from 1992 to present derived from satellite observations. Last updated on April 19, 2025. Visited on July 3, 2025.
DOI: 10.24381/cds.006f2c9a

[77] Copernicus - Europe's eyes on Earth (nd).
About Copernicus. Visited on July 3, 2025.

[78] NSF Unidata Software Documentation (2025).
NetCDF: Introduction and Overview. Visited on August 2, 2025.

[79] esri - ArcGIS Pro (nd).
ArcGIS Pro help: What is netCDF data?. Visited on August 2, 2025.

[80] Copernicus Marine Service (2025).
Introduction to the NetCDF format. Visited on August 2, 2025.

[81] Muñiz Fernandez F., Carreño Torres A., Morcillo-Suarez C., Navarro A.
Application of Array-Oriented Scientific Data Formats (NetCDF) to Genotype Data, GWASpi as an Example, Bioinformatics for Personalized Medicine, vol 6620 (2012).
DOI: 10.1007/978-3-642-28062-7_2

[82] NGA - Office of Geomatics (2014).
Department of Defense World Geodetic System 1984: Its Definition and Relationships with Local Geodetic Systems. Published on July 8, 2014. Visited on August 27, 2025.

[83] 8TH LIGHT (2023).
Geographic Coordinate Systems 101: A Primer for Software Generalists. Published on March 16, 2023. Visited on August 26, 2025.

[84] IOGP's Geomatics Committee (nd).
The EPSG Geodetic Parameter Dataset. Visited on August 27, 2025.

[85] Amatulli G., Domisch S., Tuanmu M.N., Parmentier B., Ranipeta A., Malczyk J., Jetz W.
A suite of global, cross-scale topographic variables for environmental and biodiversity modeling, Scientific Data volume 5, article 180040 (2018)
DOI: 10.1038/sdata.2018.40

[86] EarthEnv (2018).
Global 1,5,10,100-km Topography. Visited on August 27, 2025.

[87] Protected Planet (nd).
World Database on Protected Areas (WDPA). Visited on August 27, 2025.

[88] Pieton N., Abdel-Khalek H., Fragoso J., Franke K., Graf M., Holst M., Kleinschmitt C., Müller V.P., Weise F., Drechsler B., Lenivova V., Nolden C., Voglstatter C., Wietschel M., Bergup E., Sinha M.F.A.

Export Potentials of Green Hydrogen - Methodology for a Techno-Economic Assessment, Fraunhofer Institute for Systems and Innovation Research ISI (2023).
HYPAT Working Paper 02/2023.

[89] Lohr C., Schlemminger M., Peterssen F., Bensmann A., Niepelt R., Brendel R., Hanke-Rauschenbach R.
Spatial concentration of renewables in energy system optimization models, Renewable Energy (2022).
DOI: 10.1016/j.renene.2022.07.144

[90] Global Solar Atlas (nd).
Turin Caselle area: radius 100 km. Visited on September 9, 2025.

[91] Global Wind Atlas (nd).
Turin Caselle area: reduced circle. Visited on September 9, 2025.

[92] IATA - International Air Transport Association (2024).
Evolution of hydrogen aircraft fleet to 2050: A "regional first" strategy. Published on November 22, 2024. Visited on September 10, 2025.

[93] EUROCONTROL (2022).
Aviation Outlook 2050 - main report. Published on April 13, 2022. Visited on September 10, 2025.

[94] ASSAEROPORTI - Associazione degli aeroporti italiani (nd).
Archivio: dati di traffico annuali 2019. Visited on September 10, 2025.

[95] Aqueduct Water Risk Atlas (nd).
Piedmont water stress data: ratio of total water demand to available renewable surface and groundwater supplies. Visited on September 9, 2025.

[96] Kuzma S., Bierkens M.F.P., Lakshman S., Luo T., Saccoccia L., Sutanudjaja E.H., Van Beek R.
Aqueduct 4.0: Updated decision-relevant global water risk indicators, World Resources Institute (2023).
DOI: 10.46830/writn.23.00061

[97] Bardon P., Massol O.
Decarbonizing aviation with sustainable aviation fuels: Myths and realities of the roadmaps to net zero by 2050, Renewable and Sustainable Energy Reviews (2025)
DOI: 10.1016/j.rser.2024.115279

[98] Sismanidou A., Tarradellas J., Suau-Sanchez P., O'Connor K.
Breaking barriers: An assessment of the feasibility of long-haul electric flights, Journal of Transport Geography (2024)
DOI: 10.1016/j.jtrangeo.2024.103797

[99] IPCC - Intergovernmental Panel on Climate Change
Climate Change 2022: Mitigation of Climate Change, Contribution of Working Group III to the Sixth Assessment Report of the Intergovernmental Panel on Climate Change, Cambridge University Press. (2022)
DOI: 10.1017/9781009157926.001

[100] IATA - International Air Transport Association (2025).
Hydrogen for aviation: A future decarbonization solution for air travel?. Published on February, 2025. Visited on September 25, 2025.

[101] Energy Monitor (2023).
Beyond the H2ype: why the World Bank should be cautious on green hydrogen. Published on November 20, 2023. Visited on September 25, 2025.

[102] Chase, M.W. Jr.
NIST-JANAF Thermochemical Tables, Standard Reference Data Program of the National Institute of Standards and Technology (1998).
DOI: 10.18434/T42S31

[103] ReCommon (2025).
La strategia sull'idrogeno è solo un favore a Snam?. Published on July 30, 2025. Visited on October 7, 2025.

[104] Arab Reform Initiative (2022).
Who benefits from Tunisia's green hydrogen strategy?. Published on December, 2022. Visited on October 7, 2025.